A STUDY OF THE CATALYTIC PROPERTIES

OF THE SODIUM TUNGSTEN BRONZES.

Thesis Presented for the Degree of Doctor of Philosophy

by

Stuart Spencer Moody.

University of Edinburgh.

September 1969.

To my parents, brothers and sisters.

CONTENTS

ACKNOWLEDGEMENTS.

I should like to thank my Supervisor, Dr. Duncan Taylor, for his guidance and encouragement during the course of this work.

I am also indebted to Professor C. Kemball for the interest he has shown in this work, and to him and Professor Sir Edmund L. Hirst for the provision of laboratory facilities.

I am grateful to Dr. K. H. Taylor for measurements on the electron spin resonance spectrometer.

Finally, I am grateful to the Technical Staff for their assistance during my studies in the department.

Acknowledgement is made for the award of a Research Studentship from the Science Research Council.

INTRODUCTION.

The Sodium Tungsten Bronzes, with the general formula, Na_xWO_3, where x varies from 0 to ~0.8, form a series of non-stoichiometric compounds with semiconductor ($x < 0.25$) or metallic ($x > 0.25$) properties. The "free" electron concentration varies over a wide range with only very small changes in lattice parameters. They constitute, therefore, a system for which the connection between electron concentration and mobility on one hand and catalytic activity on the other can be conveniently studied.

The earliest literature reference to these compounds was by Wöhler (1), who in 1824 succeeded in preparing a sodium tungsten bronze. The designation "Wolframbronce", which was introduced to describe the yellow metallic lustre of Na_xWO_3 ($x=0.8$), was first used apparently by Phillipp and Schwebel (2), but despite this and many other reports (3-11) of their existence little work was done to establish the actual nature of these compounds until the last two decades.

In general three methods (12,13) have been used to prepare the sodium bronzes:-

(a) An electrolytic reaction in which a molten mixture of Na_2WO_4 and WO_3 are decomposed with platinum or tungsten electrodes. Here the product forms on the cathode with oxygen being liberated at the anode.

Table 1

Na_xWO_3	Colour	Crystal Structure
WO_3	Yellow-Green	Monoclinic & Orthorhombic
	Grey-Green	Tetragonal 1
$Na_{0.2}WO_3$	Dark Blue	Tet 1 & Tet 2
		Tetragonal 2
$Na_{0.4}WO_3$	Royal Blue	Cubic & Tet 2
	Purple	
$Na_{0.6}WO_3$	Dark Red	Cubic
	Brick Red	
	Orange	
$Na_{0.8}WO_3$	Yellow	

(b) A thermal reaction

$$x/2\ Na_2WO_4 + (3-2x)/3\ WO_3 + x/6\ W = Na_xWO_3$$

in which the solid reagents are finely ground and heated to give a product via the solid state reaction.

(c) One involving the reduction of molten sodium paratungstate using either electrolytic hydrogen or a metal i.e. tin or zinc.

Table 1 gives a broad outline of the change in crystallographic properties (14-25) together with colour change for the sodium bronzes. The crystal structure undergoes successive transitions through tetragonal 1 and 2 phases (18,20,22-4,27-32) in the region $x \simeq 0.1 \rightarrow 0.3$, whereafter a cubic phase (17,19,22,24-5,27,31,33) occurs up to $x \simeq 0.8$. The reported existence of a tetragonal phase in the region $x \simeq 0.4$ by some workers (20,32), has been attributed to a more gradual rate of annealing during preparation. For values of $x < 0.1$, triclinic (14-6,33) and monoclinic (pseudo-orthorhombic)(21,23-4,26-7,32,34-7) structures have been postulated.

Of special interest is the linear relationship between the lattice constant, "a" and the sodium content "x" for the cubic bronzes. This relationship, illustrating Vegard's Law (38), has proved to be of great assistance in the determination of the "x" value, which is given by the expression (39).

$$a = (3.7845 + 0.0320x)\ \text{Å}$$

Fig 1 The ReO_3 - type structure

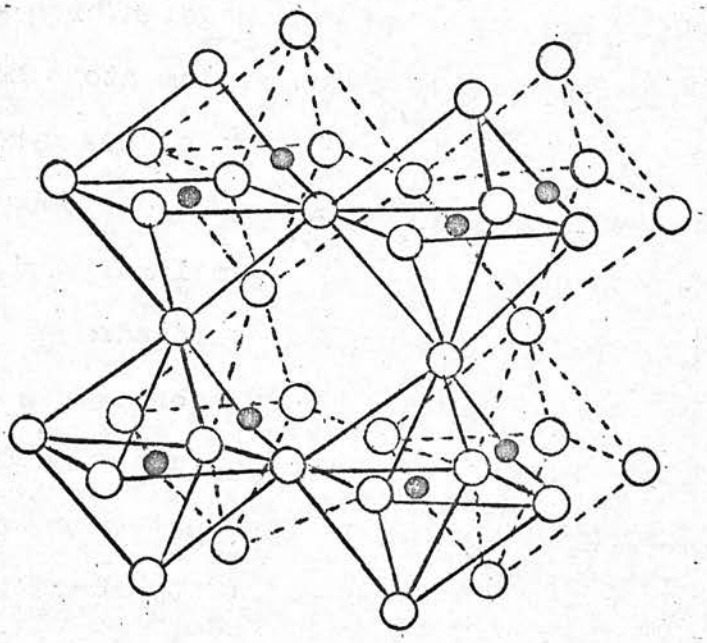

(a)

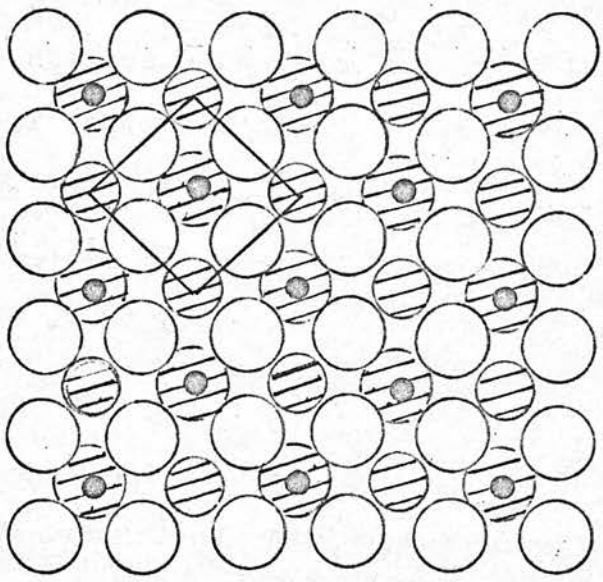

(b)

metal atoms

oxygen atoms

" " in layer immediately below

} NB Top layer omitted

The simplest model (11) for a sodium tungsten bronze, is to regard it as a host WO_3 structure in which sodium atoms have been introduced interstitially. WO_3 has a structure of low symmetry (21,23-4,26-7,32,34-7) consisting of deformed WO_6 octahedra joined by sharing corners to form an infinite 3-dimensional framework (21,27,40-2) in the same way as the regular octahedra of the ReO_3 structure (figure 1(a) and (b))(40). The loss of oxygen under vigorous conditions leads to the appearance of a new phase below composition $WO_{2.98}$ (37,40,43-9), to give a structure consisting of blocks of the basic ReO_3 type but separated by shear planes or dislocations (40,49). For the simplest case, which leads to a structure analogous to that of perovskite, $CaTiO_3$ (40), the unit cell can be represented as in figure 2, (11), with a tungsten atom at the centre, 6 oxygen atoms at the face centres and eight "interstitial sites" at the cube corners more or less occupied by alkali atoms. When these sites are completely empty i.e. where x=0in Na_xWO_3, this ideal structure resembles that of WO_3, the difference being that with WO_3, the W atoms are slightly off centre in adjacent unit cells. Figures 3(a) and 3(b), (40), give an idealised picture of the perovskite structure.

Initially (19,27,31,39,50-7) it was assumed, in order to meet the necessary requirements of neutrality, that there was a progressive change in oxidation state from W(VI), found in WO_3 (x=0), to wholly W(V), found in the hypothetically highest member of the series $Na_{1.0}WO_3$. This classical model (43) for non-

Fig 2

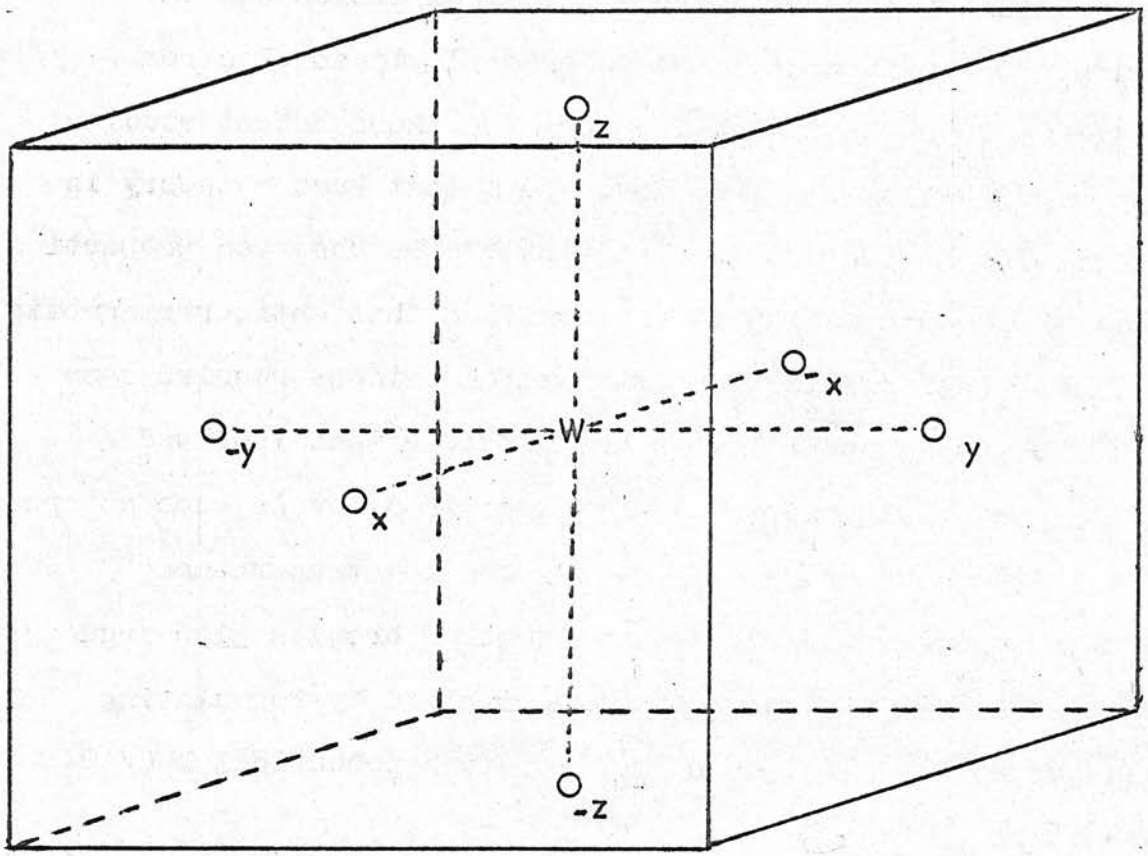

Structure of idealised tungsten bronze,

M_xWO_3

$x = 0$

stoichiometric compounds of the transition elements assumes the presence of isolated ions in several oxidation states and the conductivity process is postulated to proceed via an electron transfer from a lower to a higher valent ion. More recent studies (11,25,27,31,43,58-63), however, have shown that such a theory is unable to provide an adequate explanation of the observed properties of the tungsten bronzes. With the recognition that antiferromagnetic interactions encountered in transition metal oxides, require some overlap of the atomic orbitals, it became clear that isolated energy states have to be replaced by delocalised levels such as are postulated in the band theory of solids. The low temperature paramagnetism observed for the sodium tungsten bronzes also argues against isolated spin states of the type implied by formulating the bronzes as solid solutions of $W(VI)O_3$ in hypothetical $MW(V)O_3$ (M=alkali metal).

Sienko and Crowder (61), Mackintosh (62) and Fuchs (63), working independently, approached the problem in one of two ways based on the Molecular Orbital Theory: a "Perturbation" theory due to Frohlich and Mott (64) and to Howarth and Sondheimer (65) and an "Intermediate Coupling" theory due to Lee, Low and Pines (66-8), both of which have the common feature that each sodium atom contributes one electron to a conduction band. These theories have also proved qualitatively very useful in accounting for the metal to semiconductor discontinuities observed with decreasing temperature for some of the 3d metal oxides and for the decreasing

Fig 3

The Perovskite Structure

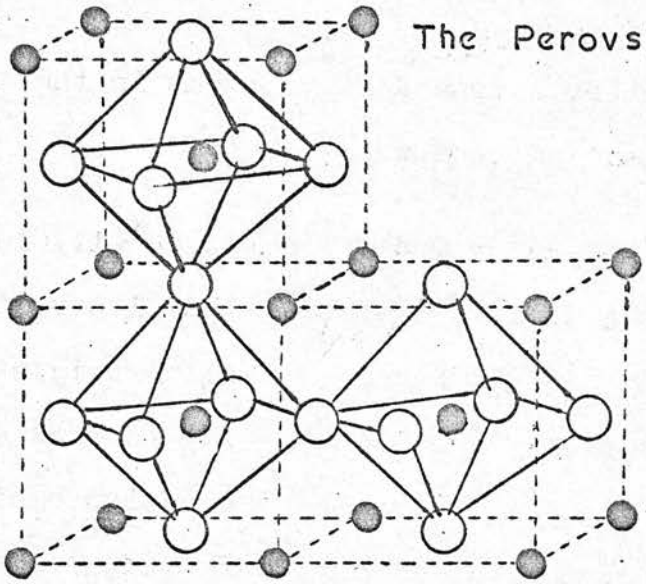

(a)

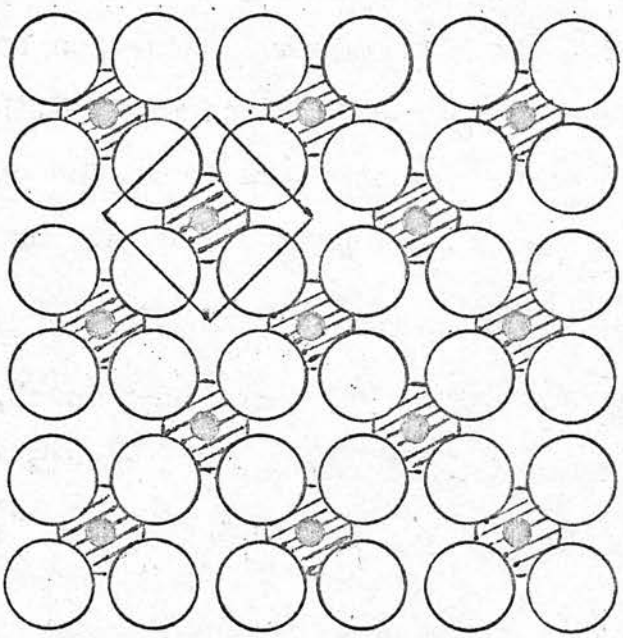

(b)

metal atoms

oxygen atoms

" " in layer immediately below

N.B. Top layer omitted

carrier mobilities observed from left to right in the conducting oxides of the 3d transition sequence.

The use of the Molecular Orbital approach (11,61-3) has proved to be a valuable tool in assessing the electronic structure of these compounds. In his studies of the electronic structure of bronzes with metallic properties, Sienko (11) adopted an essentially covalent model in which the conduction band was derived solely by overlap of the tungsten 5d (t_{2g}) orbitals. Although theoretically an insulator (69) WO_3 does exhibit semiconductor properties usually "n" type (61) in character ("p" type (70) has also been reported), owing to various impurity centres, usually associated within the region bridging the gap between the valence and conduction bands and inevitably present with polycrystalline material. With the introduction of sodium atoms to this structure, the conduction band is filled up to an extent which is determined by the "x" value.

Mackintosh (62), also adopting a covalent model, approached the problem in a different way. He sought to explain the formation of the conduction band by the overlap of the sodium "p" atomic orbitals.

The supporting evidence for both of these band models, which have led to WO_3 being called an "electronless metal" (11) which is populated by electron donors, Na, comes from various

kinds of measurements. These include resistivity vs temperature, Hall voltage, thermoelectric power, magnetic susceptibility and nuclear magnetic resonance measurements. Each of these serve in turn, to account for the suitability or inadequacy of either or both of these models.

More recently Fuchs (63), has shown that, although neither is wholly correct, they both provide a more than useful foundation from which a more complete picture of the conduction band may soon be obtained. Fuchs has suggested that clusters of sodium atoms may occur in the bronzes. Here electrons would be localised more diffusely so that they would extend over the tungsten and oxygen ions next to the sodium ions.

Indeed the broad applicability of both models may be judged from the fact that they are able to account for the observed changes in colour of the tungsten bronzes. Brown and Banks (25) have reported from their investigations of the spectral distribution of visible light reflected from Na_xWO_3 samples, that the absorption peak narrows appreciably as "x" increases. This is a consequence (63,11,71) of the widening gap between the valence band and the first vacant level of the conduction band and due to the increasing density of filled states in the conduction band.

Transient nuclear magnetic resonance studies based on the ^{23}Na resonance in the sodium bronzes, in which a negligible Knight shift has been observed, have provided evidence for Sienko's model (62,72-4) based on tungsten d orbitals. Narath, first with

Wallace (75) and then Fromhold (76), extending these studies to the ^{183}W resonance in these compounds has served to corroborate the earlier studies of the ^{23}Na resonance.

Resistivity vs temperature plots, obtained from measurements on single crystals of the bronzes with $x > \sim 0.3$, have almost without exception exhibited positive thermal coefficients of resistivity (19,24-5,54,60,77-9) consistent with metallic behaviour. Work carried out on powder samples have not, however, proved as reliable, one notable example being the results obtained by Straumanis and Hsu (52) which were consistent with semiconductor behaviour In figure 4 (77), the resistivities of single crystals of cubic and tetragonal sodium bronzes at 300°K are shown as a function of alkali metal concentration. Figure 5 (78), represents the conductivities (reciprocal resistance) of the same bronzes at 300 °K plotted as a f(x). By extrapolating to zero conductivity the curve in figure 5 strongly suggests that all bronzes will become semiconductors (or insulators) for values of "x" less than ~ 0.25. This possibility has been suggested by Sienko and Trong (80) using the theory of Mott (81) for metal-semiconductor transitions. Fuchs (63), however, has pointed out the major weaknesses of applying this approach, and in addition has suggested an alternative mechanism based on Mackintosh's work (62) Moreover, the difficulty of obtaining sufficiently homogeneous crystals have made it virtually impossible to make an accurate study of the discontinuity which would be expected from Mott's theory. Of importance here is the fact that no crystals

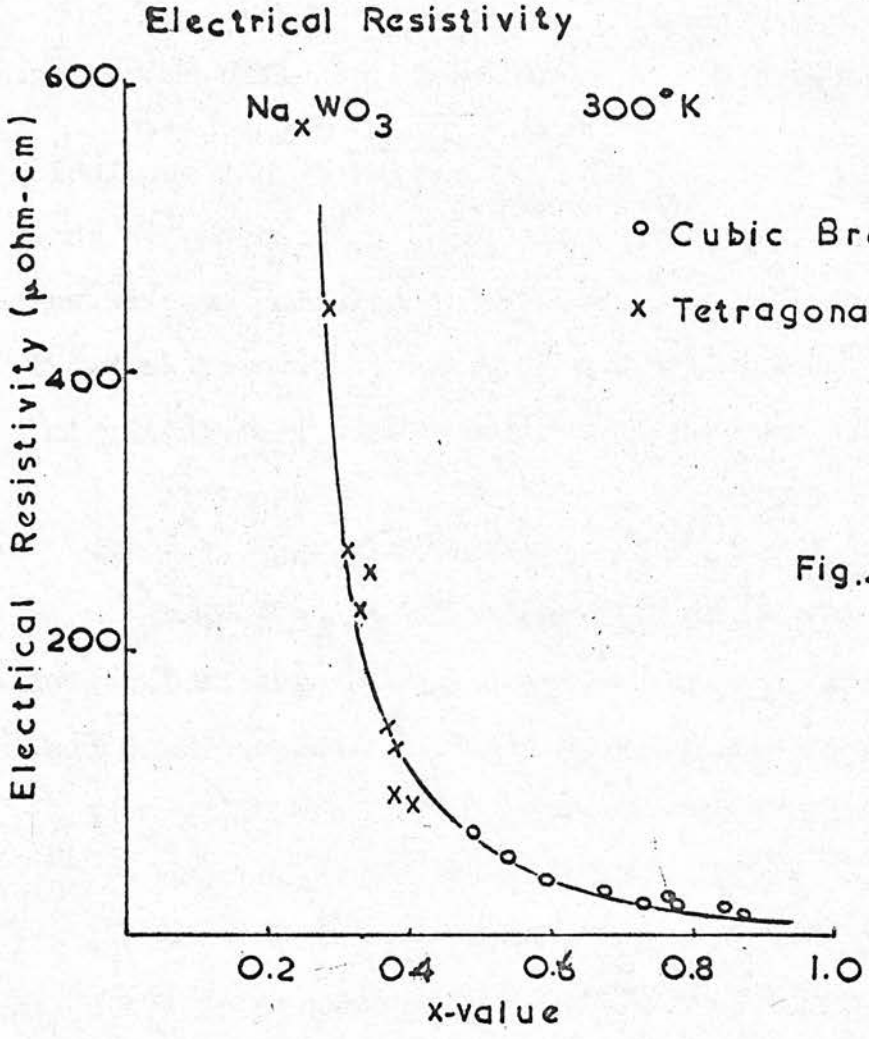
Electrical Resistivity
Na_xWO_3
300°K
o Cubic Bronze.
x Tetragonal Bronze.
Electrical Resistivity (μohm-cm)
600
400
200
0.2
0.4
0.6
0.8
1.0
x-value

Fig.4

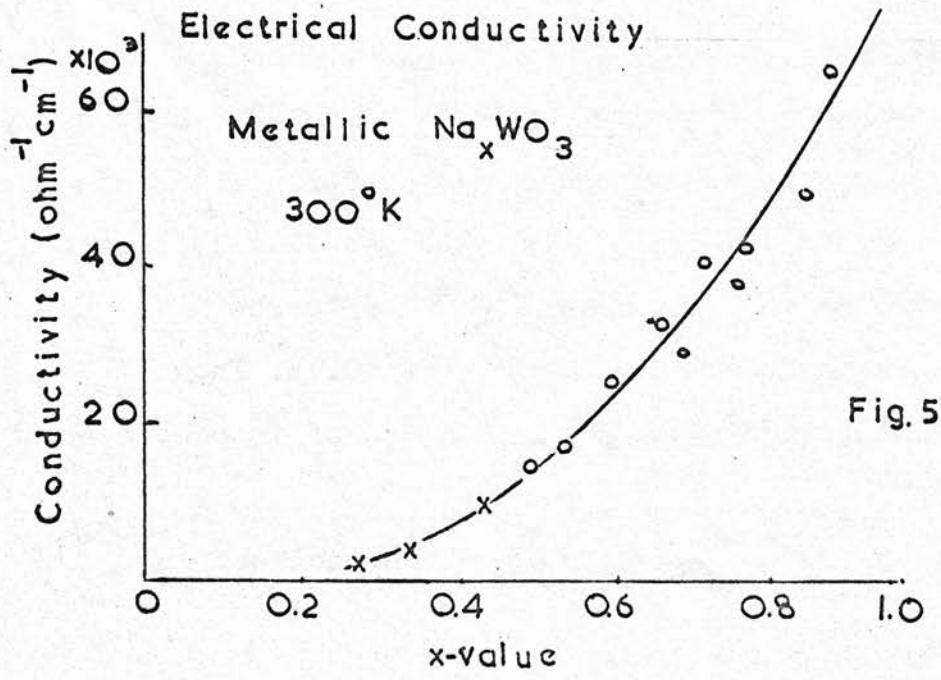
Electrical Conductivity
Metallic Na_xWO_3
300°K
Conductivity (ohm^{-1}cm^{-1})
x10^3
60
40
20
0
0.2
0.4
0.6
0.8
1.0
x-value

Fig. 5

in the region below $x \simeq 0.25$, have exhibited metallic character.

Straumanis and Hsu (52) have demonstrated that the Ionic conductivity observed with lithium tungsten bronzes, is absent in the sodium bronzes below 450°C, thus precluding any diffusion of sodium atoms through the lattice. Many references (24-5,82) have been made to the presence of a minimum in resistivity in the region $x \sim 0.75$. Brown and Banks (25), supplementing resistivity work with Hall effect studies, deduced that the mobility of the electrons in the bronzes was ~35 % of that in metallic sodium. They have put forward a tentative explanation in terms of an equilibrium between undissociated sodium atoms, sodium ions and free electrons: for values of $x < 0.75$, each sodium atom added contributes one free electron and one random scattering centre (Na^+), until at $x \simeq 0.75$ an ordered structure is formed, whereupon the continued addition of undissociated sodium atoms creates only additional scattering centres with a resultant increase in resistivity. Itwas noted by Juretschke (82) that this minimum was much less than is customarily associated with such ordered structures. Despite later reports, however, of the absence of the ordering phenomenon (60), the problem was finally resolved by Mahlestein and Danielson (79), who were able to show conclusively the presence of the minimum at $x \simeq 0.75$. They attributed the earlier discrepancies to the use of inhomogeneous crystals.

Measurements of Seebeck coefficients (thermoelectric

powers)(61, 78-9) and Hall coefficients (24-5,33,54,78,80) have provided evidence in support of the proposed free electron model. Moreover, many workers have indicated that each sodium contributes one electron for conduction processes, although, more recently, the value of using Hall coefficients has been put in doubt by Mahlestein and Danielson (79), who found that they were unable to predict the exact number of electrons consistent with the sodium content of their samples.

On the other hand, the thermodynamic properties of the bronzes obtained from magnetic susceptibility data (43,50,58,76, 83) as well as specific heat data (84), though still in agreement with the view that the bronzes contain "quasi"-free electrons, suggest that this free electron theory must be considerably modified (63,78), however well it accounts for some of the transport properties of these compounds.

Although, as we have seen, much work has been carried out on the physical properties of these compounds, the study of their catalytic properties has received much less attention. Jones (85) has studied the ortho-para-hydrogen conversion and hydrogen-deuterium exchange reactions, Balandin and Sokolova (13) the decomposition of isopropyl alcohol, ethanol and formic acid, and Dickens and Whittingham (28) the oxygen atom recombination reaction.

Jones (85), using samples with $0.30 \leqslant x \leqslant 0.98$, was able to

show that the rate constants per unit area exhibited a sharp maximum at x = 0.67; at this composition, for example, the rate constant was 840 times as large as that at x = 0.30. The maximum in activity occurred at roughly the same composition as the maximum in the electron mobility determined by other investigators (24-5,33,54,78,80). This variation in rate he attributed, mainly, to a variation in the number of active centres, since the (high temperature) activation energy was found to be constant over the whole range of composition ($\sim$6.8 K cals/ mole).

It was further observed that the bronzes underwent an "Activation process" in hydrogen, the activity being initially low and increasing to a stable maximum after a few days. This he ascribed to a slow adsorption process, since outgassing in vacuo did not impart activity, and prolonged pumping on activated bronzes caused a decrease in activity. Moreover, a rapid restoration of the activity was achieved on renewed exposure to hydrogen.

Balandin and Sokolova (13), using tungsten trioxide and bronzes prepared by reduction of sodium paratungstate, showed that the dehydrating power of the bronzes was less than that of WO_3 or the unreduced paratungstate. The dehydration activity decreased with increased degree of reduction, becoming almost zero for the most completely reduced bronze (x = 0.91). The increasing inertness to chemical change with increase of "x" value through the series was demonstrated by the resistance to oxidation

Fig. 6

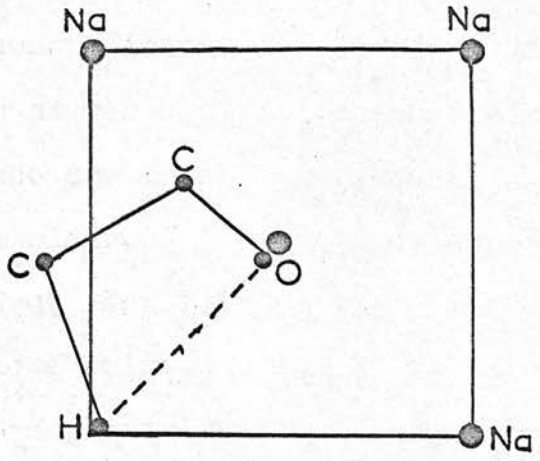

(a)

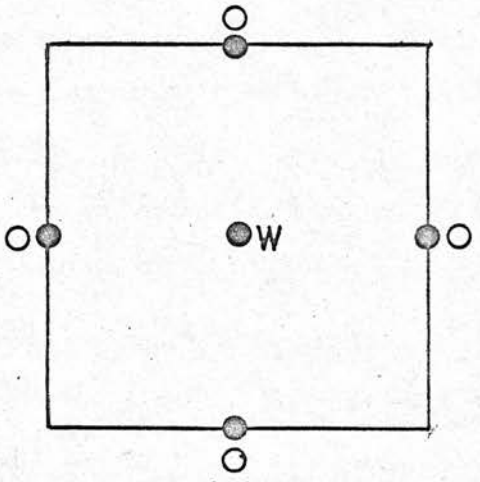

(b)

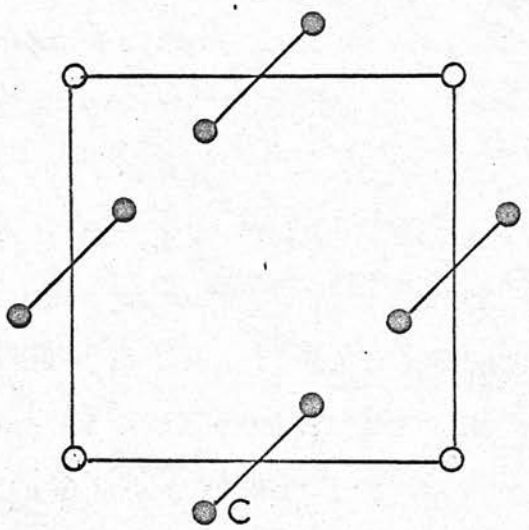

(c)

Th O

C_2

of the highest members of the series. For example, whereas the red bronze ($x = 0.63$) exhibited a substantial increase in activity after being heated in air for 1 hour, no change was observed for the higher bronze ($x = 0.91$) under identical conditions. Evidence of the readier oxidation of the lower bronzes was provided by the appreciable increase in activity of the dark blue bronze ($x = 0.28$), which, after heating in air for 3 hours, had an activity similar to that of the original paratungstate. They also found that the progressive substitution of Na by Li in the bronzes noticeably decreased their activity for the dehydration of isopropyl alcohol.

These observations, they sought to explain in terms of the Multiplet theory (86), postulating a two point adsorption on adjacent sodium and oxygen vacancies. Figure 6(a) represents the face of a unit cell in the cubic bronze, while figure 6(b) shows the atomic layer beneath it. Some vacancies arise when $x < 1$ by virtue of the lack of sufficient sodium atoms to occupy all the corners, whilst others may arise through lack of oxygen. The H and O atoms in alcohols which react during catalytic dehydration can then fill these vacancies (figure 6(a)) with the oxygen completing the WO_6 octahedron (87). In figure 6(a), which is drawn to scale, the location of the C atoms are also indicated. That the atomic distribution shown in figure 6(a) is quite feasible is seen from the fact that the C-C distribution is analogous to that adopted by thorium carbide (88) (cf. figure 6(c)) and

further that hydrogen analogs of the sodium bronzes, with almost identical parameters have been isolated (89). In accordance with this theory, the intermediate complex in figure 6(a), is a solid surface solution.

The agreement within about 16% between the distance between (Na···O) vacancies and the (H···O) distance in alcohols serves to illustrate how this model can account for the observations that the sodium bronzes promote the dehydration reaction, though weakly. It is also able to provide an explanation for the fall in catalytic activity with increased reduction of the paratungstate or introduction of lithium: both of these reduce the number of defects in the corners of the cube with the result that fewer alcohol molecules can be adsorbed in the catalytically required positions. In concluding their work, Balandin and Sokolova pointed out that although the discovered parallelism between the catalytic activity and the number of defects in the bronzes conforms with the electronic theory of catalysis, the weak catalytic activity of their defective lattices does not. In general, besides the defects, the various steric and energy relationships have also to be accounted for.

Of perhaps less significance, has been the study by Dickens and Whittingham (28) of the oxygen atom recombination reaction on the bronzes of the general formula M_xWO_3, where M = Li, Na or K and $0 \leqslant x \leqslant 0.8$. In all cases, the reaction was found to be first order, and the activities obtained, found to be closely related

to the electronic properties of the bronzes.

Of special interest with regard to the present work have been the studies by Crowder and Sienko (37, 61), Derén and Polaczkowa (90) and others (45,49,91) on the electronic properties of tungsten trioxide. These have shown that the conductivity of the semiconducting oxide increases rapidly in vacuo and that a "Quasi metallic" state is finally attained. Earlier it was stated that, according to Mott's theory (81) for metal-semiconductor transitions, a changeover from metallic to semiconducting properties would be observed at values of $x < 0.25$ in Na_xWO_3. It is now accepted, however, that under vacuum conditions, this changeover may occur at much lower values of "x", and indeed may never occur at all. This has been pointed out by Kudrak and Sienko (91), who have shown that additional electron centres are created by removal of oxygen, each missing oxygen atom being equivalent to the presence of two alkali atoms. This equivalence of oxygen defect and alkali metal addition in the WO_3 system has been demonstrated by Sienko and Banerjee (45), by the fact that the magnetic behaviour as a function of x is the same in WO_{3-x} as in M_xWO_3. This tendency of WO_3 to readily shed some of its surface oxygen (cf. Jones and Balandin and Sokolova), has also been referred to by Rabes and Schenk (92) who observed that formic acid, a strong reducing agent, quickly reduces the surface of the parent oxide WO_3.

The Formic Acid Decomposition Reaction.

Formic acid may decompose either by dehydration to yield carbon monoxide and water, or by dehydrogenation to yield carbon dioxide and hydrogen. On some catalysts, both reactions occur.

The wealth of evidence gained from infra red (93,95), kinetic isotope (93,95) and conductivity (93,94) studies support the view that, in the absence of surfaces exhibiting acidic properties, the reaction proceeds via a formate ion as intermediate.

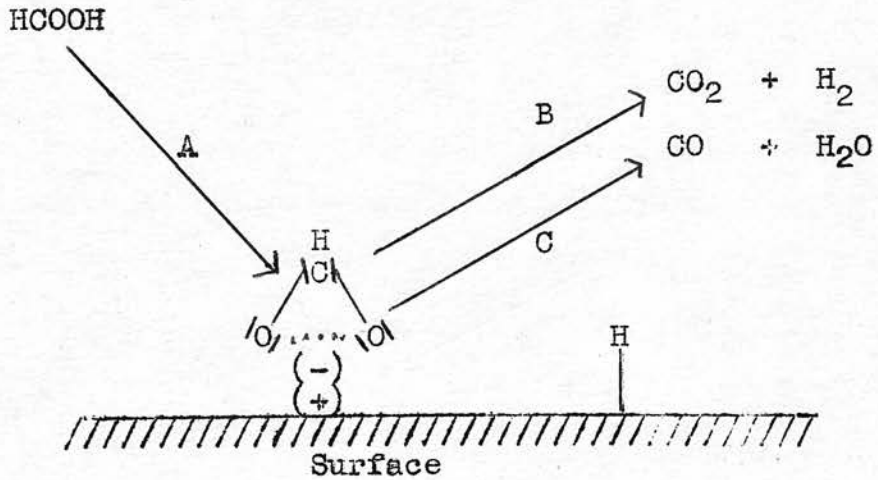

Considerable doubt, however, still exists over the actual direction of charge transfer on the surface, evidence for both positively (93,94,96) and negatively (93,95) charged species having been forwarded, and as to whether a monomolecular or bimolecular mechanism is operative. The later problem has to some degree been clarified by Hirota (95) et. al, from infra red

studies of deuterated formic acid on nickel films, and by Lawson (97) from measurements of the desorption, exchange and catalytic decomposition of ^{14}C labelled formic acid molecules on silver films. Both sets of results were found to be consistent with a bimolecular mechanism, in which a formate ion, normally stable, was rendered unstable in the presence of the vapour or the physically adsorbed species of formic acid. Moreover, they postulated that interaction between the two species could occur to form an intermediate complex of the form:

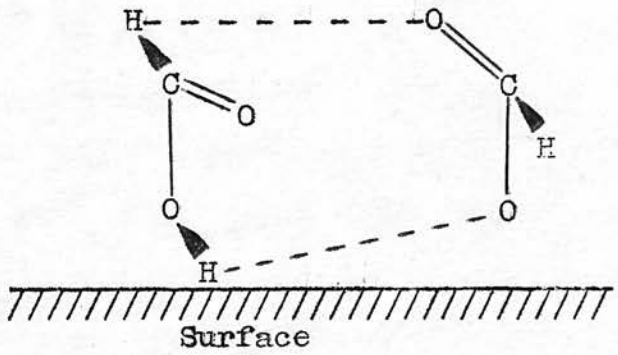

Breakdown of this complex could then occur to give CO_2 and H_2 or CO and H_2O.

The work presented in this thesis was undertaken to elucidate further the catalytic properties of the sodium tungsten bronzes. A kinetic study of the decomposition of formic acid has been carried out, together with electrical conductivity measurements, on the bronzes and also on WO_3.

EXPERIMENTAL

Preparation of the Sodium Tungsten Bronzes.

Of the various methods (12,13) available for the preparation of the sodium bronzes, the most versatile and the one adopted in this study, is the solid state reaction:

$$x/2\ Na_2WO_4 + (3-2x)/3\ WO_3 + x/6\ W = Na_xWO_3$$

Here the appropriate quanties of sodium tungstate, tungstic oxide and tungsten powder were finely ground and heated in a silica tube (6 cm long and 1 cm wide) at 850°C under vacuum (10^{-5} mm Hg), for a minimum of 5 hours. A sample of pure tungsten oxide was heated in the same manner. Owing to the strong devitrifying action of sodium tungstate on vitreoussilica, a tube could not be used for more than two or three preparations, more especially during the preparation of the higher members of the series. After cooling, the samples were finely ground and then leached successively with boiling dilute NaOH, concentrated HCl, distilled water and acetone (28). This treatment removes unreacted Na_2WO_4, WO_3 and tungsten metal.

Analysis of bronzes.

Analyses for sodium content were carried out by fusion with a 3:1 fusion mixture of KNO_3:K_2CO_3 in a platinum crucible, the bronze going rapidly into solution with gentle heating. After cooling, the white cake was dissolved in boiling water and then transferred to a 250 ml graduated flask. The amount of dissolved

sodium, and hence the percentage of sodium in the bronze, was then measured by use of an Eel flame photometer. The flame photometer was calibrated using solutions containing different known concentrations of sodium ions together with a constant concentration of potassium ions, both ions being introduced as their respective chlorides. Care was taken to ensure that all fusions were carried out with a potassium ion weight identical to that present in the calibration solutions.

X-ray Diffraction Results.

X-ray powder diffraction traces were determined with a Philips x-ray diffractometer (35kv-20ma. beam, copper target) and scanning the range $2\theta = 8°-60°$.

For members of the series exhibiting both cubic symmetry ($0.3 < x < 0.8$) and distorted cubic symmetry ($0.1 < x < 0.3$), the spacings were calculated from the relation.

$$2d\sin\theta = n\lambda$$

and by use of the expression.

$$d = \frac{a}{\sqrt{h^2 + k^2 + l^2}}$$

most of the peaks on the diffraction trace could be indexed.

Table 2 shows that the results obtained compare favourably with those of other workers (14-27). Without exception, all lattice parameters "a A° (present study)" are mean values for the 100, 110, 111, 200, 210 and 211 lattice planes.

Traces taken after exposure to formic acid showed negligible change in the value of 2θ or the intensity of individual peaks, indicating that little reorganisation of the crystal lattice had occurred during the reaction sequence.

Table 2

X-ray Diffraction Measurements

Copper target 35kV 20 mA unfiltered

k α radiation λ= 1.5405°A

x value	Lattice constant. α °A
0.11	3.80
0.16	3.80
0.28	3.81
0.38	3.80
0.52	3.82
0.60	3.81
0.66	3.82
0.73	3.83
0.77	3.83
0.81	3.84
0.85	3.86

Surface Area Measurements.

The method adopted was that derived by Brunauer, Emmett, and Teller (99), universally known as the B.E.T. method.

Here, a gas is adsorbed onto the previously degassed solid at low temperatures. Near ideal gases are generally used since they obey the B.E.T. theory in its simplest form. On the assumption that several layers of gas can be adsorbed onto the solid surface, this theory may be shown to lead to an expression from which the volume of gas necessary to form a mono layer on the surface is readily obtained.

The volume of gas adsorbed at N.T.P. is given by:-

$$V = \frac{cPVm}{(Po - P)(1 + (c-1)\ P/Po)}$$

where P = pressure of gas.

Po = vapour pressure of gas at the temperature of the adsorbate.

c = constant related to the heat of adsorption.

Vm = volume of gas at N.T.P. necessary to form a mono layer on the surface.

From this expression it can be seen that by plotting $P/(Po - P)\ V$ against P/Po, a value for Vm can be obtained. Knowledge of this quantity then enables the number of molecules involved in covering the surface and hence the surface area to be calculated. This isotherm is generally found to hold up to a relative pressure (P/Po) of ~ 0.25.

With the sole exception that pressure measurements were made directly using a small Mc. leod gauge, the experimental procedure was that outlined by Inglis (100), using krypton as adsorbate gas at -196°C and helium for dead space determination. The cross sectional area occupied by an adsorbed krypton atom was taken to be 19.5 $\mathring{A}^2$. The various fixed volumes were determined using helium since the gas is not appriecably adsorbed on glass. Table 3 gives a summary of the measured surface areas, both before and after the leaching and washing procedure. The surface area quoted for each catalyst is the mean of at least two determinations, reproducibility being $\pm$ 5 %.

Table 3

'X' value	Surface Area metres^2/gm.	
	Before Leaching	After Leaching
0	2.00	-
0.11	0.41	2.13
0.16	1.65	4.44
0.28	1.25	2.58
0.38	0.32	1.33
0.52	0.55	1.23
0.60	0.23	0.95
0.66	0.06	0.19
0.73	0.18	0.53
0.77	0.13	0.42
0.81	0.11	0.33
0.85	0.16	0.50

Magnetic Susceptibility Measurements.

Measurements of the magnetic susceptibility of substances containing transition elements are useful in giving an indication of the presence of unpaired electrons due to holes in the d-band, and as such have proved of value in elucidating the electronic properties of the tungsten bronzes.

Measurements of the susceptibilities of tungsten trioxide and the sodium tungsten bronzes were made by the Gouy method at room temperature and a field strength of about 10,000 gauss, the Gouy tube being calibrated with $Hg(Co(CNS)_4)$(101). Measurements of specific susceptibility were also made on samples which had been pretreated in a manner identical to that experienced by samples during the study of the kinetics of the formic acid decomposition reaction.

The 3mm diameter pyrex Gouy tube, having a reference mark 9cm from the closed end, was suspended by aluminium wire so that the bottom was on the axis of the horizontal pole pieces of the magnet (figure 7). Before any weighings were carried out (with the tube empty or filled, or with the magnet switch on or off), the tube was suspended for ten minutes, to allow it to reach the temperature of thesurrounding air and as necessary to allow the magnetic field to become uniform.

The tube was weighed empty with the magnet switched off and then again with it on. In this way the diamagnetic correction for

the tube was obtained. The volume of the tube was then determined by filling it to the reference mark with water and weighing with the magnetic off. The tube calibration constant was found by use of $Hg(Co(CNS)_4)$, the magnetic susceptibility of which is 16.44×10^{-6} cgs units at room temperature.

In the preparation of pretreated samples, use was made of the apparatus shown in figure 8. The sample was placed in the horizontal reaction vessel and subjected to a reaction sequence identical to that adopted in the study of the kinetics of the formic acid decomposition reaction. After about four reaction cycles each involving the expansion of formic acid to the reacting system followed by heating at 180-230°C for ~2 hours, and outgassing for a minimum of 3 hours at 470-500°C, the catalyst was allowed to cool to room temperature. Stopcock T was then closed, the apparatus detached from the vacuum line and the sample carefully transferred from the reaction vessel to the adjoining Gouy tube. Thereafter, the Gouy tube was sealed and removed from the reaction vessel. Measurements were then carried out in a similar manner to those for normal samples. In all these cases, the volume of the sample was recorded by a scratch on the outside of the tube and the tube calibrated using a volume of calibrant equal to the volume of the catalyst previously employed.

The specific susceptibility of the sample is given by (102):

$$10^6 \chi = \frac{\alpha + \beta F'}{W}$$

where $F' = F - \delta$

α = constant for displaced air = 0.029 x specimen volume.

β = tube calibration constant.

W = weight of specimen.

F' = force on specimen.

F = observed force.

δ = diamagnetic correction for the tube.

By convention α, F and δ are measured in mg and W in gm.

Fig 7

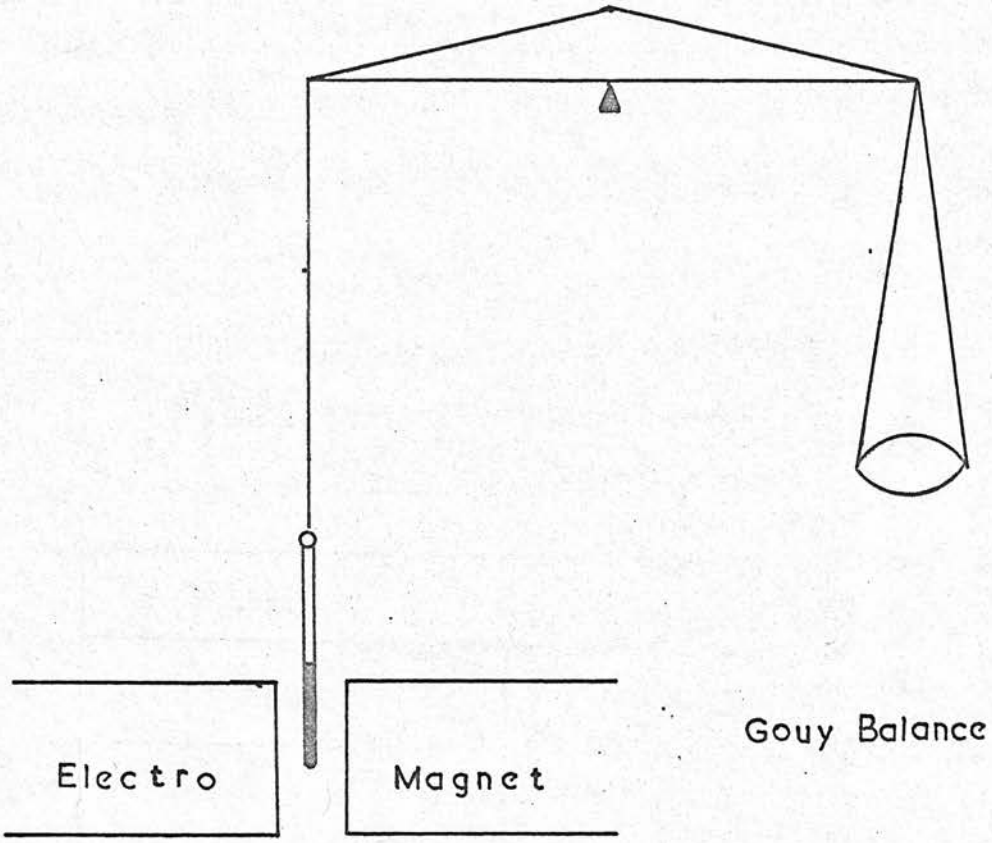

Gouy Balance

Fig 8

Apparatus For Sample Preparation
Under Vacuo

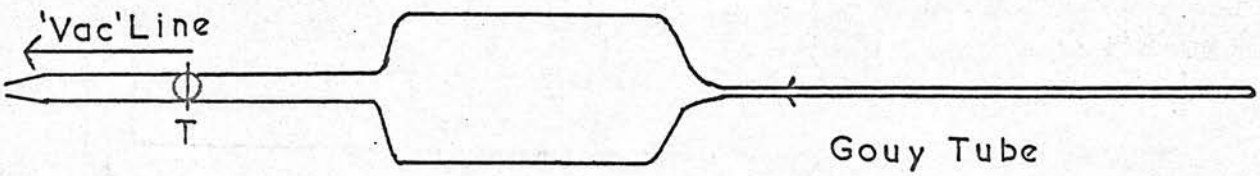

Table 4

Magnetic Susceptibility Data

'X' value	Specific Susceptibility 10^6X c.gs. units	
	Normal Samples	Pretreated Samples
0	0.57	2.45
0.11	0.13	0.01
0.16	0.10	0.05
0.28	0.15	0.10
0.38	0.19	0.14
0.52	0.22	0.16
0.60	0.12	0.06
0.66	0.14	0.07
0.77	0.35	0.29
0.85	0.19	0.13

Electron Spin Resonance Studies.

In principle, electron spin resonance (e.s.r.) may be observed in any system that has unpaired electrons. Moreover, electron spin resonance absorption can be shown (103, 104) to take place at any frequency provided the value of the magnetic field is adjusted to satisfy the equation:-

$$h\nu = g\beta Ho$$

in which β is the Bohr magneton and Ho is the strength of the applied field. The quantity 'g' is the Landé spectroscopic splitting factor and has the value 2.0023 for a free electron. In practice mixing of spin momentum with orbital momentum in atoms and molecules, may cause 'g' to depart from this value.

In the present study measurements of the e. s. r. spectra were carried out using a Hilger Watt Microspin electron spin resonance spectrometer. The electromagnet and stabilised power pack were supplied by Newport Instruments. Spectra were taken both of normal samples and of samples pretreated in a manner analogous to that used in the study of the magnetic susceptibility of these catalysts. The apparatus used for the pretreatment was identical to figure 8 except that the quartz sample tube and pyrex reaction vessel were cemented together with araldite. Care was taken to ensure that the araldite seal was kept cool when the reaction vessel section was being heated. Preliminary studies of spectra taken at room temperature were supplemented by measurements at low

temperatures and with increased magnetic field strength to give higher sensitivity.

Although, no detectable signals were observed for any of the sodium bronzes, whether pretreated or not, a signal was observed for pretreated WO_3. This occurred at a g value of $\sim$1.6 and indicated that pentavalent tungsten was present on the surface. The absence of any such signal for non-pretreated WO_3 refutes the possibility of the line being due to impurities present in the WO_3.

Preparation of Gases.

The gas handling lines were arranged so that the gases and vapours used in these experiments could be obtained and stored in high purity.

(a) Formic Acid.

500 ml Analar Formic Acid were distilled in the presence of phthalic anhydride (to remove any water present) and the fraction collected in the range 99-101°C. The distillation was repeated a further three times. Thereafter the purified formic acid was frozen out using a drikold/ acetone bath; allowed to melt and when half melted, the melt was discarded and the remaining solid allowed to warm to room temperature. This cycle was repeated at least six times, noting the melting point of the solid each time. After this series of operations, the acid was found to melt at a constant temperature of 8.4°C in excellent agreement with literature values (98). A small quantity of the purified acid was placed in a detachable tube and connected to the gas handling line. The acid was then frozen with liquid nitrogen and the sample tube evacuated. Vacuum distillation of the acid was then carried out between a storage vessel and the detachable tube several times (A and B in figure 9), discarding the first and last 10 % at each cycle. The acid was finally frozen out in the storage vessel and maintained at -196°C when not in use.

(b) Krypton.

99-100 % Krypton with balance Xenon was supplied by the British Oxygen Co. in break seal bulbs. The bulb was glass blown to the gas handling line via a liquid nitrogen trap, so that the pressure of krypton could be reduced to $<$ 3mm Hg for ease of handling during surface area measurements.

(c) Helium.

Mineral helium was admitted through a charcoal trap at a rate not exceeding 30 ml/ min. The charcoal was first activated by baking the trap at 300 °C overnight with continual pumping. The system was isolated from the pumps, and if the pressure in the system was $<$ 1×10^{-5} mm Hg, as measured on a McLeod gauge, the trap was cooled in liquid nitrogen and helium admitted. The gas was stored in a 2 litre bulb.

(d) Hydrogen, Carbon Monoxide and Carbon Dioxide.

These gases were used for surface adsorption experiments. Hydrogen and carbon monoxide were simply expanded into the system from a cylinder through a liquid nitrogen trap and stored in a 2 litre bulb. Carbon dioxide was obtained by placing a small quantity of drikold in a detachable tube and connecting it to the gas handling line. The tube was cooled in liquid nitrogen and evacuated. Vacuum distillation of the gas was then carried out between two detachable vessels several times in the usual manner.

Thereafter, it was finally stored in a detachable tube at -196°C. Since, in many instances, ultra high purity was not necessary these preparations were considered sufficiently good.

(e) Water.

A small quantity of distilled water was introduced into the gas handling line and distilled in a manner analogous to that adopted for formic acid. The purified water was stored in a detachable tube and kept at -196°C when not in use.

Fig 9

Static Reaction System

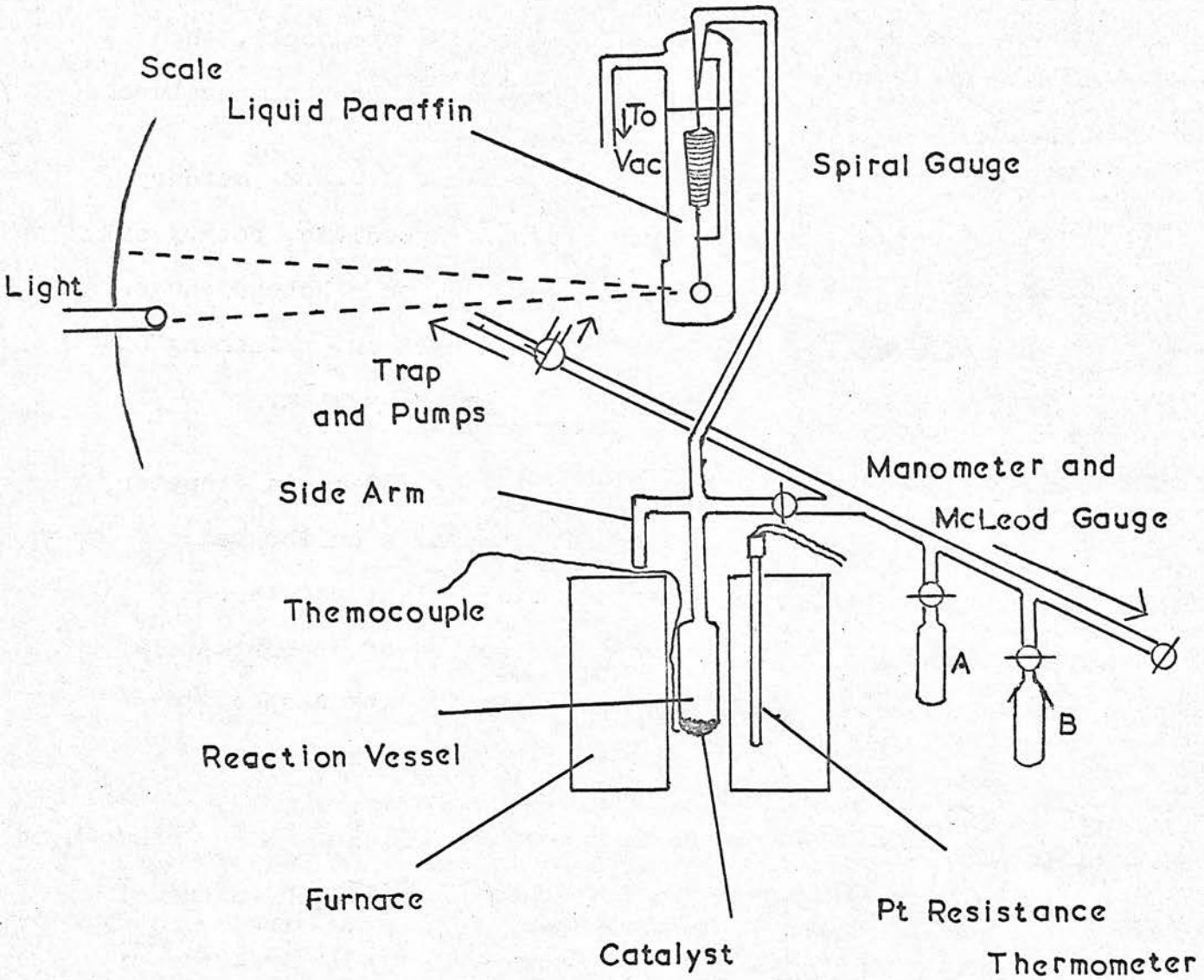

Reaction System for Kinetic Measurements.

Figure 9 shows the static system used for kinetic experiments. The whole system was constructed of 'Pyrex' glass, 'Apiezon' L or T greases being used to lubricate all joints and stopcocks, the latter grease more especially for regions above room temperature.

The pumping system consisted of an Edwards G.M.2. mercury diffusion pump backed by a Edwards E.D.35., speedivac, rotary oil pump and gave pressures less than 10^{-5} mm Hg, on a McLeod gauge. Two liquid nitrogen traps were used to minimise any poisoning of the catalysts by mercury vapours present in the system.

The reaction vessel was a vertical tube, 30 mm in diameter and 37 ml volume and was connected directly to a calibrated glass spiral pressure gauge equipped with a light pointer. A pressure change of 1 mm Hg giving a deflection of approximately 5 mm on the scale. This deflection was linear with respect to pressure over the range of pressures used in the kinetics measurements.

The reaction vessel temperature was controlled by means of an electric furnace and electronic controller to within $\pm$ 0.2°C. By a system of counter weights and pulleys, the furnace could be easily raised or lowered round the reaction vessel.

Temperatures were measured with a thermocouple of Driver Harris T_1/ T_2 alloy calibrated against a standard thermocouple.

Thermocouple voltages were measured on a 'Cropico' type P3 potentiometer which enabled temperature changes of $\pm$ 0.2°C to be measured. Ice water was used for the cold junctions of the thermocouple.

Procedure for Decomposition Experiments.

Identical procedures were adopted for all catalysts. When the reaction vessel containing a known weight (~ 2gm) of catalyst had reached the desired temperature, formic acid was allowed to enter the reaction vessel to an initial pressure of 25-30 mm Hg. As soon as the system had been isolated, the initial pressure was read on the spiral gauge and the stopclock started. Pressure readings were recorded at 15 second intervals during the first minute, and 30 second intervals thereafter. With all samples pressure/ time curves were linear after the first two or three minutes indicating zero order kinetics. The extent of this linear relationship was found to increase from ~7 %, for the lowest members of the series to ~30 %, of the total reaction, for the highest members of the series. Thereafter, the rate of pressure increase gradually diminished. At low reaction temperatures a pressure decrease was observed during the first minute or two due to adsorption of the reactant. All catalysts were found to undergo an "Activation Process" in formic acid. The activity, initially low, increased to a stable maximum after about two decomposition runs. Reaction rates quoted in the results section, apply exclusively to measurements in the zero order region. The reproducibility of reaction rates was within ± 5 %. All catalsts were outgassed between runs for a minimum of 3 hours at 470-500°C and 10^{-5} mm Hg pressure. If at any time the pressure was greater than this, a slight falling off in the activity of the catalyst

was noticed. For reference purposes 'normal conditions' shall refer to the adsorption of a reaction sequence similar to that outlined above. Blank runs in the absence of catalyst showed that the 'Pyrex' reaction vessel did not catalyse the decomposition below 270°C. Blake and Hinshelwood (105) have shown that homogeneous decomposition of formic acid does not take place under these experimental conditions below 400°C. The results reported clearly relate only to bronze catalysed reactions.

As a further guide to the reaction, the effect of the presence of the individual product gases on the reaction rate was investigated. In addition, adsorption experiments were carried out by expanding a known volume of either carbon dioxide, carbon monoxide, hydrogen or water at a known pressure into the reaction system, all pressures being measured accurately with the aid of the spiral gauge, the decrease in pressure providing a measure of the amount adsorbed.

Finally the effect of pretreatment in oxygen on the reaction rate was investigated. The procedure adopted involved exposure to oxygen ($\sim$150 mm Hg) for a period of approximately 12 hours at temperatures ($>$ 350°C), arbitarily chosen for individual catalysts from measurements of the change in resistance with time in the presence of oxygen ($\sim$150 mm Hg).

Investigation of the Water-Gas Shift Reaction.

Known mixtures of known partial pressures of CO_2 and H_2, and

similarly CO and H_2O were expanded into the reaction vessel and maintained at between 180-230°C for a minimum of 3 hours. The individual component pressures were then analysed by freezing, according to the procedure outlined in the sub-section headed 'Product Analysis by Pressure Measurements'.

All reaction rates were corrected for the dimerisation of formic acid which occurs below 110°C. This was to allow for the fact that approximately 25 % of the reaction system, namely the capilliary linkage to the spiral gauge, was always maintained at room temperature.

In all cases, activation energy plots of log rate/ 1/ T were constructed from the study of the decomposition reaction at a minimum of six different temperatures, usually at 5°C intervals.

The Analysis of Reaction Products.

Mass Spectrometric Analysis.

The product mixtures were analysed using an AEI MS 10 mass spectrometer. Carbon monoxide and carbon dioxide samples were run individually to obtain their standard cracking patterns. The peaks in the spectra were then expressed as percentages of the parent peaks at mass 28 and mass 44 respectively. The spectra overlap at mass 28, so that, using the data from the individual spectra, the relative contributions of carbon monoxide and carbon dioxide to the mass 28 peak could be separated, when an unknown mixture of the two gases was analysed.

To calibrate the spectrometer, to take account of sensitivity variations for different gases, synthetic mixtures of hydrogen together with carbon monoxide and carbon dioxide were made up using a combination of a gas burette and Toepler pump.

Mass spectra were obtained for a series of such mixtures of known partial pressure ratio. After correction for background and the overlap at mass 28, the ratio of the peak height at mass 44 to the corrected peak height at mass 28 was measured and plotted against the ratio of the corresponding partial pressures. The resultant straight line was used to determine a sensitivity factor S defined as:

$$S = \frac{p(CO_2)}{p(CO)} \cdot \frac{h(CO)}{h(CO_2)}$$

where h denotes the corrected peak height. A similar S value was determined for a plot of hydrogen/ carbon dioxide ratios, so that the (CO_2/ CO) and (CO_2/ H_2) ratios could be determined from the ratio of the corresponding peak heights.

Direct product analyses were achieved by constructing a reaction set-up similar to that adopted for the study of the kinetics of the decomposition reaction. The reaction vessel was fitted with a capillary leak which allowed $\leq 1\%$ per hour of the reaction mixture to leak continuously into the mass spectrometer. It was then possible to make a detailed continuous study of the reaction products without stopping the reaction. Formic acid and water were frozen out from the products before the latter were admitted to the spectrometer by interposing a U-tube, filled with glass beads and maintained at -110 °C with a propanol/ liquid nitrogen freezing mixture, between the capillary leak and the inlet port of the spectrometer. To provide a comparision with analysis results from pressure measurements (see below), reactions in some experiments were stopped by cooling the reaction vessel with a drikold/ acetone freezing mixture at -78 °C before the products were leaked to the mass spectrometer.

The results showed that, for all catalysts studied, the pressure of hydrogen was very much less than the corresponding pressure of carbon dioxide, with this anomaly being maintained throughout the complete reaction cycle. A comparision of the

product ratios obtained from reactions frozen at drikold temperatures with those recorded immediately before terminating the reaction, provided conclusive proof for the physical adsorption of carbon dioxide on the catalyst during freezing at -78°C.

Analysis by Pressure Measurements.

Analyses were carried out using pressure data to supplement mass spectrometric analyses. This method was found to be rapid and convenient.

After decomposition had been allowed to proceed for the desired percentage conversion, the furnace was removed and the reaction vessel cooled rapidly in a drikold/ acetone freezing mixture. When the system had come to equilibrium, with the drikold/ acetone bath set at a fixed level, the pressure in the system was measured using the glass spiral gauge. The reaction vessel was then allowed to warm to room temperature and the pressure again noted. Finally the side arm of the reaction vessel (figure 9) was immersed to a fixed level in liquid nitrogen, and the pressure recorded. Since a temperature gradient existed in the system, a calibration was necessary. Helium was admitted to the system to a pressure of up to 100 mm Hg and the pressure in the system noted at room temperature, drikold temperature and liquid nitrogen temperatures in turn. This was repeated for different initial pressures of helium and calibration plots drawn of pressure at room temperature against pressure observed at -78°C and -196°C.

The pressures of the non-condensible gases in the product mixtures at -78°C were converted, with the calibration plots to pressures at room temperature, denoted P_{RT}, and similarly the pressures at -196°C.

Hence

P_{RT} (CO + H_2 + CO_2) = Pressure observed at -78°C after correction to room temperature.

P_{RT} (CO + H_2) = Pressure observed at -196°C after correction to room temperature.

Therefore P_{RT} (CO_2) = P_{RT} (CO + H_2 + CO_2) - P_{RT} (CO + H_2) and so P_{RT}(CO_2) could be determined.

From comparision with pCO_2/ pH_2 ratios obtained from mass spectrometric studies of reactions terminated by freezing at drikold temperatures, after a similar percentage conversion, it was possible to assign a value to P_{RT}(H_2) so that P_{RT}(CO) and hence the CO_2/CO ratio could be determined.

To obtain complete ageement with analyses carried out on the mass spectrometer, it was necessary to correct for the adsorption of carbon dioxide at -78°C. This was found to vary according to the pressure of carbon dioxide present in the system and to the surface area of individual catalysts. Adsorption experiments carried out with different initial pressures of carbon dioxide

indicated that this preferential adsorption of carbon dioxide became critical only for those higher members of the series which favoured the dehydrogenation reaction. In cases suitable corrections were applied, bringing pressure results in line with those obtained from mass spectrometric analyses.

Product analysis by pressure measurements were also carried out on catalysts which had been exposed to oxygen and on synthetic mixtures of CO_2 and H_2, and CO and H_2O according to the procedure outlined in the previous section.

Results of Rate Measurements.

Zero order reaction rate constants were measured from the slope of the pressure/ time curves obtained for each catalyst at a number of temperatures. Typical pressure/ time curves are shown in graphs 1, 2, 3 and 4 for bronzes of x = 0.73, 0.60, 0.38 and 0.16 respectively (Tables 6-9). The rates were then expressed in units of molecules per ~~optimum~~ reaction site per sec.

A certain amount of doubt existed over what in fact should constitute an actual reaction site. For convenience, and as a consequence of the similarity of crystal structure in going through the series, it was decided to adopt, as an arbitrary site, the face of the cubic or distorted cubic unit cell of the bronzes. On an average the cell edge is $\sim$3.80°A, so that each face occupied an area of 14.4°A^2, and there were $\sim 7.0 \times 10^{18}$ faces for each metre^2 of surface.

To obtain a more accurate picture of the actual area (or number of faces) associated with individual molecules of formic acid, adsorption experiments were carried out on each catalyst. These were carried out at temperatures for individual catalysts at which the reaction rate was finite but very slow, and the procedure was in every way identical to that adopted to check for product adsorption.

Knowledge of the area and number of molecules adsorbed thus enabled the area and hence the number of faces per molecule of

formic acid to be calculated, the results of which are shown in Table 5.

With the exception of H_2O, which was found to retard the reaction, the addition of the individual product gases was found to have a negligible effect on the rate of reaction. Furthermore, none of the product gases were adsorbed appreciably at reaction temperatures.

In addition oxygen pretreatment resulted in an irreversible change in the rate of reaction for catalysts with $x > 0.11$. However, with WO_3 and $Na_{0.11}WO_3$ the original rate was recovered upon renewed exposure to formic acid.

Tables, numbers 6a-9a inclusive, give the values of log rate constant and $10^3/T$ used in the Arrhenius plots shown in graphs 1a-4a. Two sets of log rate constant are quoted for each catalyst, one in units of molecules of formic acid per sec per cube face area and the other in units of molecules per sec per adsorption site area.

The activation energies in K. joules. $mole^{-1}$ and the logarithm of the frequency factor log A, where A is in molecules $site^{-1}$ sec^{-1} were calculated, in the majority of cases without having to use the method of least squares.

Table 5

x value	Area/mol. HCOOH $^{o}A^{2}$	No. of cube faces/ mol. HCOOH	No. of mols. of HCOOH/cube face
0	25.9 44.6*	1.8 3.1*	0.56 0.32
0.11	63.3 83.5*	4.4 5.8*	0.23 0.17
0.16	51.8	3.6	0.28
0.28	37.4	2.6	0.38
0.38	57.5	4.0	0.25
0.52	50.4	3.5	0.29
0.60	46.0	3.2	0.31
0.66	18.7	1.2	0.83
0.73	24.5	1.7	0.59
0.77	25.9	1.8	0.56
0.81	33.1	2.3	0.44
0.85	36.0	2.5	0.40

*Denotes measurements on catalysts subjected to oxygen pretreatment.

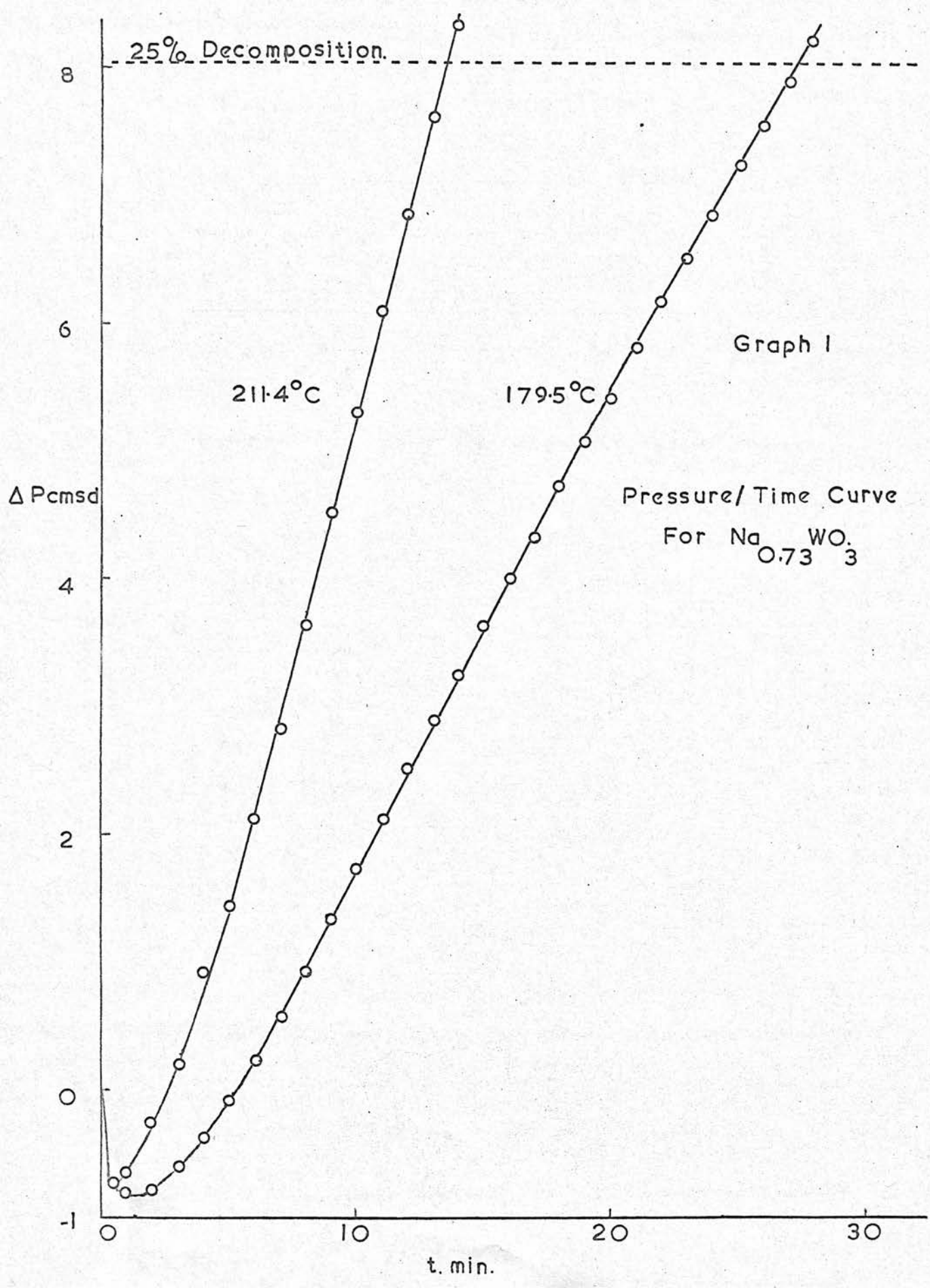
25% Decomposition.
8
6
4
2
0
-1
ΔPcmsd
211·4°C
179·5°C
Graph I
Pressure/Time Curve
For $Na_{0.73}WO_3$
0
10
20
30
t. min.

Table 6

Examples of Pressure-Time Plots

Catalyst $Na_{0.73}WO_3$. Runs 3 and 14 at 211.4° C and 179.5° C respectively.

t. mins.	Δ p cm. s.d.	
	run 3	run 14
0	0	0
0.25	-0.65	-0.53
0.5	-0.71	-0.67
0.75	-0.67	-0.75
1	-0.63	-0.78
2	-0.45	-0.76
3	0.25	-0.58
4	0.94	-0.36
5	1.45	-0.06
6	2.13	0.24
7	2.85	0.59
8	3.65	0.95
9	4.53	1.35
10	5.32	1.75
11	6.11	2.15
12	6.86	2.54
13	7.65	2.92
14	8.35	3.26
15	9.02	3.64
16		4.02
17		4.36
18		4.76
19		5.10
20		5.45
21		5.85
22		6.19
23		6.53
24		6.88
25		7.24
26		7.55
27		8.24

Graph 1a.

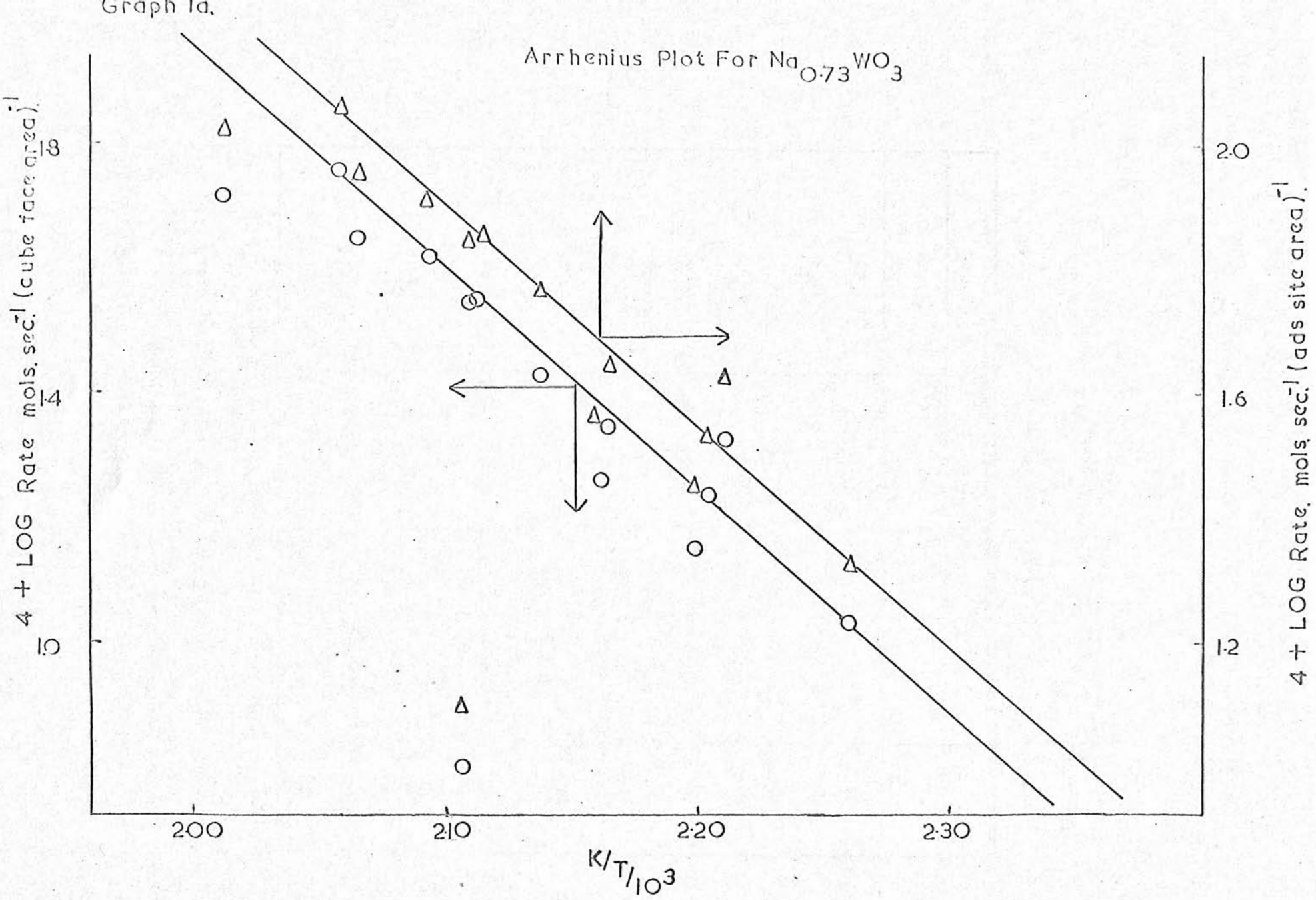
Arrhenius Plot For $Na_{0.73}WO_3$
4 + LOG Rate mols. sec.$^{-1}$ (cube face area)$^{-1}$
4 + LOG Rate. mols sec.$^{-1}$ (ads site area)$^{-1}$
1·8
1·4
1·0
2·0
1·6
1·2
2·00
2·10
2·20
2·30
K/T/10^3

Table 6a

$Na_{0.73}WO_3$

$K/T/10^3$	Run No.	4 + log Rate	
		mols. sec^{-1} (cubic face area)$^{-1}$	mols. sec^{-1} (ads. site area)$^{-1}$
2.260	11	1.15	1.45
2.210	10	1.32	1.62
2.203	14	1.02	1.32
2.198	5	1.15	1.45
2.165	12	1.34	1.64
2.161	4	1.25	1.55
2.137	7	1.42	1.72
2.113	13	1.55	1.85
2.110	6	1.54	1.84
2.107	1	0.80	1.10
2.092	8	1.61	1.91
2.065	3	1.65	1.95
2.058	9	1.76	2.06
2.012	2	1.72	2.02

$E = 68.7 \pm 3.5$ K. joules. $mole^{-1}$

$\log A = 9.2 \pm 0.8$ (9.5 $\pm$ 0.8 for 'ads. site area' plot).

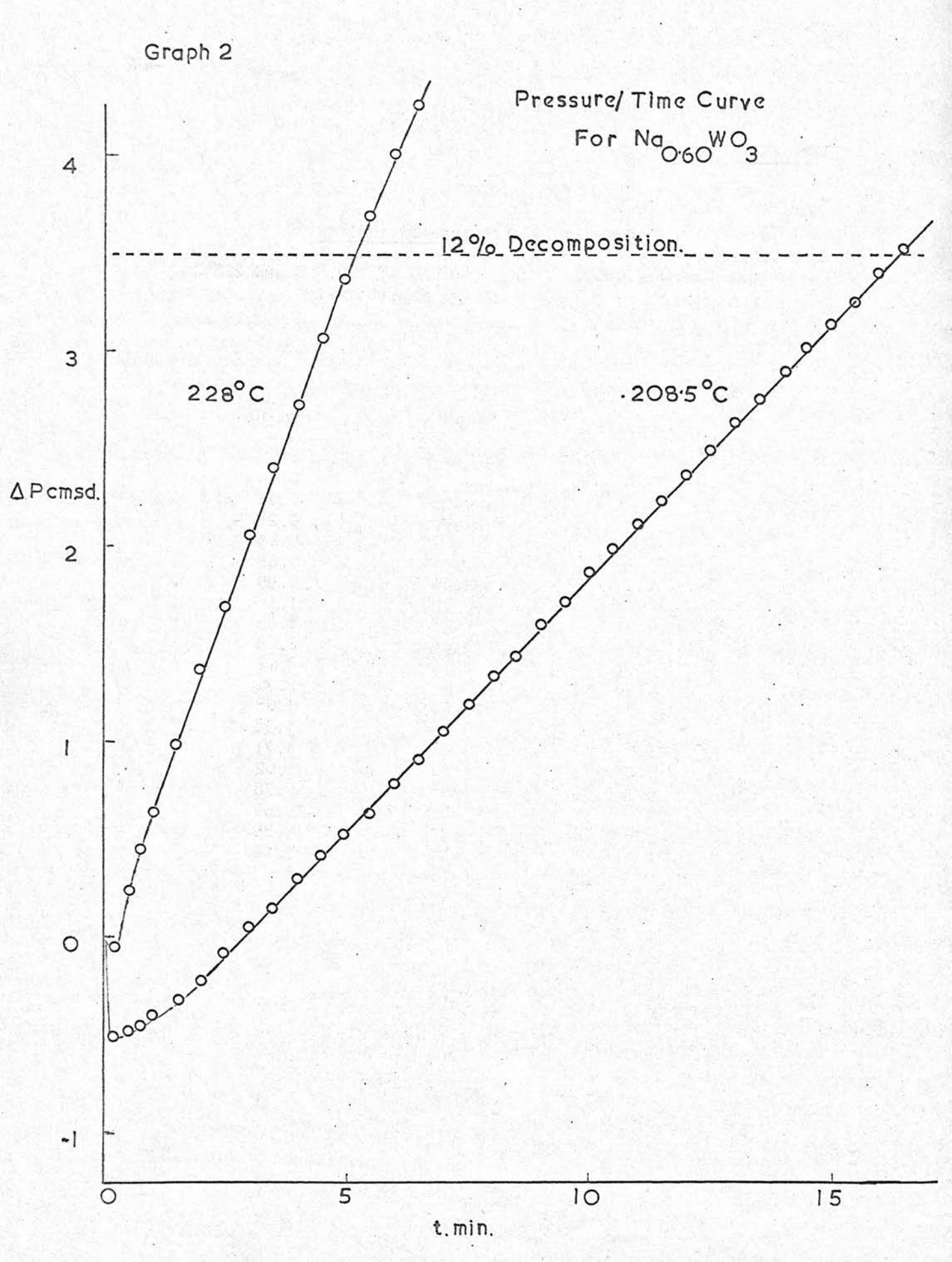
Graph 2
Pressure/ Time Curve
For $Na_{0.60}WO_3$
12% Decomposition.
228°C
208·5°C
ΔP cmsd.
4
3
2
1
0
-1
0
5
10
15
t. min.

Table 7

Examples of Pressure-Time Plots

Catalyst $Na_{0.6}WO_3$. Runs 3 and 10 at 208.5°C and 228°C respectively.

t. mins.	Δp cm. s.d.	
	Run 3	Run 10
0	0	0
0.25	-0.50	-0.05
0.5	-0.47	0.25
0.25	-0.45	0.45
1	-0.41	0.65
1.5	-0.33	0.99
2	-0.22	1.38
2.5	-0.05	1.69
3	0.05	2.08
3.5	0.16	2.42
4	0.31	2.74
4.5	0.43	3.08
5	0.53	3.38
5.5	0.66	3.71
6	0.80	4.02
6.5	0.93	4.28
7	1.07	4.59
7.5	1.21	4.85
8	1.35	5.12
8.5	1.45	
9	1.60	
9.5	1.73	
10	1.87	
11	2.13	
12	2.35	
13	2.65	
14	2.91	
15	3.15	
16	3.42	
17	3.65	

Graph 2a

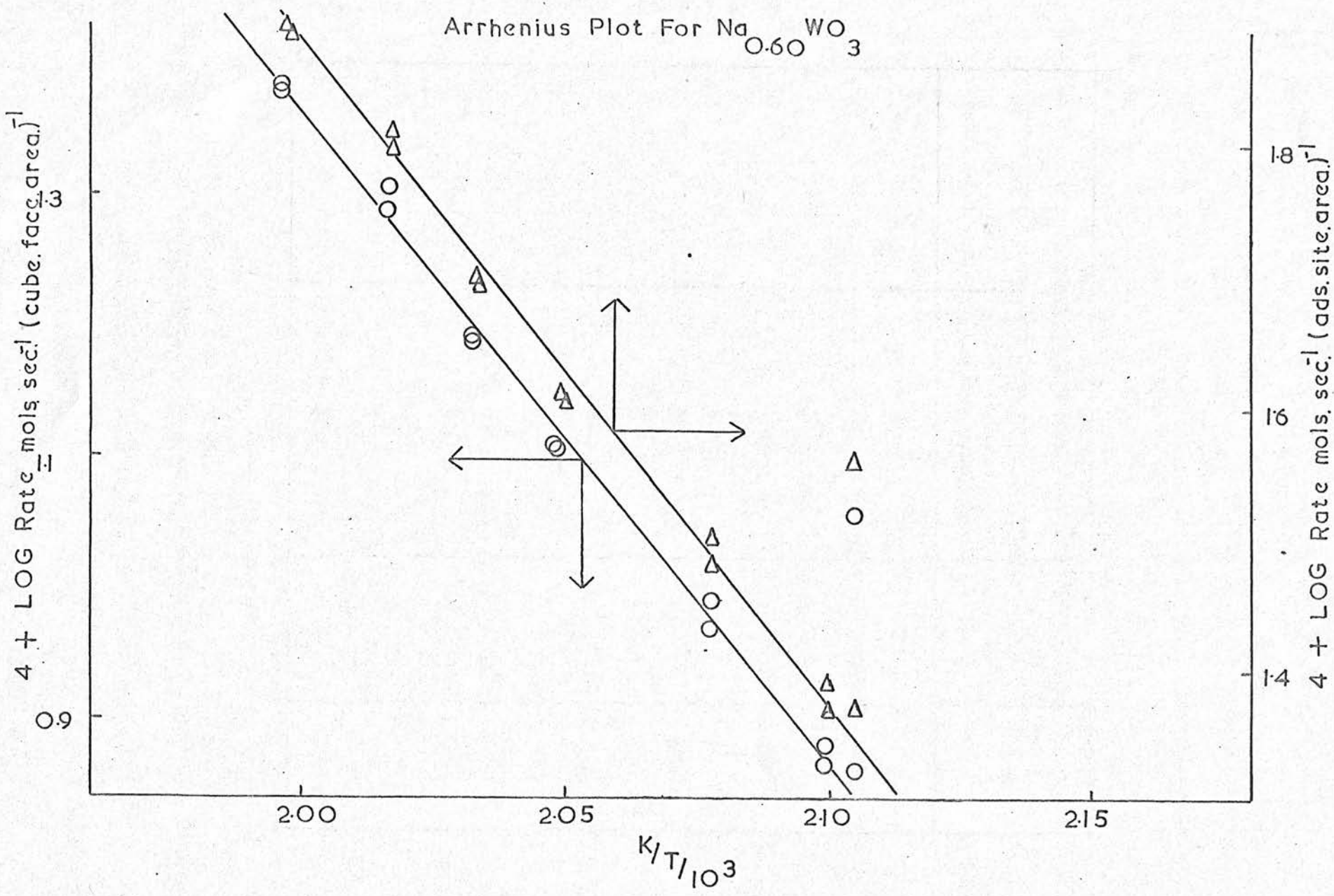
Arrhenius Plot For $Na_{0.60}WO_3$
4 + LOG Rate mols. sec.$^{-1}$ (cube. face. area.)$^{-1}$
4 + LOG Rate mols. sec.$^{-1}$ (ads. site. area.)$^{-1}$
0.9
1.3
1.4
1.6
1.8
2.00
2.05
2.10
2.15
$K/T/10^3$

Table 7a

$Na_{0.60}WO_3$

$K/T/10^3$	Run No.	4 + log Rate	
		mols. sec^{-1} (cubic face area)$^{-1}$	mols. sec^{-1} (ads. site area)$^{-1}$
2.104	1	0.86	1.37
2.104	2	1.06	1.56
2.099	13	0.88	1.39
2.099	14	0.86	1.37
2.077	3	0.99	1.50
2.077	4	0.97	1.48
2.048	5	1.11	1.61
2.048	6	1.11	1.61
2.032	7	1.19	1.70
2.032	8	1.19	1.70
2.016	11	1.31	1.81
2.016	12	1.29	1.80
1.996	9	1.38	1.44
1.996	10	1.38	1.89

$E = 95 \pm 5$ K. joules. $mole^{-1}$

$\log A = 11.3 \pm 0.8$ (11.8 ± 0.8 for 'ads. site area' plot)

Graph 3

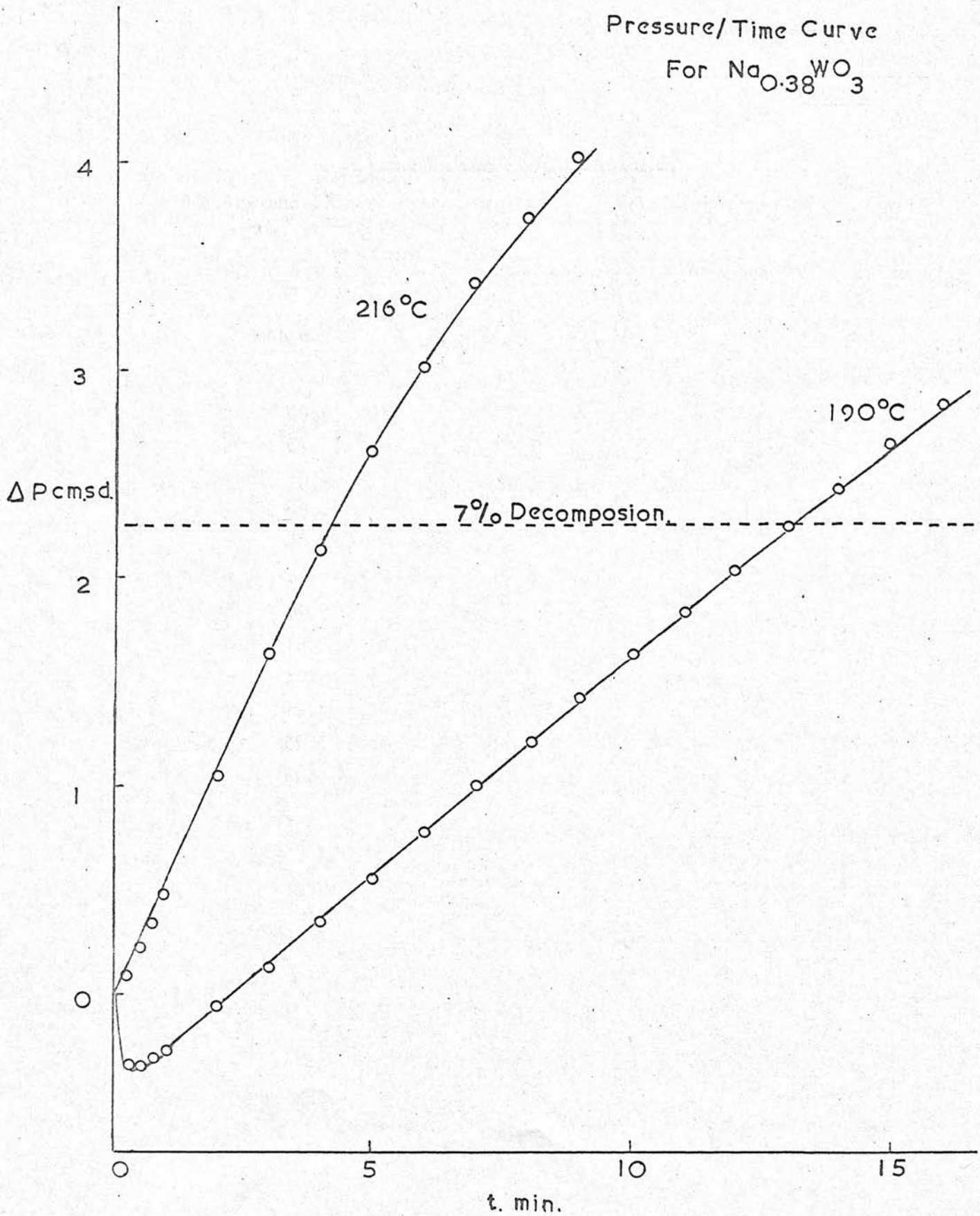
Pressure/Time Curve
For $Na_{0.38}WO_3$
216°C
190°C
7% Decomposion.
ΔPcmsd.
0
1
2
3
4
0
5
10
15
t. min.

Table 8

Examples of Pressure-Time Plots

Catalyst $Na_{0.38}WO_3$. Runs 1 and 13 at 190.8°C and 216.5°C respectively.

t. mins.	Δp cm. s.d.	
	run 1	run 13
0	0	0
0.25	-0.32	0.05
0.5	-0.32	0.23
0.75	-0.29	0.35
1	-0.25	0.48
2	-0.06	1.06
3	0.14	1.64
4	0.35	2.14
5	0.56	2.61
6	0.78	3.01
7	1.00	3.41
8	1.22	3.73
9	1.44	4.02
10	1.64	
11	1.84	
12	2.04	
13	2.24	
14	2.43	
15	2.64	
16	2.82	
17	3.01	

Graph 3a

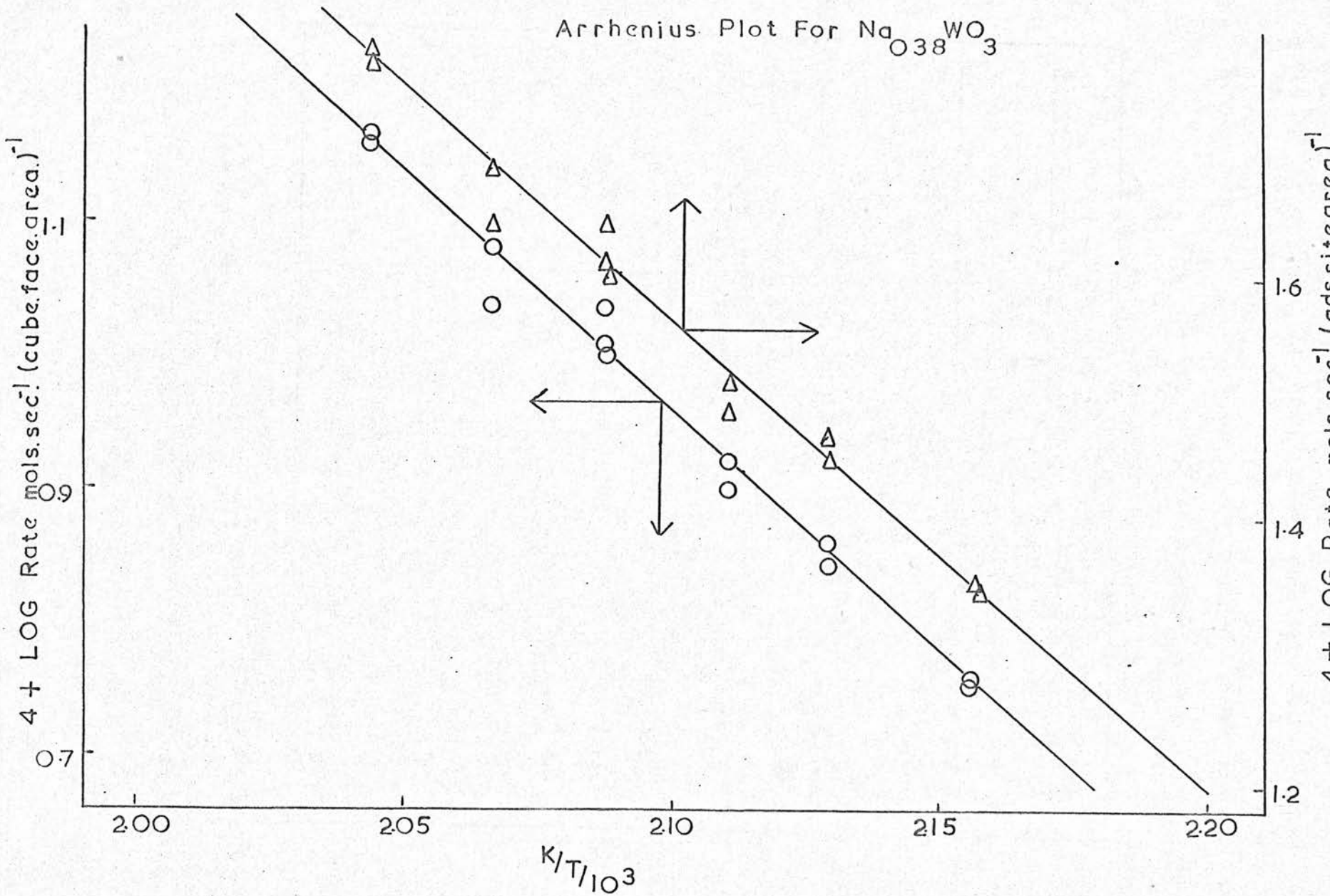
Arrhenius Plot For $Na_{0.38}WO_3$
4 + LOG Rate mols.sec.$^{-1}$ (cube.face.area.)$^{-1}$
1·1
0·9
0·7
4 + LOG Rate mols.sec.$^{-1}$ (ads.site.area.)$^{-1}$
1·6
1·4
1·2
2·00
2·05
2·10
2·15
2·20
K/T/10^3

Table 8a

$Na_{0.38}WO_3$

$K/T/10^3$	Run No.	4 + log Rate	
		mols. sec^{-1} (cubic face area)$^{-1}$	mols. sec^{-1} (ads. site area)$^{-1}$
2.156	1	0.75	1.35
2.156	2	0.78	1.38
2.129	5	0.84	1.44
2.129	6	0.86	1.46
2.110	7	0.90	1.50
2.110	8	0.92	1.52
2.087	3	1.04	1.64
2.087	4	1.00	1.60
2.087	9	1.01	1.61
2.066	10	1.08	1.68
2.066	11	1.08	1.68
2.066	12	1.04	1.64
2.043	13	1.16	1.76
2.043	14	1.17	1.77

$E = 68.8 \pm 7.1$ K. joules. $mole^{-1}$

$\log A = 8.5 \pm 0.3$ (9.1 ± 0.3 for 'ads. site area' plot)

Graph 4

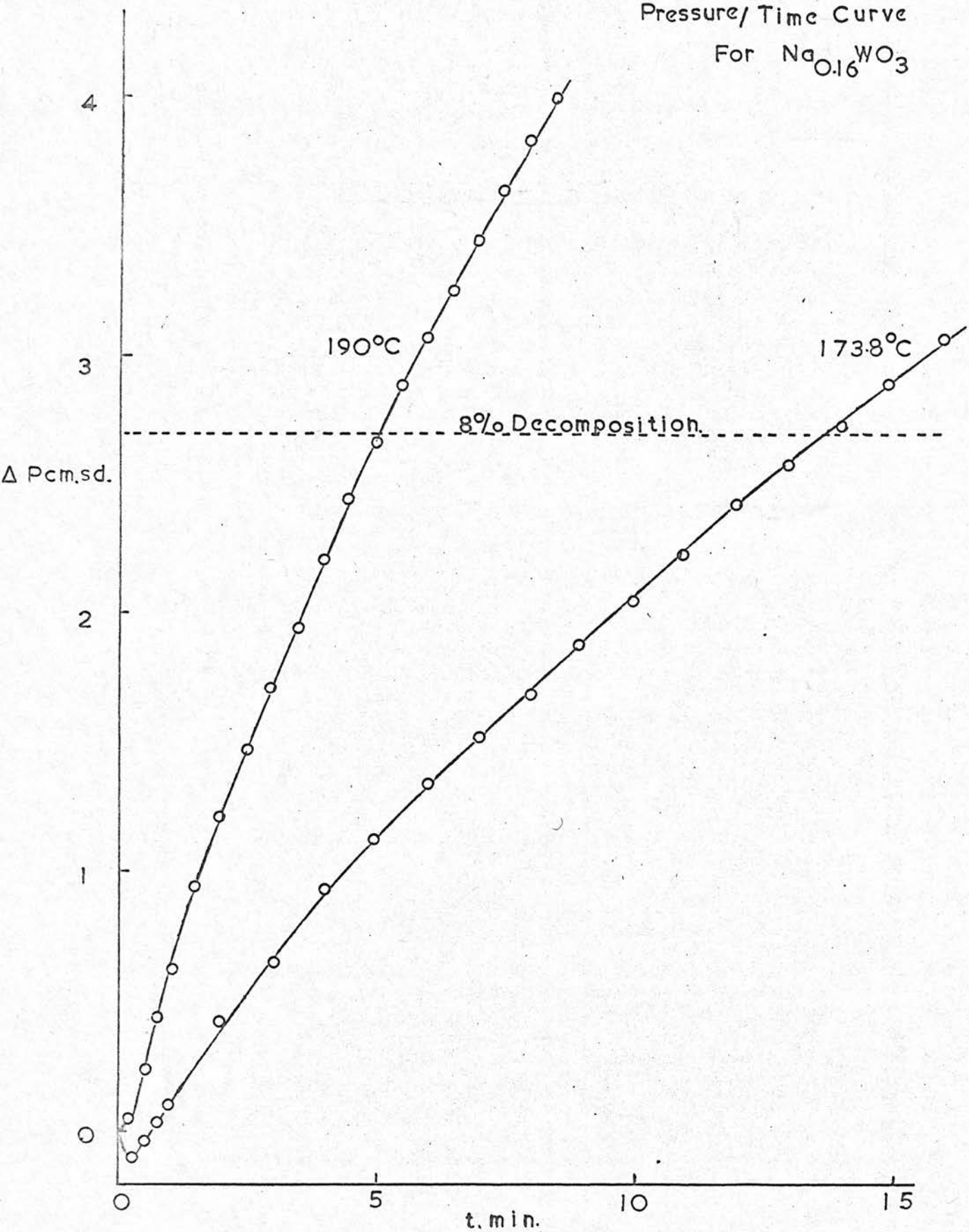
Pressure/ Time Curve
For $Na_{0.16}WO_3$
190°C
173.8°C
8% Decomposition
Δ Pcm.sd.
0
1
2
3
4
0
5
10
15
t. min.

Table 9

Examples of Pressure-Time Plots

Catalyst $Na_{0.18}WO_3$. Runs 6 and 12 at 173.8°C and 190°C respectively.

t. mins.	Δ p cm. s.d.	
	run 6	run 12
0	0	0
0.25	-0.10	0.05
0.15	-0.03	0.25
0.75	0.05	0.45
1	0.12	0.63
2	0.43	1.21
3	0.66	1.72
4	0.93	2.22
5	1.13	2.67
6	1.35	3.08
7	1.53	3.45
8	1.70	3.84
9	1.89	
10	2.06	
11	2.24	
12	2.43	
13	2.58	
14	2.74	
15	2.90	
16	3.07	
17	3.22	
18	3.35	

Graph 4a

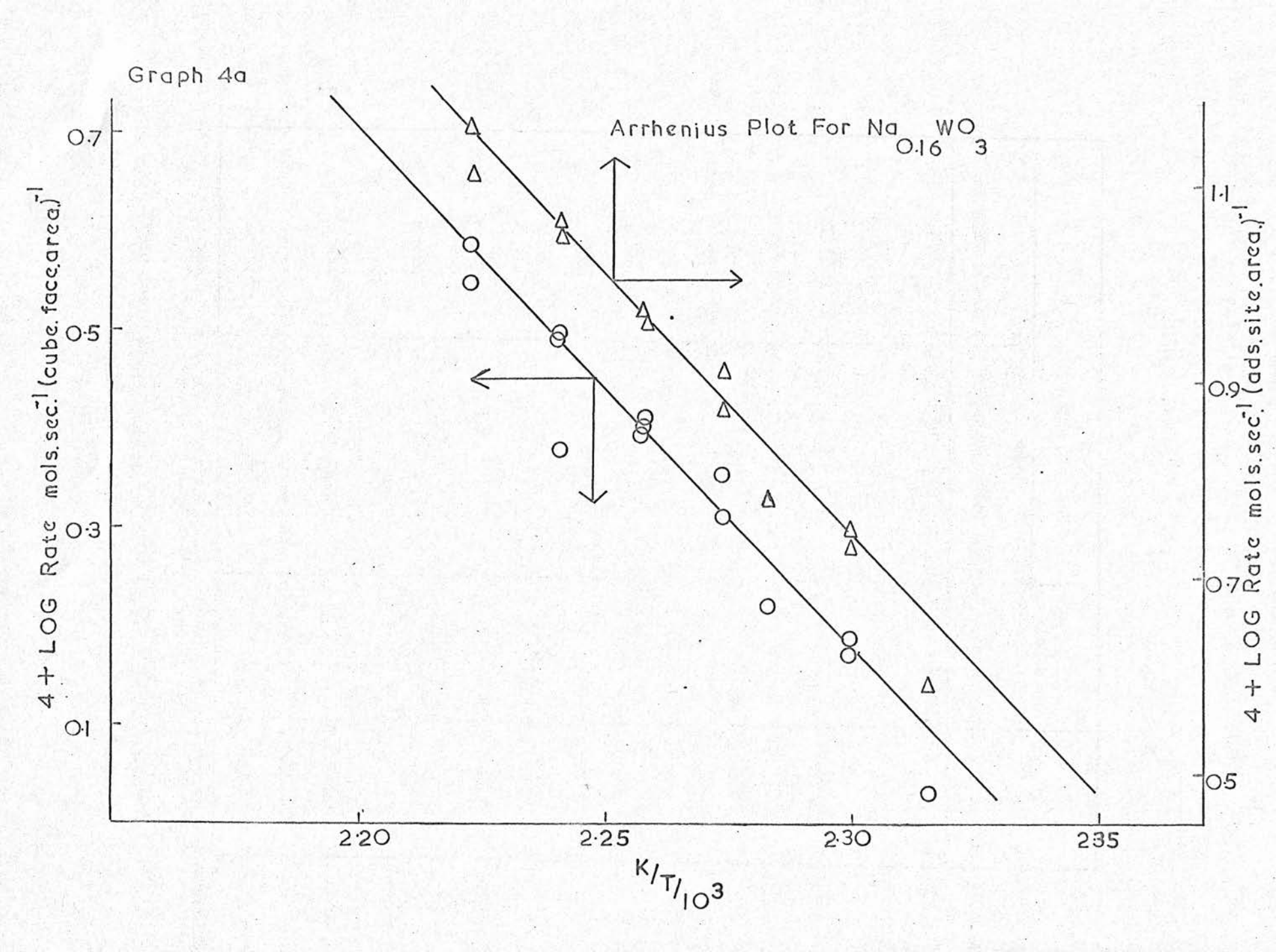
Arrhenius Plot For Na0.16WO3
0.7
0.5
0.3
0.1
4 + LOG Rate mols.sec.-1 (cube.face.area.)-1
1.1
0.9
0.7
0.5
4 + LOG Rate mols.sec.-1 (ads.site.area.)-1
2·20
2·25
2·30
2·35
K/T/10³

Table 9a

$Na_{0.16}WO_3$

$K/T/_{10^3}$	Run No.	4 + log Rate	
		mols. sec^{-1} (cubic face area)$^{-1}$	mols. sec^{-1} (ads. site area)$^{-1}$
2.315	16	0.03	0.59
2.315	7	0.03	0.59
2.299	8	0.19	0.75
2.299	9	0.17	0.73
2.282	4	0.22	0.78
2.282	5	0.22	0.78
2.273	10	0.31	0.87
2.273	11	0.35	0.91
2.257	15	0.41	0.97
2.257	16	0.40	0.96
2.257	17	0.40	0.96
2.240	1	0.38	0.94
2.240	2	0.50	1.06
2.240	3	0.49	1.05
2.222	12	0.70	1.26
2.222	13	0.55	1.11
2.222	14	0.59	1.15

$E = 102 \pm 7$ K. joules. $mole.^{-1}$

$\log A = 12.4 \pm 1.7$ (13.0 $\pm$ 1.8 for 'ads site area' plot)

Results of Product Analysis.

Tables 10, 11, 12 and 13 give values of the relative peak heights of carbon monoxide, carbon dioxide and hydrogen together with CO_2/CO and CO_2/H_2 ratios, calculated by the procedure given above, as a function of time for catalysts, x = 0.16, 0.38, 0.66 and 0.73 at 165°C, 202°C, 204°C and 167°C respectively, as shown in graphs 5(a-c), 6(a-c), 7(a-c) and 8(a-c).

Results of product analysis by mass spectrometric analysis and by pressure measurements are given in Tables 14 and 15 respectively. Initial product ratios represent analyses made at less than 10 % of total decomposition, whereas final product ratios represent analyses made when the reaction rate was virtually zero.

In practically all cases (within the limits of experimental error), the CO_2/CO ratio was found to be independent of temperature for a given catalyst at a given % decomposition. (see Table 14). The ratio was, however, dependent on percentage reaction and for a given set of conditions varied from one catalyst to another. In the majority of cases , an increase in CO_2/CO ratio with extent of reaction was observed. The lack of evidence for the presence of the water-gas shift reaction clearly supports the view that this variation in CO_2/CO ratio is a property characteristic of the bronzes. The fact that the CO_2/H_2 ratios are "anomalous" in that their values are not unity, together with the variation

with % decomposition, indicates that varying quantities of hydrogen are retained by the catalyst.

Graph 5a

Relative Peak Heights Of CO, CO_2 & H_2, For $Na_{0.16}WO_3$

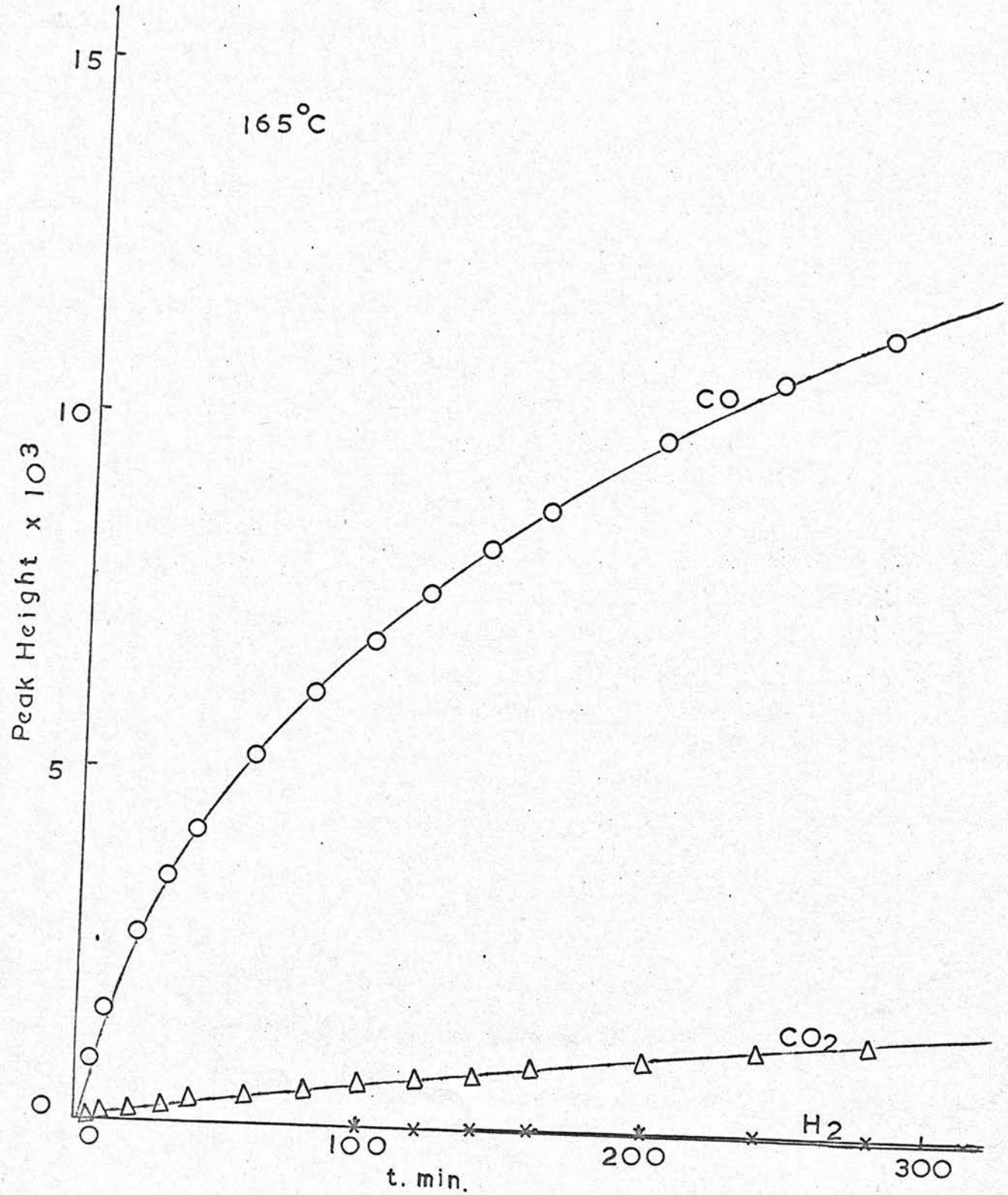

Graph 5b.

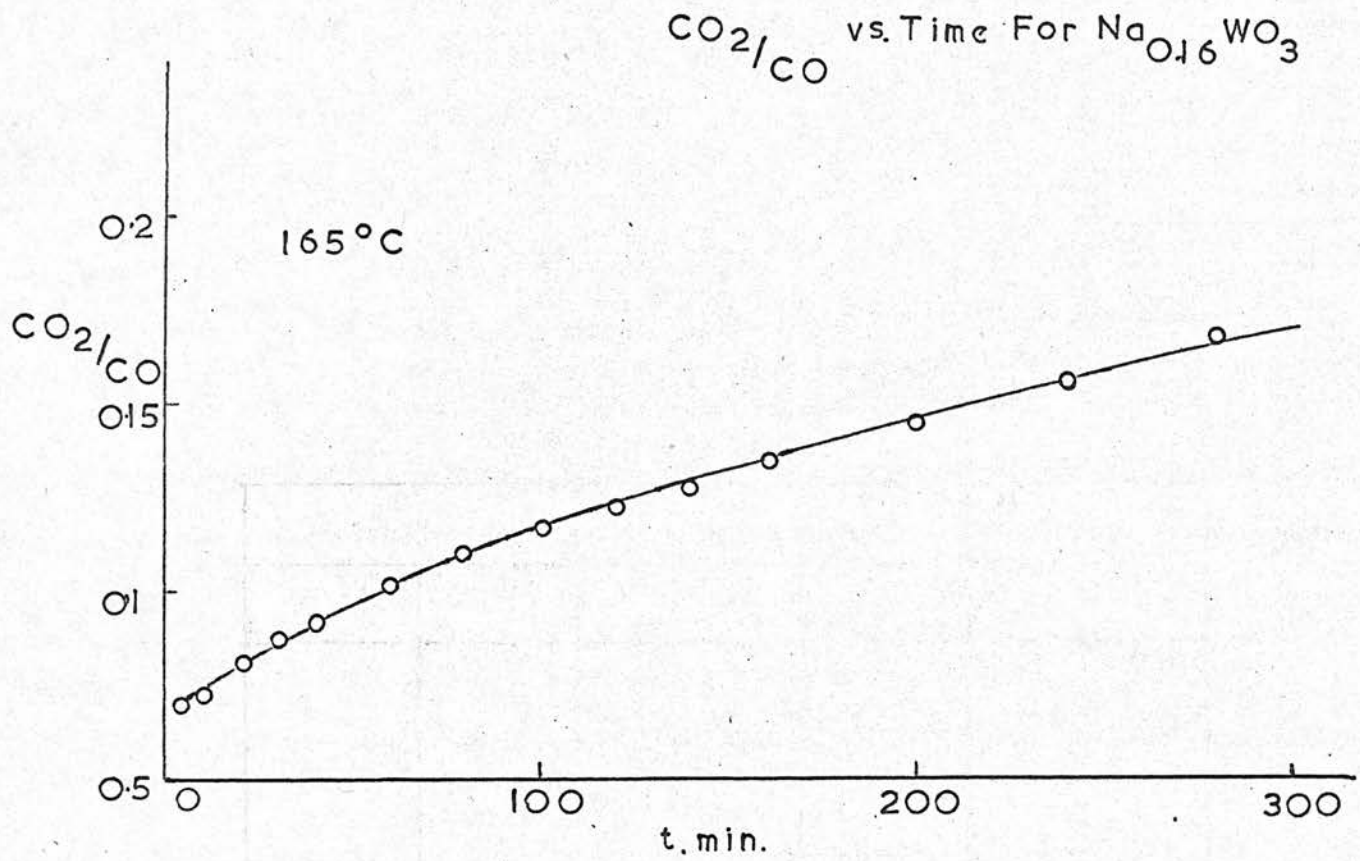

Graph 5c

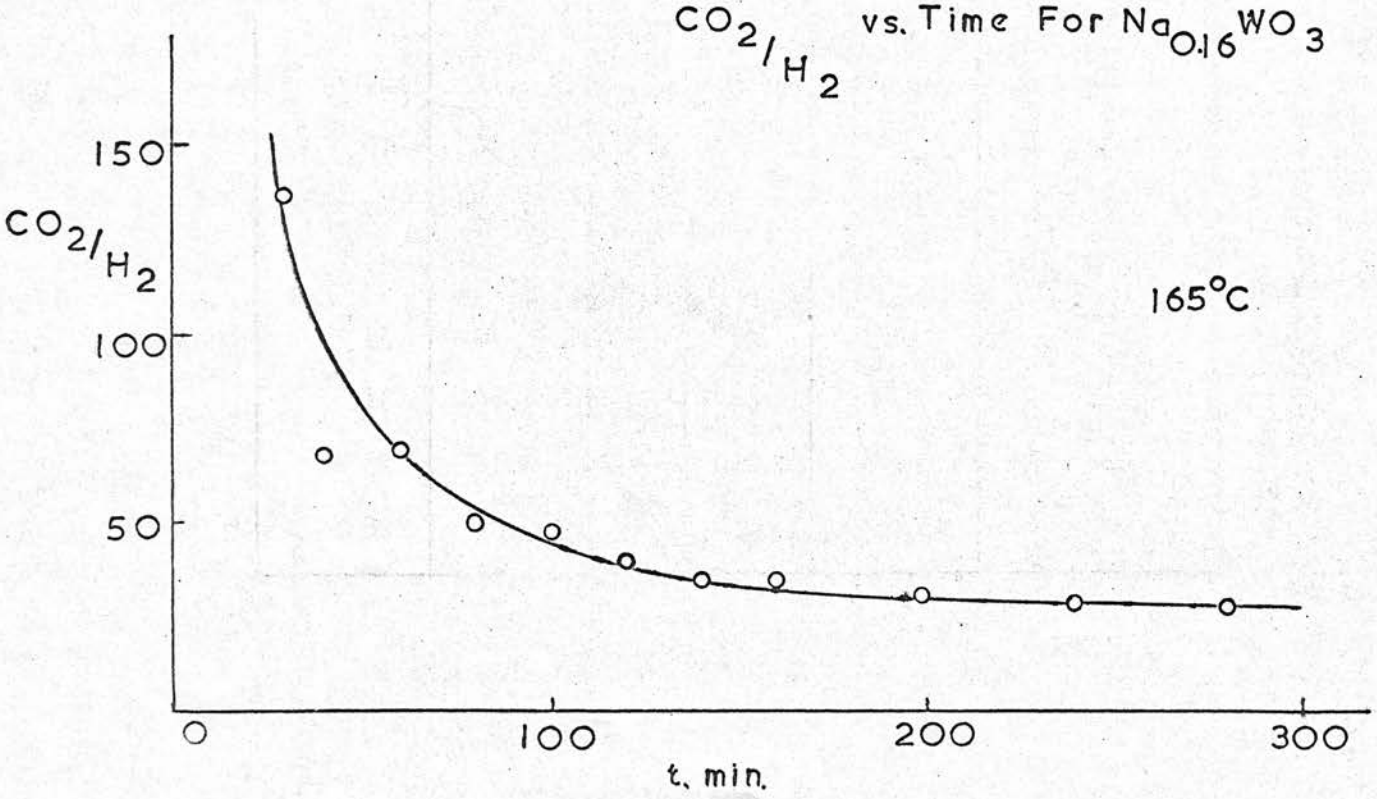

Table 10

Product Ratios for $Na_{0.16}WO_3$

t. mins.	Peak Height			Molar Ratios	
	CO	CO_2	H_2	CO_2/CO	CO_2/H_2
5	860	45	0	0.07	∞
10	1,580	87	0	0.07	∞
20	2,650	162	0	0.08	∞
30	3,500	230	2	0.09	100
40	4,150	288	5	0.09	69
60	5,230	400	7	0.10	69
80	6,090	503	12	0.11	50
100	6,870	603	15	0.12	48
120	7,550	700	21	0.12	40
140	8,220	794	27	0.13	35
160	8,800	890	31	0.14	35
200	9,850	1,070	42	0.15	31
240	10,680	1,250	52	0.16	29
280	11,370	1,430	62	0.17	28

Graph 6a

Relative Peak Heights Of CO, CO_2 & H_2, For $Na_{0.38}WO_3$.

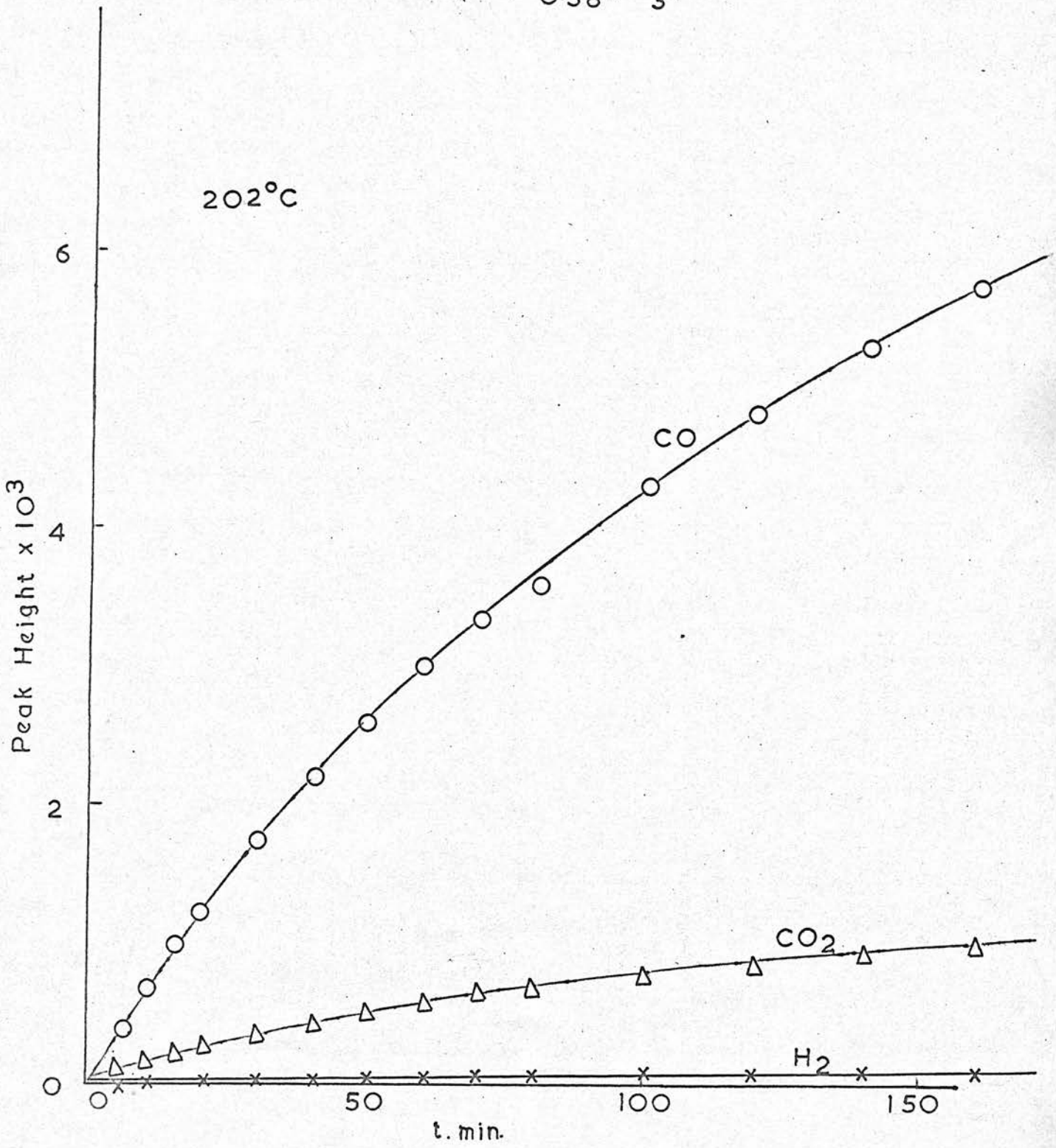

Graph 6b

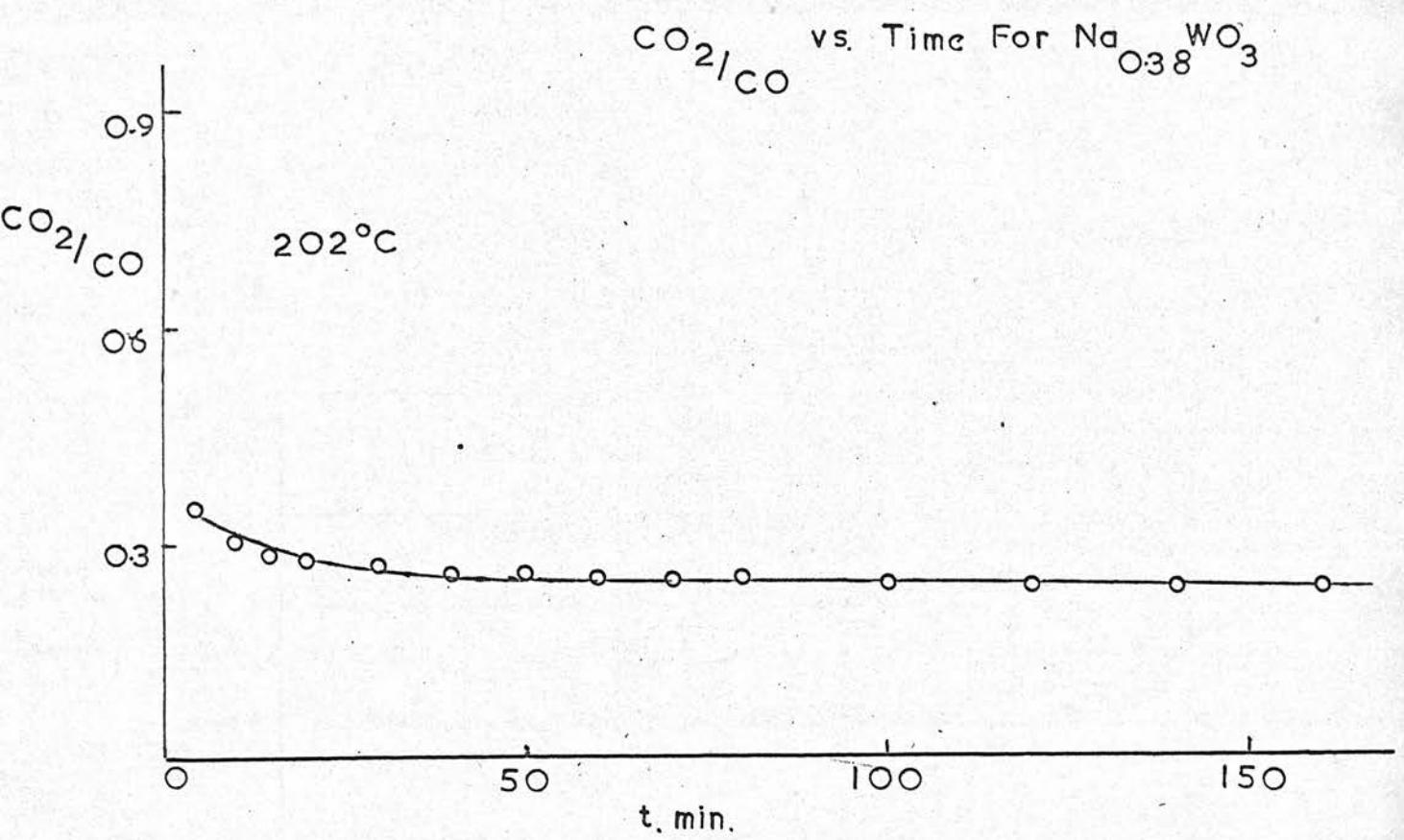

Graph 6c

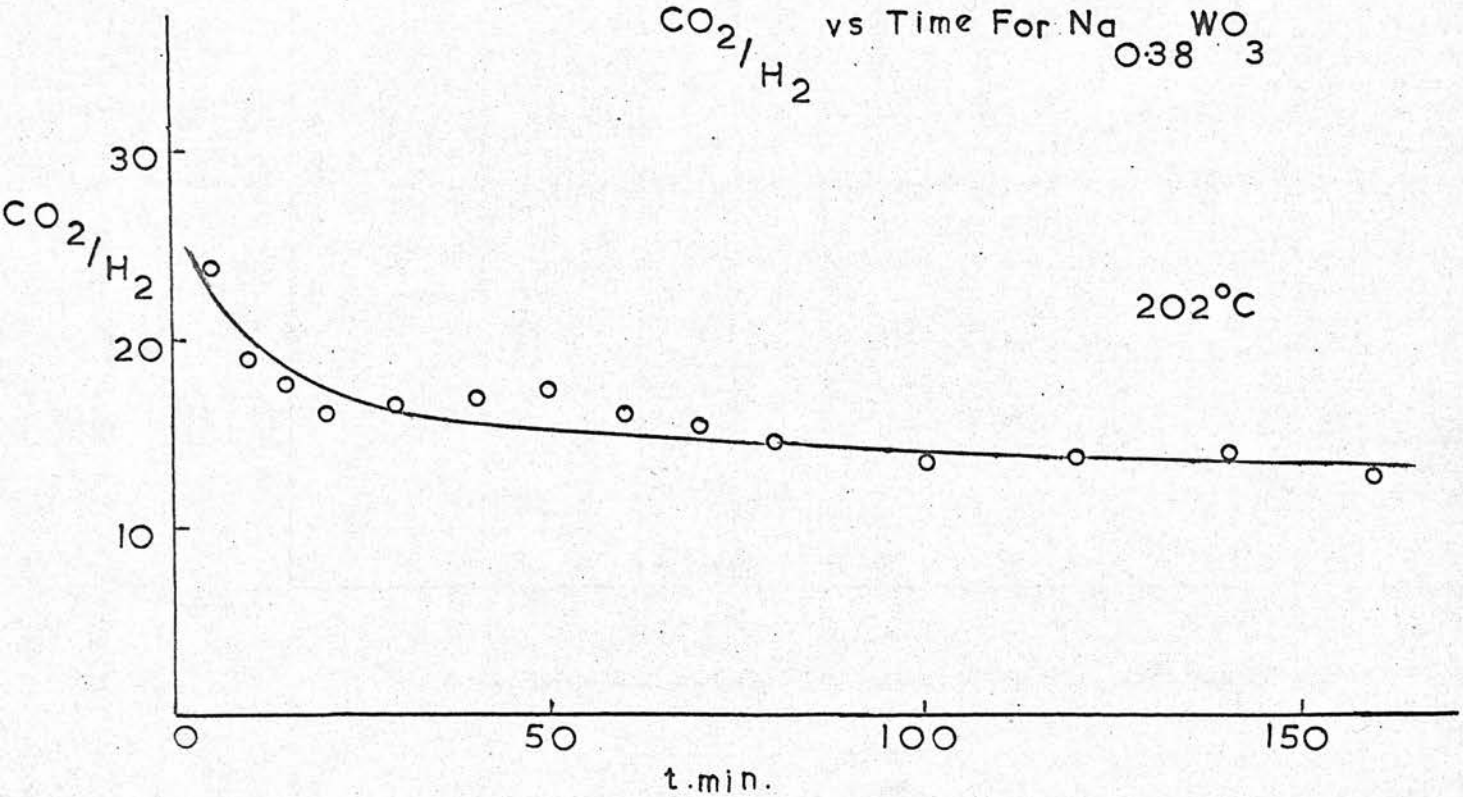

Table 11

Product Ratios for $Na_{0.38}WO_3$

t. mins.	Peak Height			Molar Ratios	
	CO	CO_2	H_2	CO_2/CO	CO_2/H_2
5	400	100	5	0.35	24
10	700	160	10	0.31	19
15	990	210	14	0.28	18
20	1,240	260	19	0.28	17
30	1,740	350	25	0.27	17
40	2,200	430	30	0.26	17
50	2,610	510	35	0.26	18
60	3,010	570	42	0.25	16
70	3,370	640	49	0.25	16
80	3,610	690	56	0.26	15
100	4,320	780	69	0.24	14
120	4,870	870	76	0.24	14
140	5,340	950	81	0.24	14
160	5,790	1,030	97	0.24	13

Graph 7a

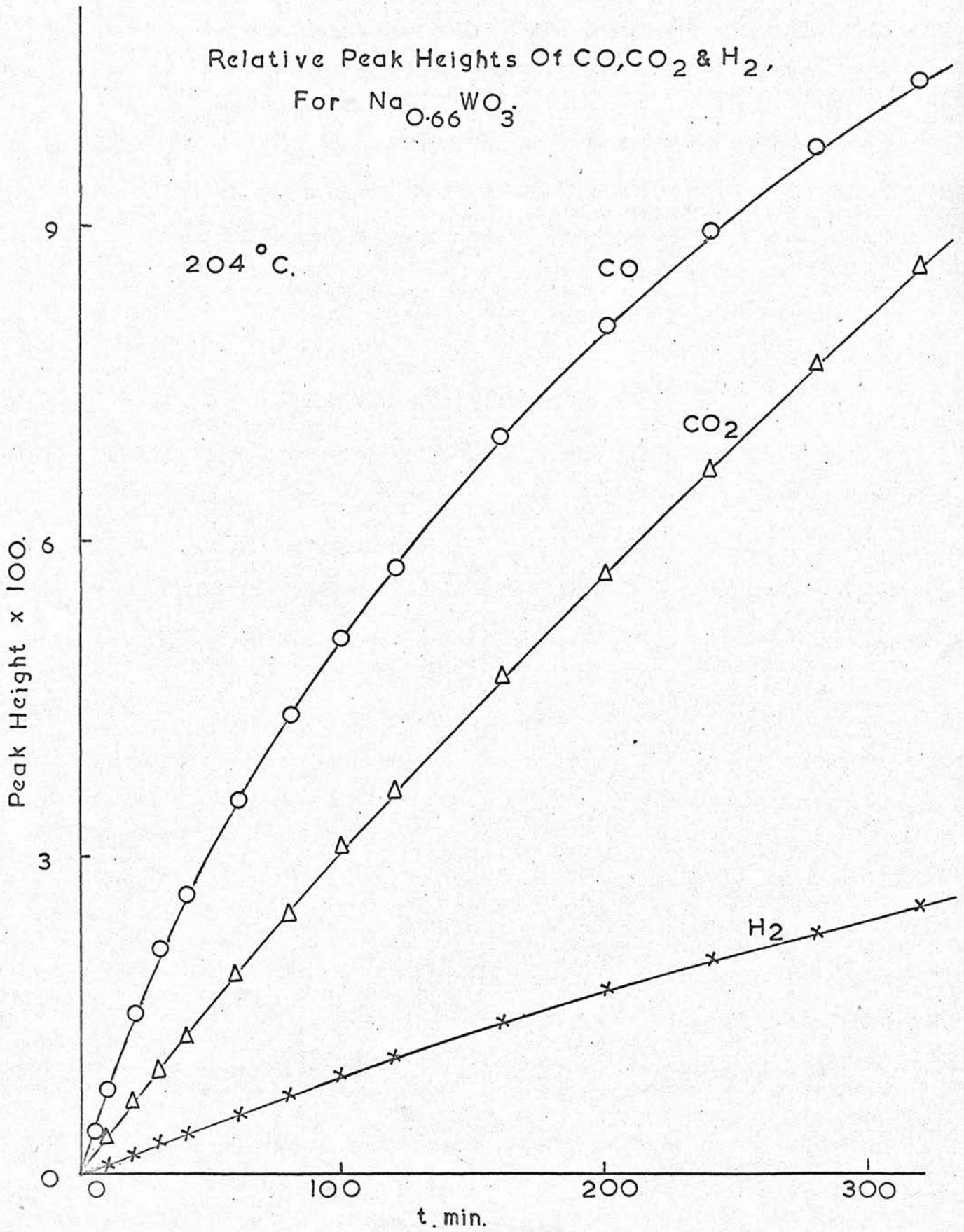
Relative Peak Heights Of CO, CO_2 & H_2.
For $Na_{0.66}WO_3$.
204 °C.
CO
CO_2
H_2
Peak Height x 100.
0
3
6
9
0
100
200
300
t. min.

Graph 7b

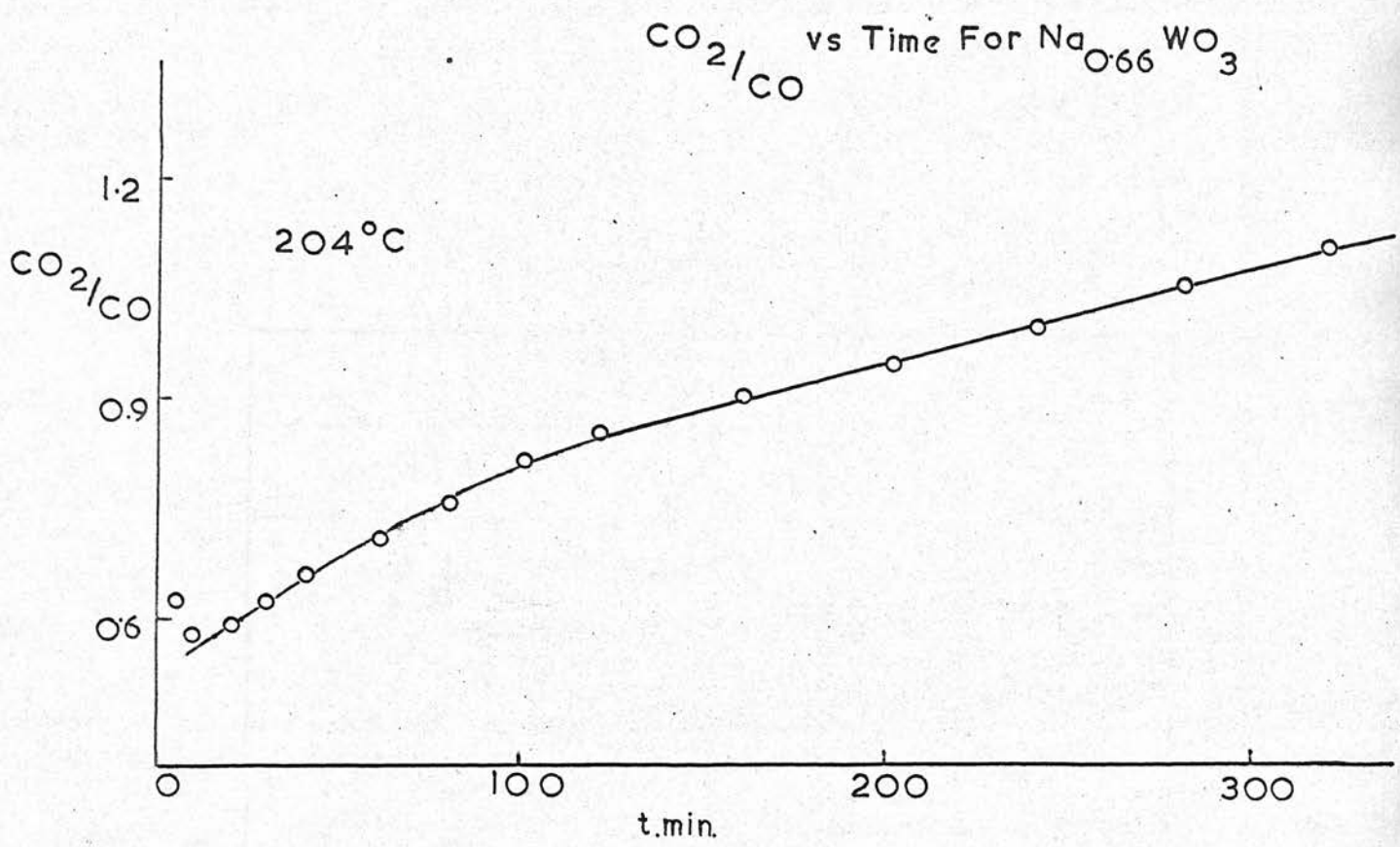

Graph 7c

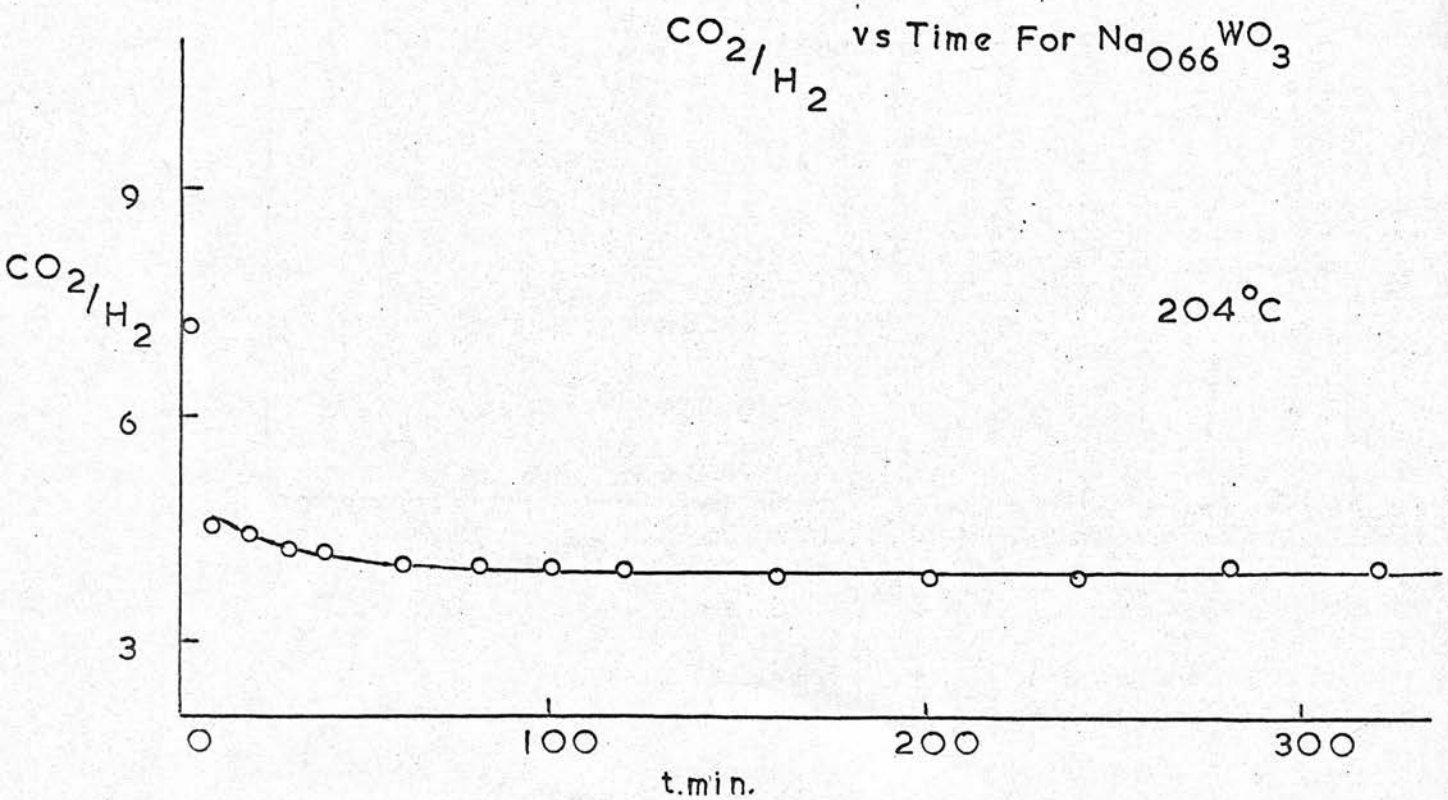

Table 12

Product Ratios for $Na_{0.66}WO_3$

t. mins.	Peak Heights			Molar Ratios	
	CO	CO_2	H_2	CO_2/CO	CO_2/H_2
5	39	18	3	0.62	7.2
10	79	34	9	0.58	4.5
20	153	67	18	0.58	4.5
30	213	99	28	0.62	4.2
40	264	129	37	0.65	4.2
60	357	189	56	0.71	4.0
80	437	248	74	0.76	4.0
100	511	310	93	0.81	4.0
120	576	367	111	0.85	4.0
160	700	473	145	0.91	3.9
200	805	571	176	0.95	3.9
240	987	669	205	1.00	3.9
280	975	767	230	1.06	4.0
320	1,038	864	255	1.12	4.1

Graph 8a

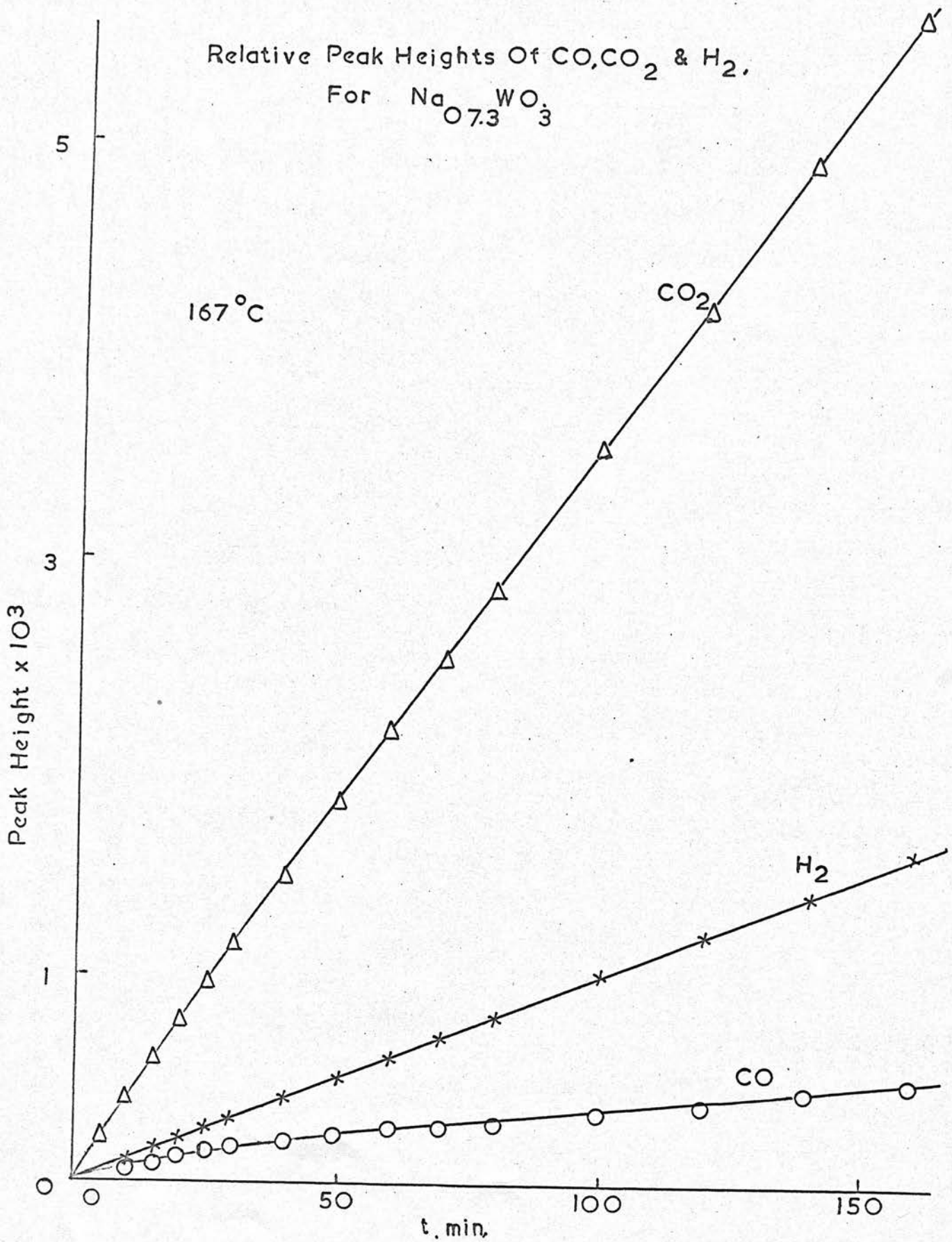
Relative Peak Heights Of CO, CO_2 & H_2.
For $Na_{0.7.3}WO_3$
167 °C
CO_2
H_2
CO
Peak Height x 10³
0
1
3
5
0
50
100
150
t. min.

Graph 8b

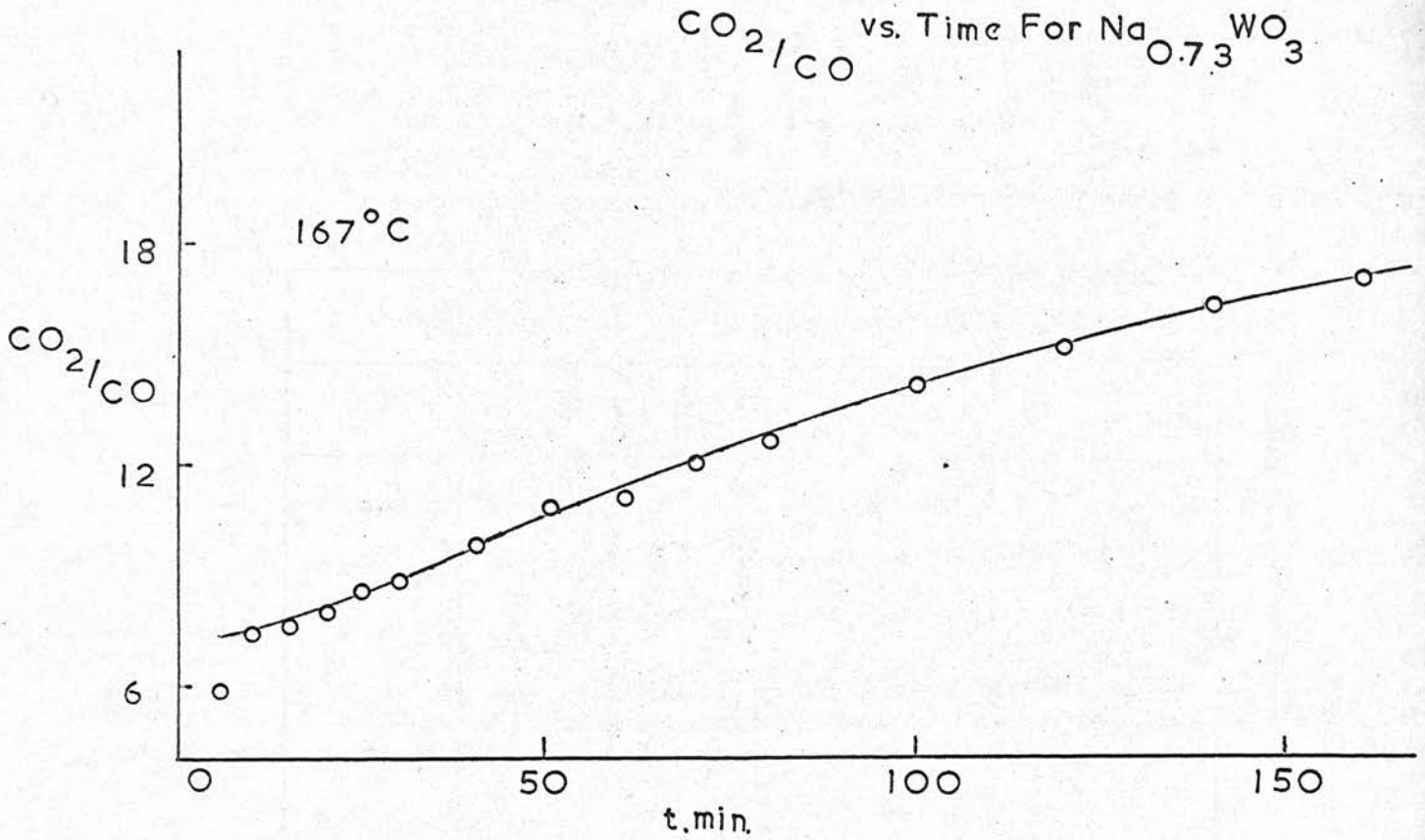

Graph 8c

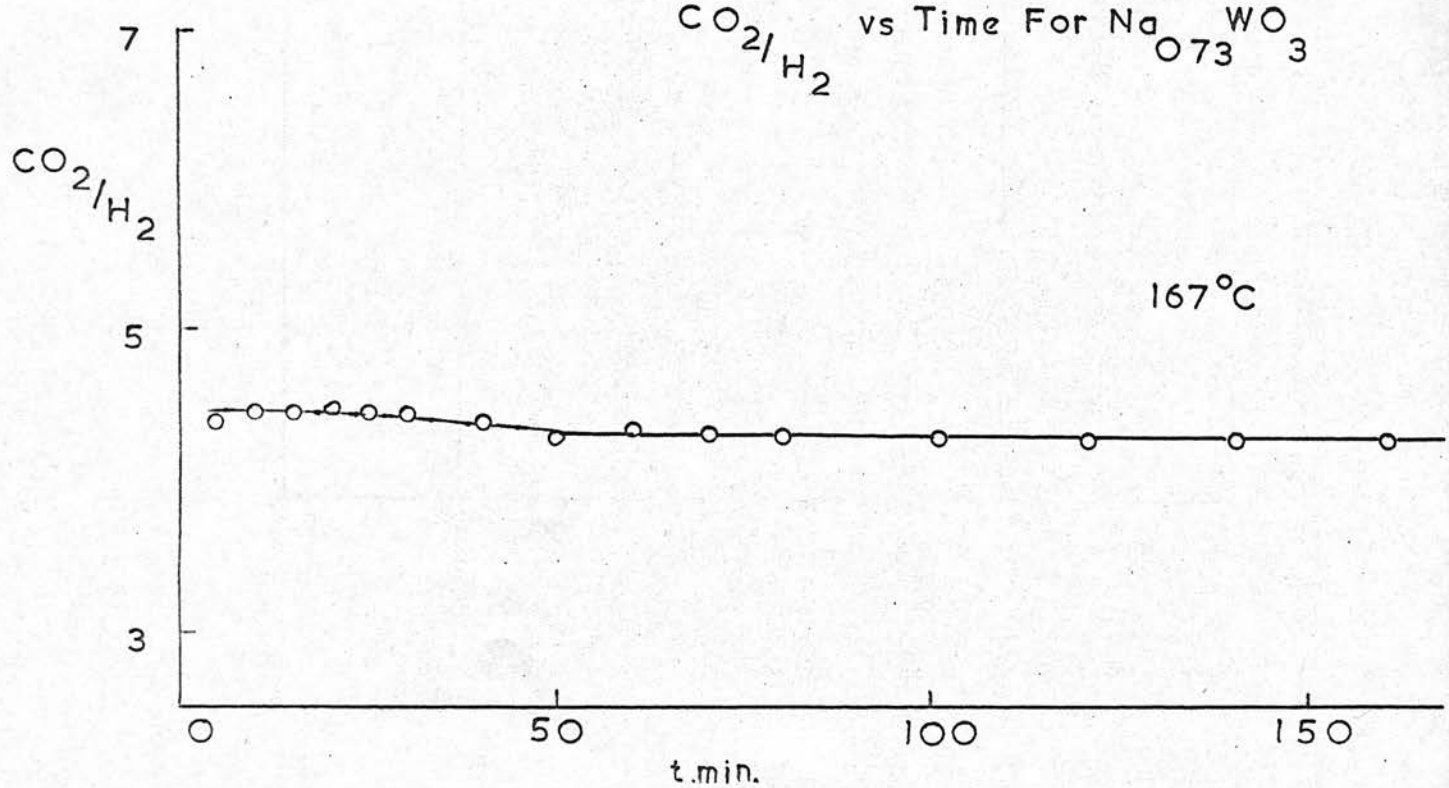

Table 13

Product Ratios for $Na_{0.7}WO_3$

t. mins.	Peak Heights			Molar Ratios	
	CO	CO_2	H_2	CO_2/CO	CO_2/H_2
5	50	220	60	5.9	4.4
10	73	410	110	7.5	4.5
15	103	590	160	7.7	4.4
20	130	780	210	8.0	4.5
25	150	960	260	8.6	4.4
30	173	1,130	310	8.8	4.4
40	200	1,470	410	9.8	4.3
50	223	1,820	500	11	4.4
60	260	2,160	600	11	4.3
70	277	2,500	700	12	4.3
80	303	2,840	790	13	4.3
100	333	3,530	990	14	4.3
120	373	4,220	1,190	15	4.3
140	403	4,910	1,380	16	4.3
160	440	5,600	1,580	17	4.3

Table 14

Product Analysis by Mass Spectrometer Measurements

Catalyst	Temperature °C	$[CO_2/CO]$ Initial	Final	$[CO_2/H_2]$ Initial	Final
WO_3	170	0	0	∞	∞
	220	0	0	∞	∞
$Na_{0.11}WO_3$	170	0.1	0.1	∞	8
	185	0	0.1	∞	5
	195	$<$ 0.1	0.1	∞	4
$Na_{0.18}WO_3$	165	$<$ 0.1	0.2	∞	20
	202	$<$ 0.1	0.1	∞	16
$Na_{0.28}WO_3$	180	0.2	0.3	∞	28
	200	0.1	0.2	30	12
	212	0.2	0.3	60	25
$Na_{0.38}WO_3$	202	0.3	0.2	34	16
	212	0.3	0.2	28	13
	225	0.4	0.2	24	12

Table 14 (contd.)

Catalyst	Temperature °C	$[CO_2/CO]$		$[CO_2/H_2]$	
		Initial	Final	Initial	Final
$Na_{0.52}WO_3$	190	0.1	0.4	3	5
	215	0.2	0.4	2.0	3.5
	218	0.1	0.2	2.4	4
	234	0.1	0.5	6	5
$Na_{0.60}WO_3$	192	0.2	0.4	20	6
	202	0.1	0.3	∞	5
	210	0.1	0.3	9	6
$Na_{0.86}WO_3$	185	0.3	0.9	2.8	4
	204	0.6	1.3	7.2	3.5
$Na_{0.73}WO_3$	167	1.6	8	3.3	4.2
	200	4.7	10	6.3	4.7
	212	6	10	4.4	4
$Na_{0.77}WO_3$	196	0.8	1.6	4.5	4
	210	0.7	1.5	5	4
$Na_{0.81}WO_3$	173	5.3	3.8	14	5
	200	>10	4.4	40	6

Table 15

Product Analysis by Pressure Measurements

*Denotes first run

Catalyst	Temperature °C	% Reaction	$[CO_2/CO]$
WO_3	151.8	18.0	0
	156	15.3	0
	165.7*	10.2	0
	166	8.4	0
	172	11.3	0
	180.4	28	0
$Na_{0.11}WO_3$	173.8	11.9	0.2
	180	9.7	0.1
	185.2	12.4	0.2
	197.4*	12.5	0.2
	197.4	13	0.2
	210	38	0.3
$Na_{0.16}WO_3$	159	6.9	0
	159	25	0.1
	165.2	14.3	0
	165.2	28	0.1
	173.2	10.1	0
	173.2	31	0.1
	202.3*	16	0
$Na_{0.28}WO_3$	178.8	11	0
	180.2	10.2	0.2
	180.7*	10.9	0.4
	180.7	11	0.1
	186.8	11.5	0
	196.1	10.5	0
	223 *	18.8*	0.3
	223	34	0.4
	226	9.5	0.3
	234 *	32.2*	0.1
	242	31.6	0.2

Table 15 (contd.)

Catalyst	Temperature °C	% Reaction	[CO_2/CO]
$Na_{0.38}WO_3$	190.8*	9.1	0.4
	190.8	9.3	0.4
	196.5	11.1	0.3
	196.5	12	0.3
	206	39	0.3
	206	40.6	0.4
$Na_{0.52}WO_3$	188.3*	11.7	0.2
	194.7	8.9	0.1
	199.8	9.7	0.2
	202.5	9.8	0.2
	217.5	29.8	0.2
	224	45.7	0.5
	225 *	31.4	0.4
	240	29.8	0.3
	242.5	42	0.3
$Na_{0.60}WO_3$	202.2*	7	0.2
	202.2	64	0.5
	208.5	11.9	0.2
	208.5	60.7	0.5
	215.2	10.3	0.1
	215.2	75	0.6
	215.2	82	0.6
	223	11.7	0.2
	223	74	0.6
	227.9	12.2	0.2

Table 15 (contd.)

Catalyst	Temperature °C	% Reaction	$[CO_2/CO]$
$Na_{0.66}WO_3$	202.1	66	1.1
	212.2*	14	0.7
	223.1	26.5	0.8
	231.8	38	1.0
	238.8	46.4	0.9
$Na_{0.73}WO_3$	178.5	13.1	2.3
	181	21.8	1.9
	182 *	24.5	2.4
	189	20.7	2.0
	200	18.6	1.7
	201	87	1.5
	205	25.5	1.8
$Na_{0.77}WO_3$	190 *	55.3	1.2
	210	60	1.5
	218.2	16.7	1.4
	218.2	61.6	0.7
	229.8	17.3	1.0
	229.8	18.4	0.8
	237	60.2	1.5
$Na_{0.81}WO_3$	215	14.2	7.3
	2.18	56.3	2.2
	2.27	38	1.9
	2.27	77.4	3.5
	236.5	53.2	2.0
	246.4	38.3	1.5
$Na_{0.85}WO_3$	182 *	67	2.5
	183.2	20.2	2.4
	192.4	76	2.5
	193	21.8	2.3
	194.7	25.2	2.1
	217.2	38.5	2.4

Table 15 (contd.)

(b) For Catalysts subjected to Oxygen Pretreatment

+ Denotes subsequent runs on catalysts without further oxygen pretreatment.

Catalyst	Temperature °C	% Reaction	$[CO_2/CO]$
$Na_{0.11}WO_3$	189.2	41.6	0.5
	189.2	41.8	0.5
	189.2+	11	0.2
	189.2	6.9	0.1
	189.2+	5.9	0.1
	189.2+	7.9	0
	189.2+	60	0.2
	189.2	16.3	0.1
	189.2	17.4	0.2
	196.4	7.3	0.2
	214	7.3	0.1
	214	63	0.4
	220	12	0.2
	228.3	14.8	0.1
	228.3	56	0.4
$Na_{0.38}WO_3$	195	10.2	0
	195	35	0
	210	7.6	0
	210	26	0
	210+	20	0
$Na_{0.77}WO_3$	190	11.3	0
	211	25	0
	211+	33	0
	221+	36	0

Table 16 gives the activation energy, log frequency factor, activities calculated at a fixed rate of 0.00016 mol. per cube face area. per sec. (or mol. per adsorption site area. per sec.) together with the initial and final CO_2/ CO ratio for the series.

Graphs 9 and 10 give the activation energy pattern and log frequency factor pattern respectively.

The presence of a compensation effect (100) has been shown in graph 11.

The activities used in the activity pattern of graph 12 have been calculated by defining activity as 10^3/ Ts where Ts is the temperature required to give a fixed rate of 0.00016 mol. per cube face area. per sec. (or mol. per ads. site area. per sec.) This method of defining activity, adopted by Fahrenfort (106), is more reasonable than calculating the rates of reaction at a fixed temperature, since the latter would involve extrapolation over a wide range. In the present work to obtain relative activities, as defined above, little extrapolation of the Arrhenius plots was required.

Graphs 13 and 14 show the individual contributions of the dehydrogenation and dehydration reactions to the total activity.

These were calculated using the assumption that the ratio CO_2/ CO is a measure of the ratio Dehydrogenation/ Dehydration. For example, if the ratio CO_2/ CO = x, then:

the dehydrogenation component = $x \times 10^3 / Ts$, whereas the the dehydration component = $1 - x \times 10^3 / Ts$. Both initial and final CO_2 / CO ratios were used.

Table 16

'x' value	E i.e. joules mole^{-1}	CO_2/CO		Based on 'Cubic face Area' results		Based on 'ads site area' results	
		Initial	Final	log A	$10^3/TS$	log A	$10^3/TS$
0	138	0	0	17.8	2.286	18.2	2.321
0.11	111.4	< 0.1	0.2	13.1	2.131	13.7	2.238
0.16	102	< 0.1	0.2	12.4	2.106	13.0	2.211
0.28	98.2	0.1	0.3	12.4	2.073	12.8	2.152
0.38	68.8	0.4	0.2	8.5	2.033	9.1	2.200
0.52	83	0.1	0.5	10.1	2.05	10.7	2.177
0.60	95	0.1	0.6	11.3	2.032	11.8	2.133
0.66	67.2	0.3	1.3	8.9	2.195	9.0	2.228
0.73	68.6	2	> 10	9.2	2.209	9.5	2.269
0.77	73.2	1.0	1.6	9.5	2.146	9.7	2.215
0.81	85	> 10	4	10.3	2.04	10.7	2.131
0.85	63.6	2.0	2.5	8.6	2.216	8.9	2.295

Graph 9

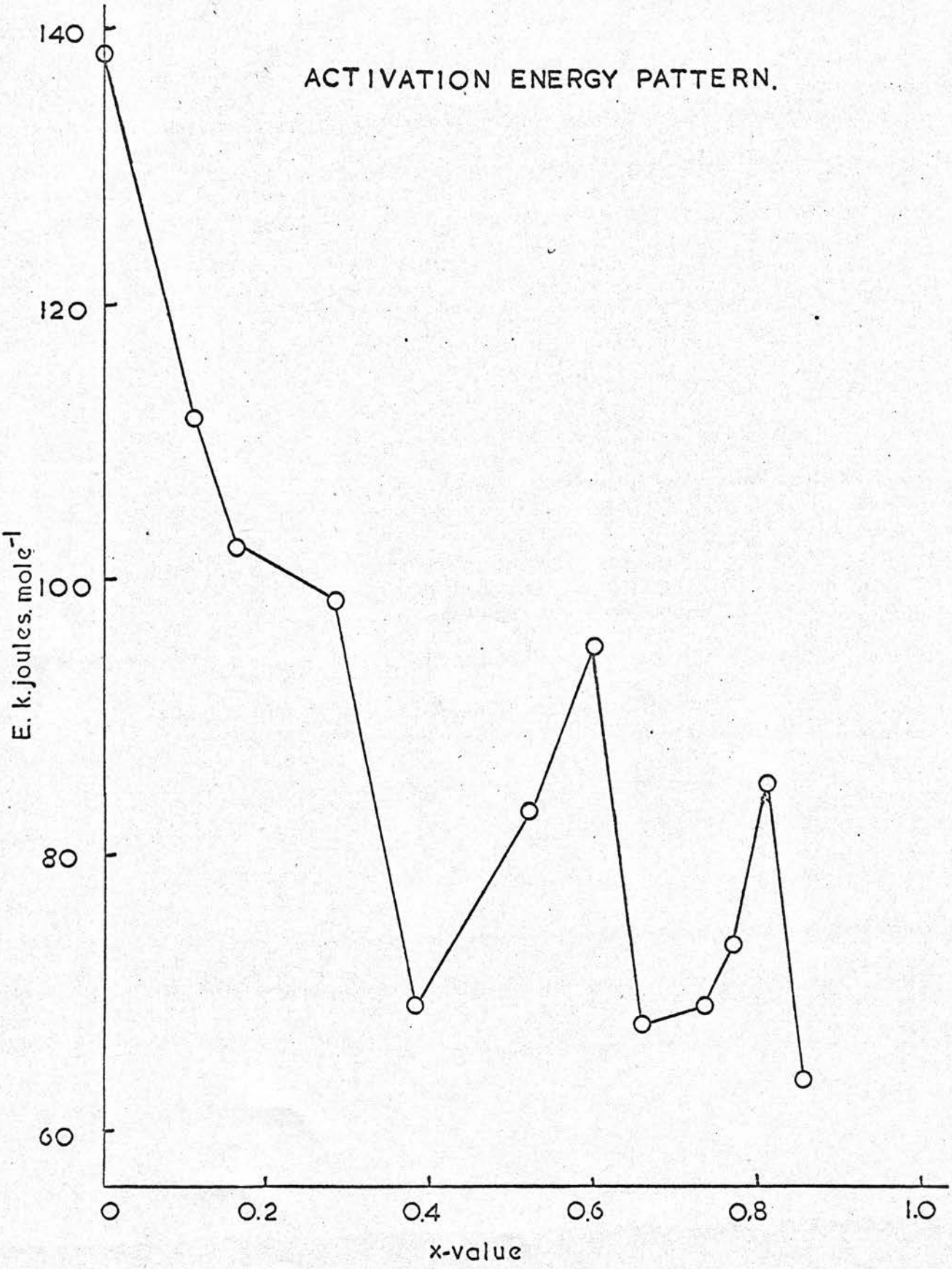
ACTIVATION ENERGY PATTERN.
140
120
100
80
60
E. k.joules. mole^{-1}
0
0.2
0.4
0.6
0.8
1.0
x-value

Graph 10

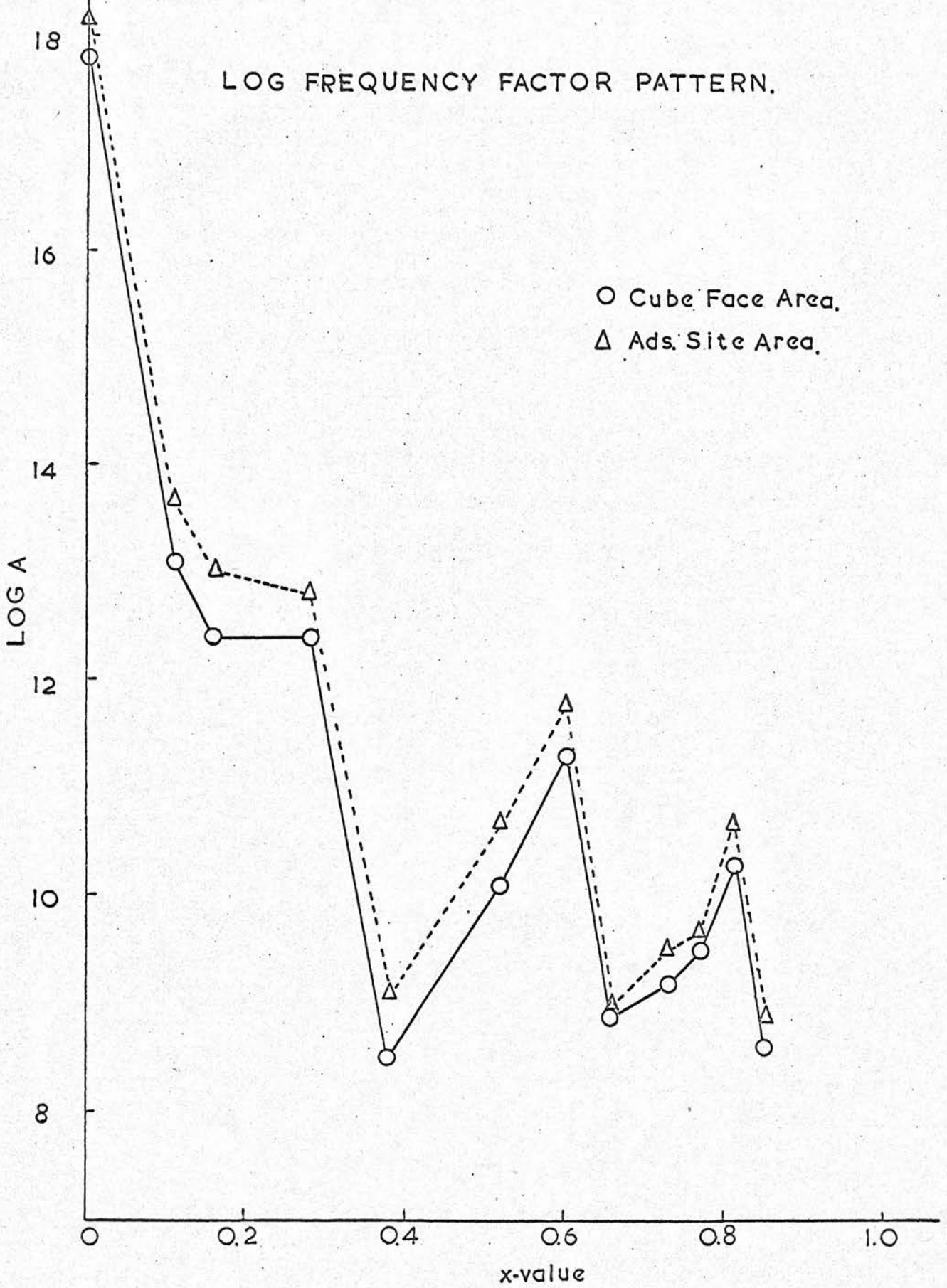
LOG FREQUENCY FACTOR PATTERN.
O Cube Face Area.
Δ Ads. Site Area.
LOG A
18
16
14
12
10
8
0
0.2
0.4
0.6
0.8
1.0
x-value

Graph II

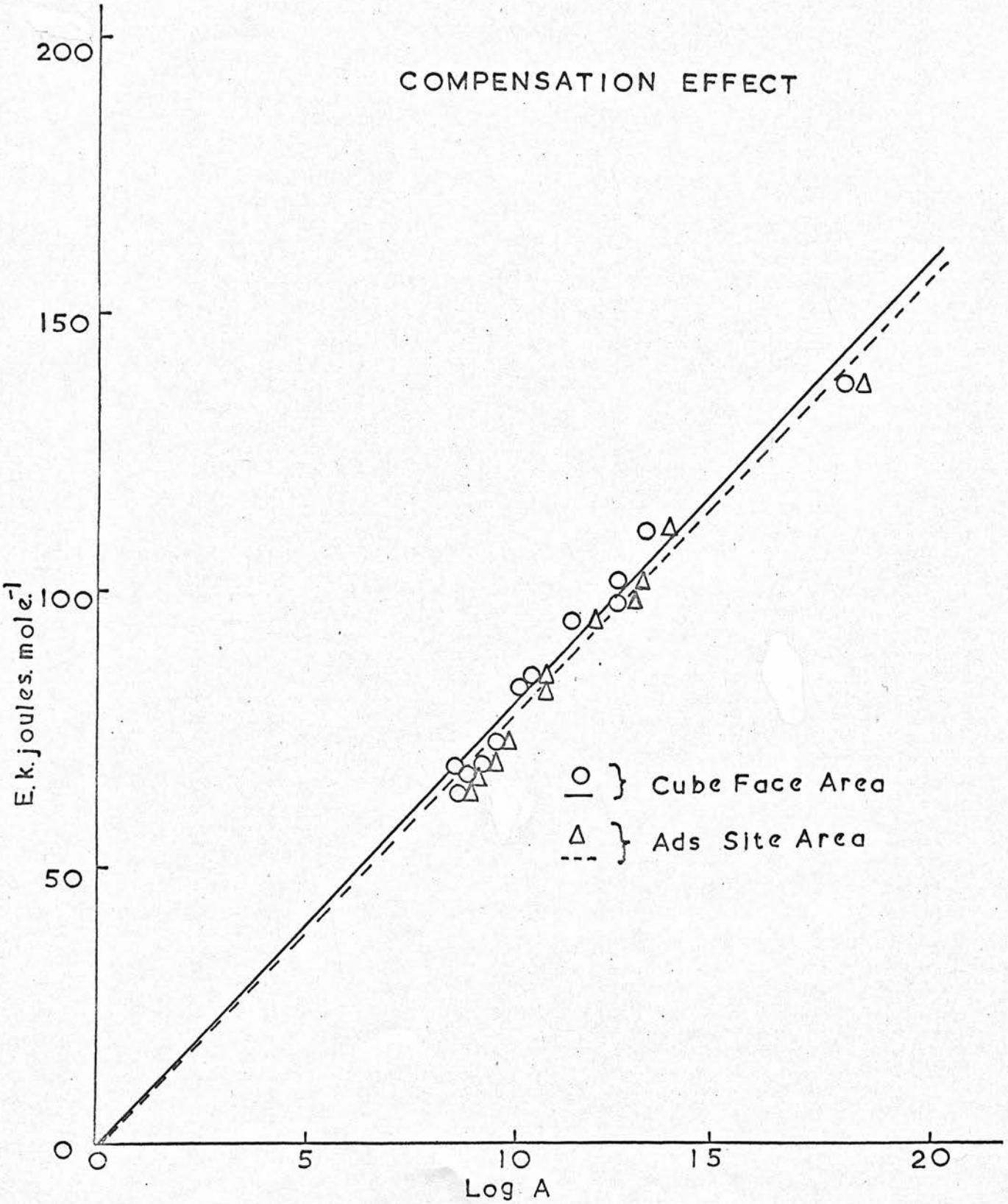
COMPENSATION EFFECT
200
150
100
50
0
E. k. joules. mole^{-1}
0
5
10
15
20
Log A
Cube Face Area
Ads Site Area

Graph 12

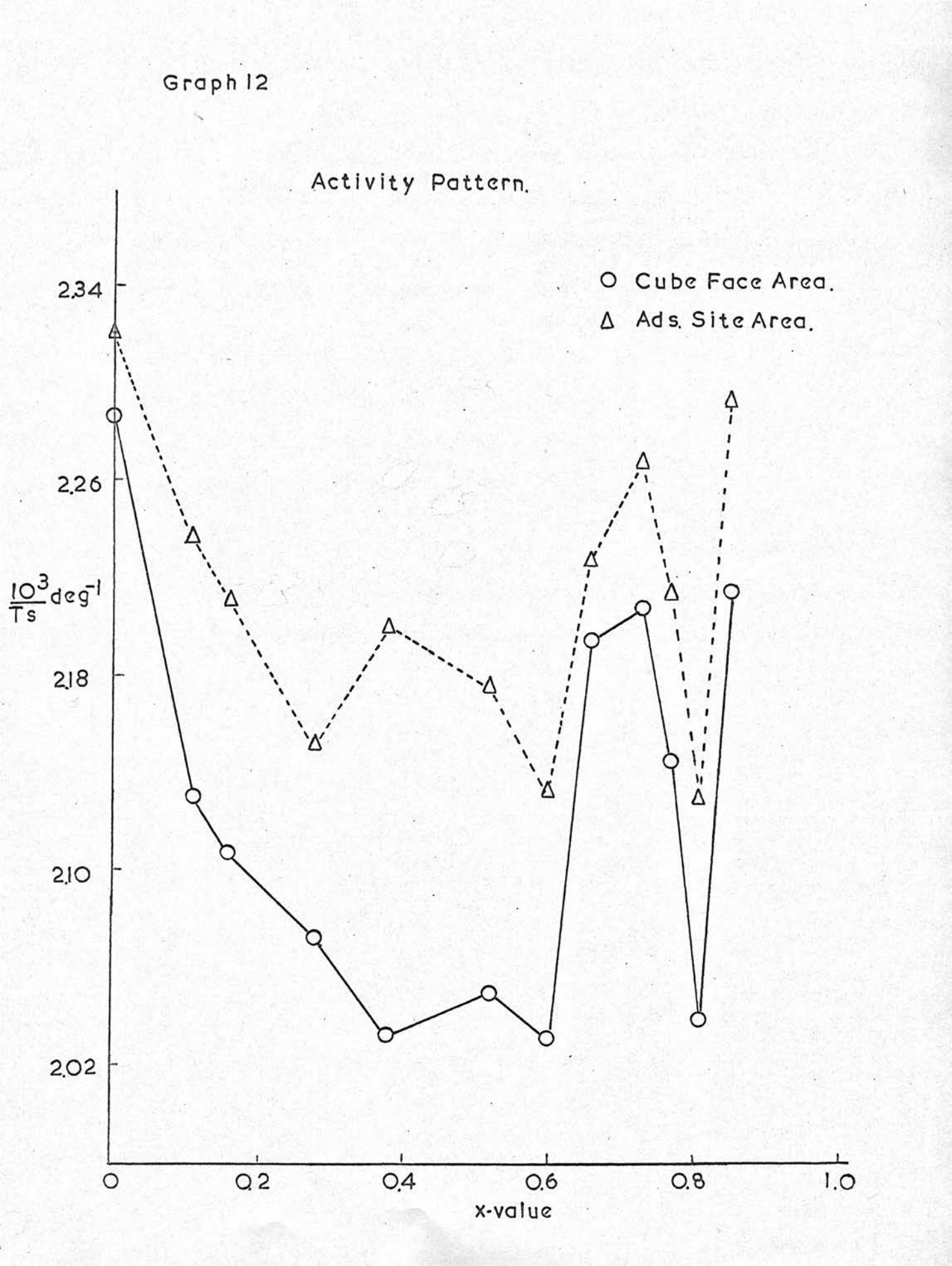
Activity Pattern.
O Cube Face Area.
Δ Ads. Site Area.
2.34
2.26
2.18
2.10
2.02
$\frac{10^3}{Ts}$ deg^{-1}
0
0.2
0.4
0.6
0.8
1.0
x-value

Graph 13.

Activity Pattern For Dehydrogenation.

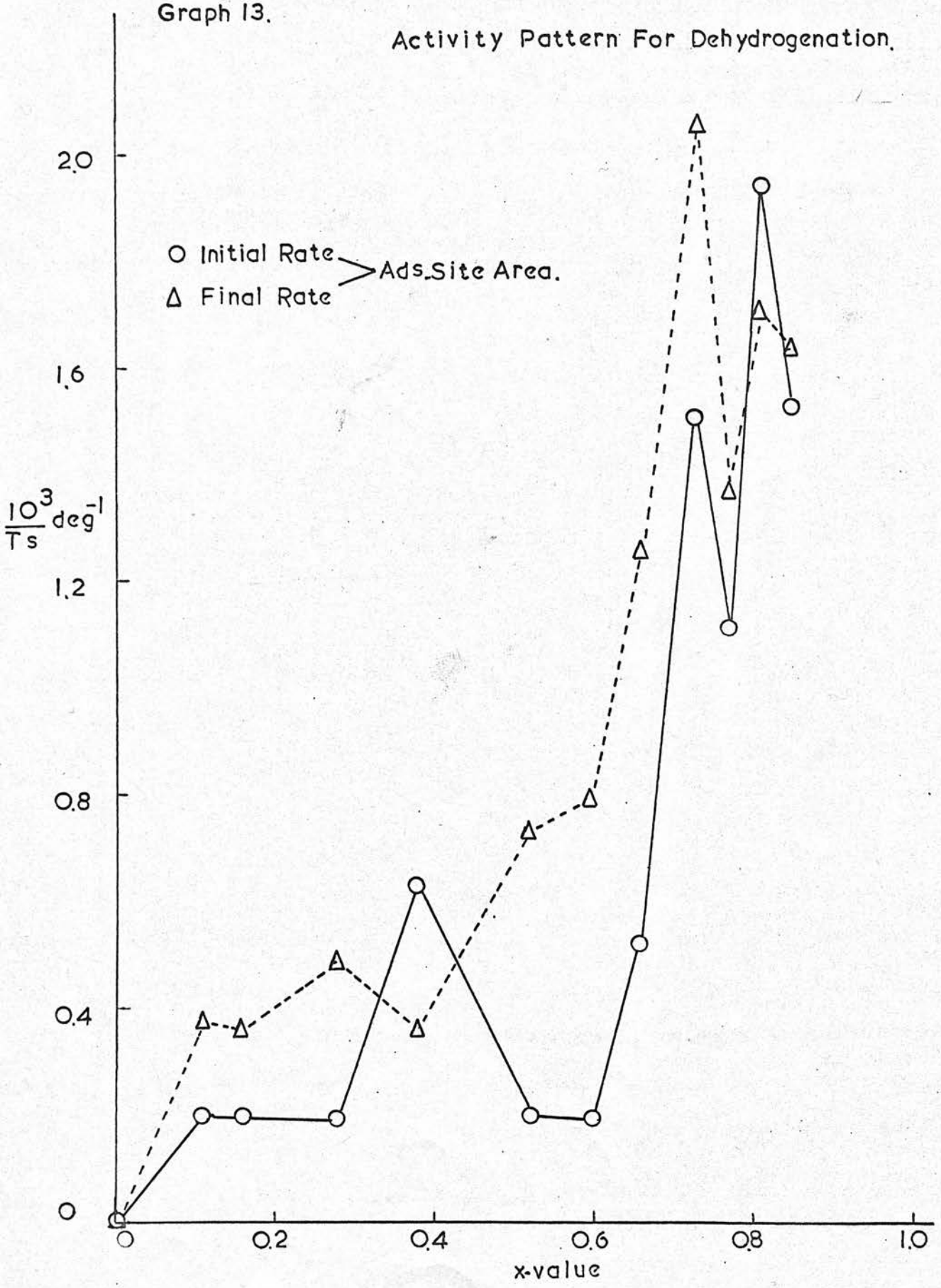

Graph 14

Activity Pattern For Dehydration.

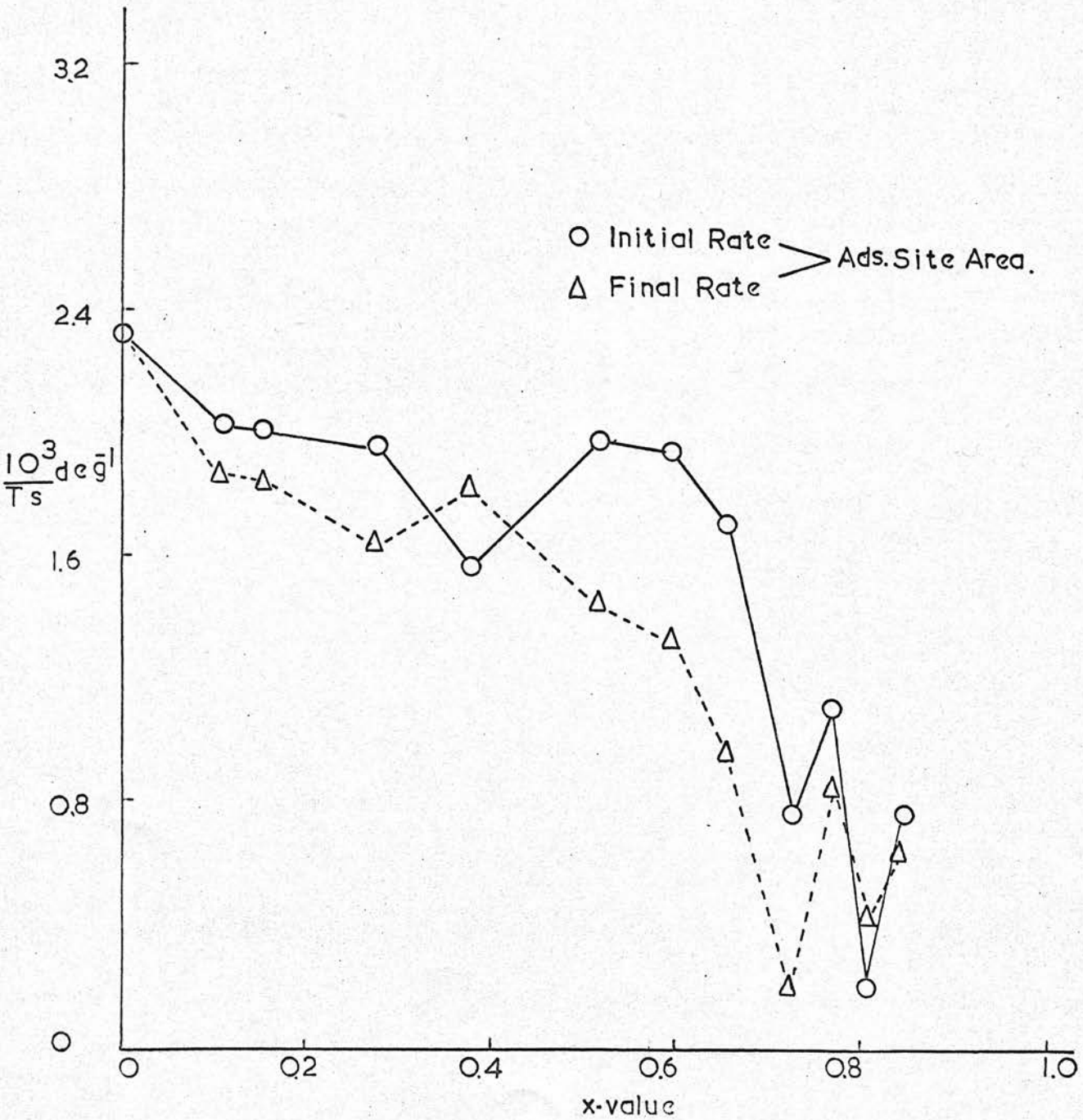

Fig 10

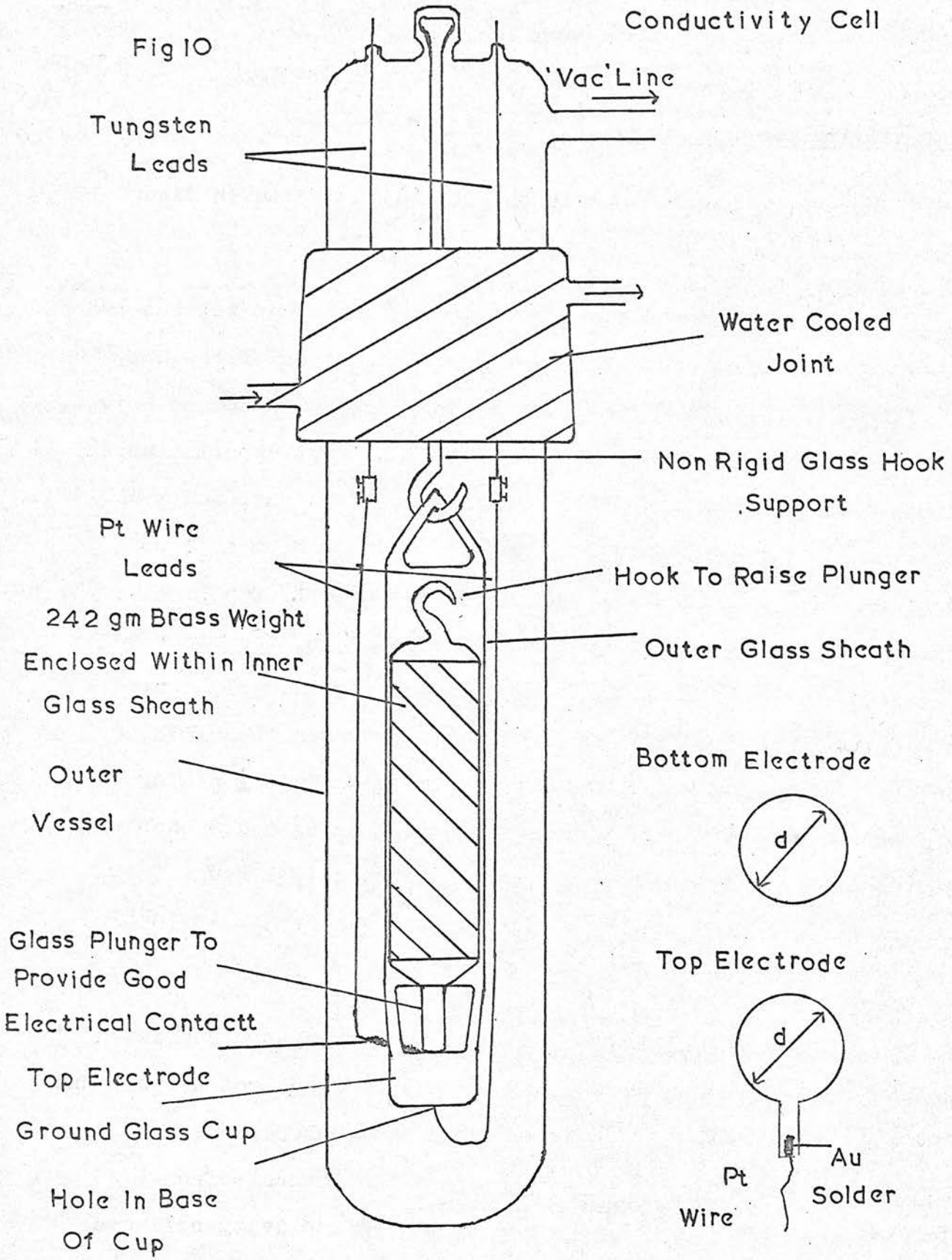
Conductivity Cell
'Vac' Line
Tungsten Leads
Water Cooled Joint
Non Rigid Glass Hook Support
Pt Wire Leads
Hook To Raise Plunger
242 gm Brass Weight Enclosed Within Inner Glass Sheath
Outer Glass Sheath
Outer Vessel
Bottom Electrode
d
Glass Plunger To Provide Good Electrical Contactt
Top Electrode
d
Top Electrode
Ground Glass Cup
Au Solder
Pt Wire
Hole In Base Of Cup
d~8mm.

Conductivity Measurements.

These were carried out in the cell illustrated in figure 10. This cell was connected to a high vacuum system.

The sample was contained in a ground glass cup between two platinum foil electrodes, one resting on the floor of the cup, the other on top of the sample. A cylindrical 242 gm brass weight, sealed within a glass sheath, was allowed to rest upon the upper platinum electrode to ensure good electrical contact, and was contained within another glass sheath suspended from a glass hook, non-rigidly attached to the top of the cell. Two platinum wires, one through a hole in the base of the cup, the other connected to the upper electrode by way of a gold seal, served as electrical connections to a couple of tungsten leads. These provided external electrical contacts via glass metal seals. Easy access to the sample was made possible using a detachable outer tube and a water cooled joint. A glass spiral gauge connected to the cell allowed the pressure of any gas in the cell to be measured.

As with the Kinetics set-up, the pumping system consisted of a mercury diffusion pump backed by a speedivac, rotary pump and gave pressures $< 1 \times 10^{-5}$ mm Hg, measured on a McLeod gauge. A liquid nitrogen trap was used to prevent contaminants from entering the cell. The temperature of the conductivity cell was controlled to within $\pm$ 0.2°C by means of an electrically heated

furnace and electronic relay.

A.C. ($1592^{Hz}_{\wedge}$) and D.C. resistance measurements were made with a Wayne-Kerr Universal Bridge, B 221 A, and a Universal Avometer (Model 8) respectively.

Experimental Procedure.

Approximately 1.8 gm catalyst was placed in the conductivity cell and the apparatus assembled. After noting the resistance of the sample in air at room temperature, the cell was evacuated to $< 1 \times 10^{-5}$ mm Hg, the resistance measured again, and the temperature raised slowly to approximately 500°C. Resistance measurements were taken at convenient intervals at known temperatures. Graphs 15-18 inclusive, show typical examples of the results obtained for all samples studied. A short point of procedure, explaining the function of the curves has been included after the appropriate graph.

Thereafter, formic acid was admitted to the cell, to a pressure of 25-30 mm Hg and a study of the change of resistance with time made. With the exception of WO_3, which showed a marked rise in resistance in the presence of formic acid, little change in resistance was observed for those catalysts studied. In the main, measurements were confined to temperatures at which the decomposition reaction occurred. Tables 17 and 18 and graphs 19 and 20 illustrate the change in resistance during the decomposition reaction. Similar studies carried out in the presence of the individual product gases exhibited no visible change in resistance with time.

After the above measurements, samples were degassed at 500°C overnight and then exposed to oxygen at a pressure of $\sim$150 mm Hg at 360°C, 400°C, 450°C for $Na_{0.11}WO_3$, $Na_{0.38}WO_3$ and $Na_{0.77}WO_3$

respectively, and the increase of resistance with time noted. Subsequent evacuation after a reaction span of ~12 hours, was followed immediately by exposure to formic acid at temperatures both greater and less than that just sufficient to promote the decomposition reaction. For catalysts with $x \geq 0.11$, the original low resistance could not be recovered either by degassing at 500°C or by repeated addition of formic acid at decomposition temperatures. In fact, eventual recovery was only possible after continued roasting in formic acid at 500°C. X-ray diffraction traces carried out on samples pretreated in oxygen showed that a complete reorganisation of the crystal structure had occurred, for those samples with $x \geq 0.11$. However, for WO_3 and $Na_{0.11}WO_3$, original resistances could be recovered, although slowly, without having to resort to this high temperature formic acid treatment.

Tables 19 and 20 and graphs 21 and 22 (a and b) show typical examples for the change in resistance with time for $Na_{0.11}WO_3$ upon exposure to oxygen and formic acid respectively. From the curves, it can be seen that there is a linear dependence of resistance with time for oxygen adsorption, and an approximately exponential decrease, with first order kinetics being followed initially on subsequent exposure to formic acid.

In all cases, the wide spread of points for rate of change of resistance - $K/T/10^3$ plots made it virtually impossible to obtain even an estimate of the activation energy for oxygen

adsorption.

Whenever possible simultaneous A.C. and D.C. measurements of resistance were made; the limiting factor being the difficulty of measuring values of resistance $< 10^6\Omega$ by the A.C. method.

Although of less importance to the present study, it should be noted that a rapid fall in resistance was observed on formic acid admission to oxygen pretreated samples with $x > 0.11$, at temperatures just sufficient to promote the decomposition reaction. At lower temperatures, only very slow initial falls in resistance were observed. In spite of the fact that x-ray diffraction traces indicated that complete reorganisation of the crystal lattices had occurred, awareness of this rapid fall in resistance might be, qualitatively very useful in understanding the actual surface processes occurring immediately upon admission of formic acid.

Analysis of Resistance Measurements.

Such a procedure outlined above cannot be used to determine absolute conductivities. It can, however, be used to obtain a measure of the relative rates of change of resistance since this is independent of the size of the sample and the area of contact. This also precludes the making of accurate conclusions as to the actual component conduction processes, so that only the total conductivity may be obtained for any one sample.

Graph 15.

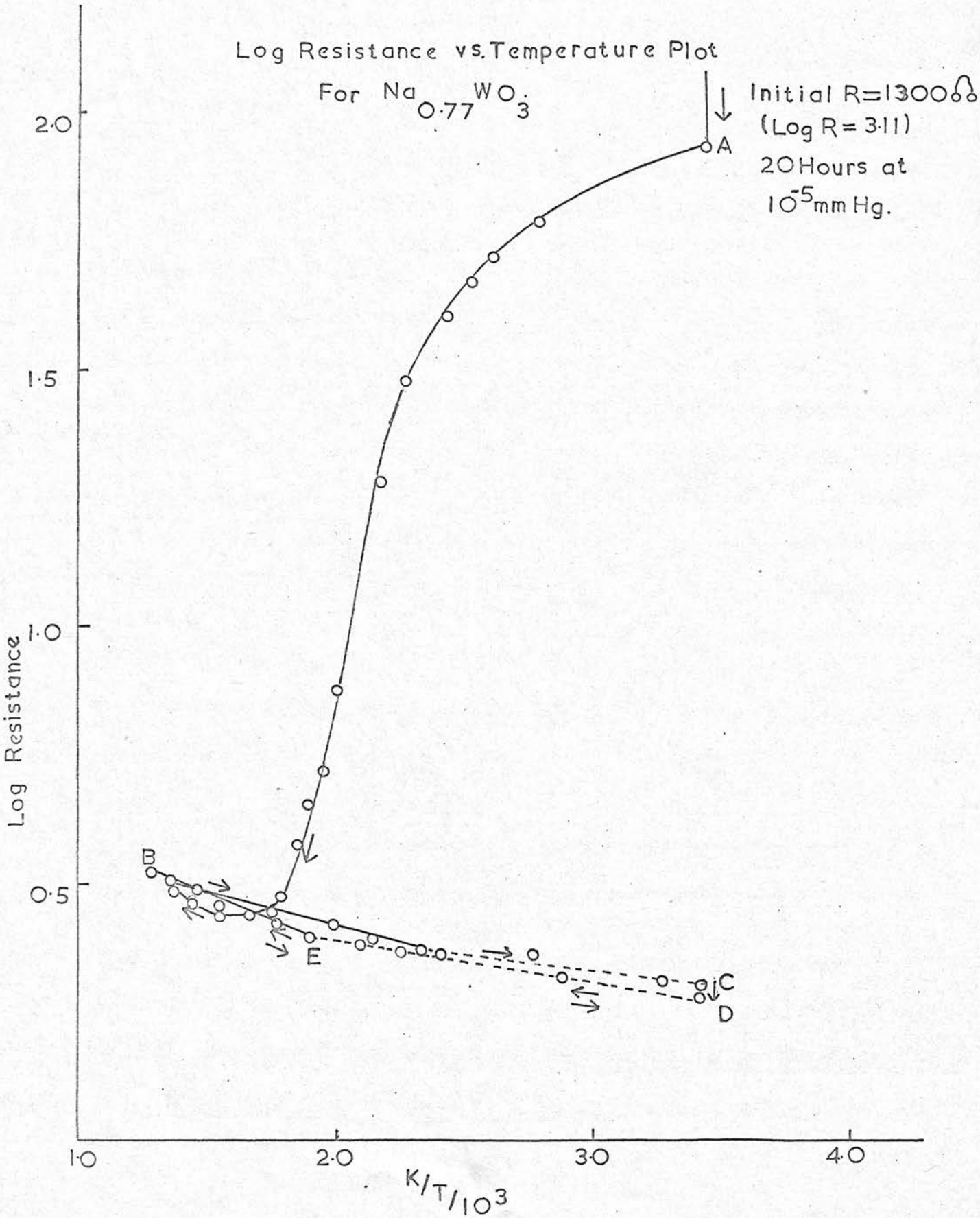
Log Resistance vs. Temperature Plot
For $Na_{0.77}WO_3$
Initial R=1300Ω
(Log R = 3.11)
20 Hours at
10^{-5} mm Hg.
A
B
C
D
E
Log Resistance
2.0
1.5
1.0
0.5
1.0
2.0
3.0
4.0
K/T/10³

Graph 16

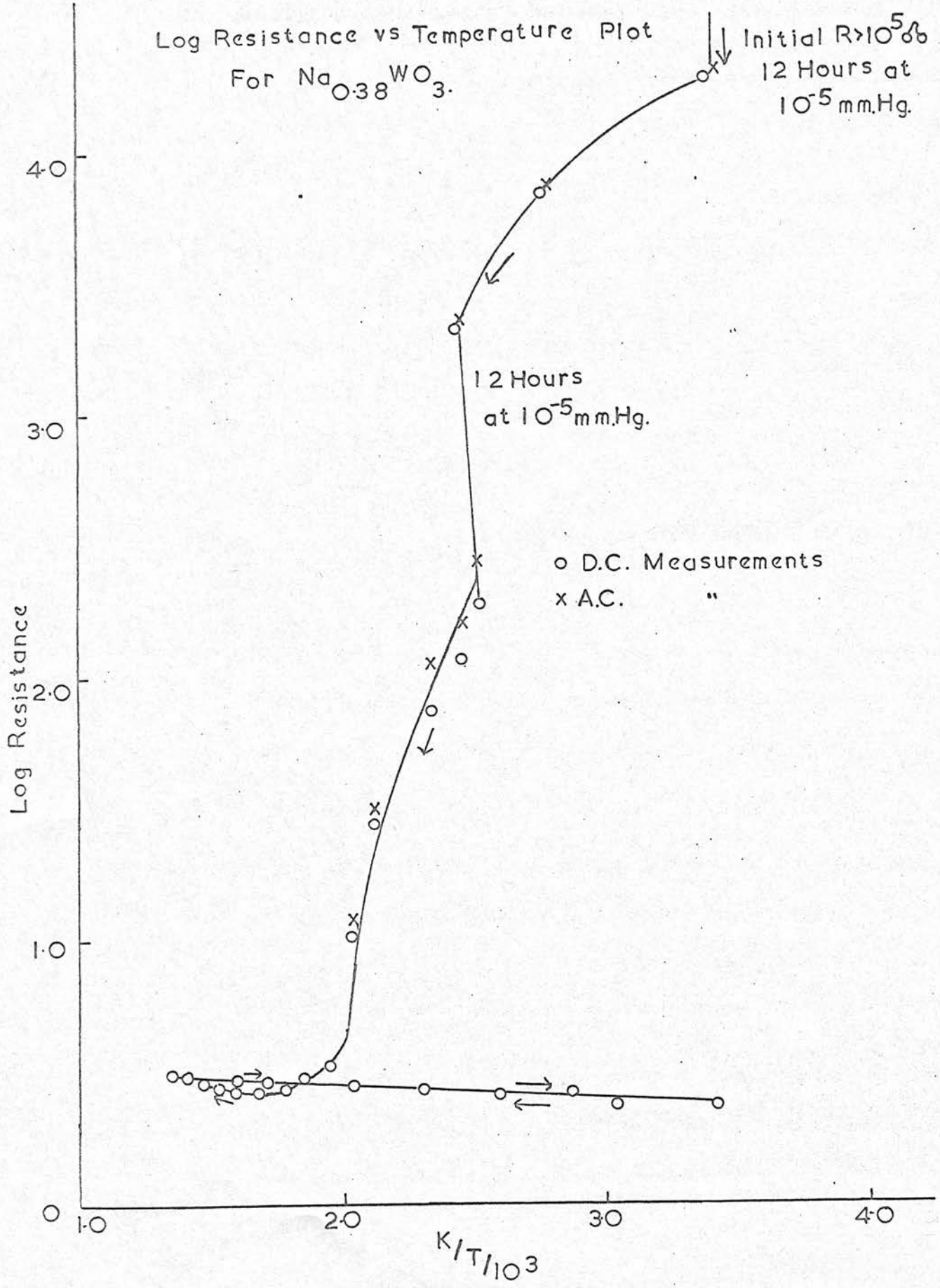
Log Resistance vs Temperature Plot
For $Na_{0.38}WO_3$.
Initial R>10^5 Ω
12 Hours at
10^{-5} mm.Hg.
12 Hours
at 10^{-5} mm.Hg.
o D.C. Measurements
x A.C. "
Log Resistance
4·0
3·0
2·0
1·0
0
1·0
2·0
3·0
4·0
K/T/10^3

Graph 17

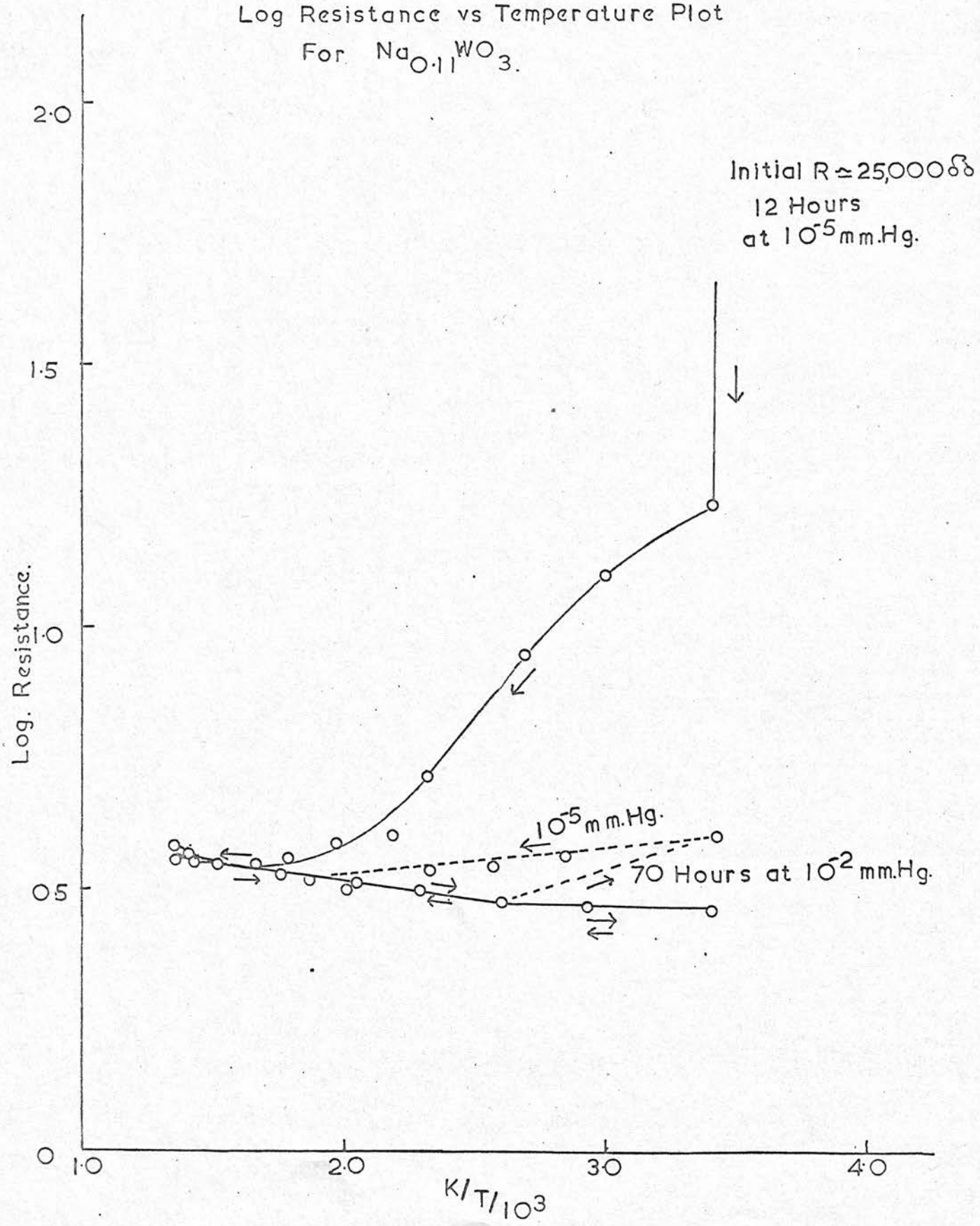
Log Resistance vs Temperature Plot
For $Na_{0.11}WO_3$.
Initial R ≃ 25,000 δδ
12 Hours
at 10^{-5} mm.Hg.
10^{-5} m m.Hg.
70 Hours at 10^{-2} mm.Hg.
Log. Resistance.
2·0
1·5
1·0
0·5
0
1·0
2·0
3·0
4·0
K/T/10^3

Graph 18

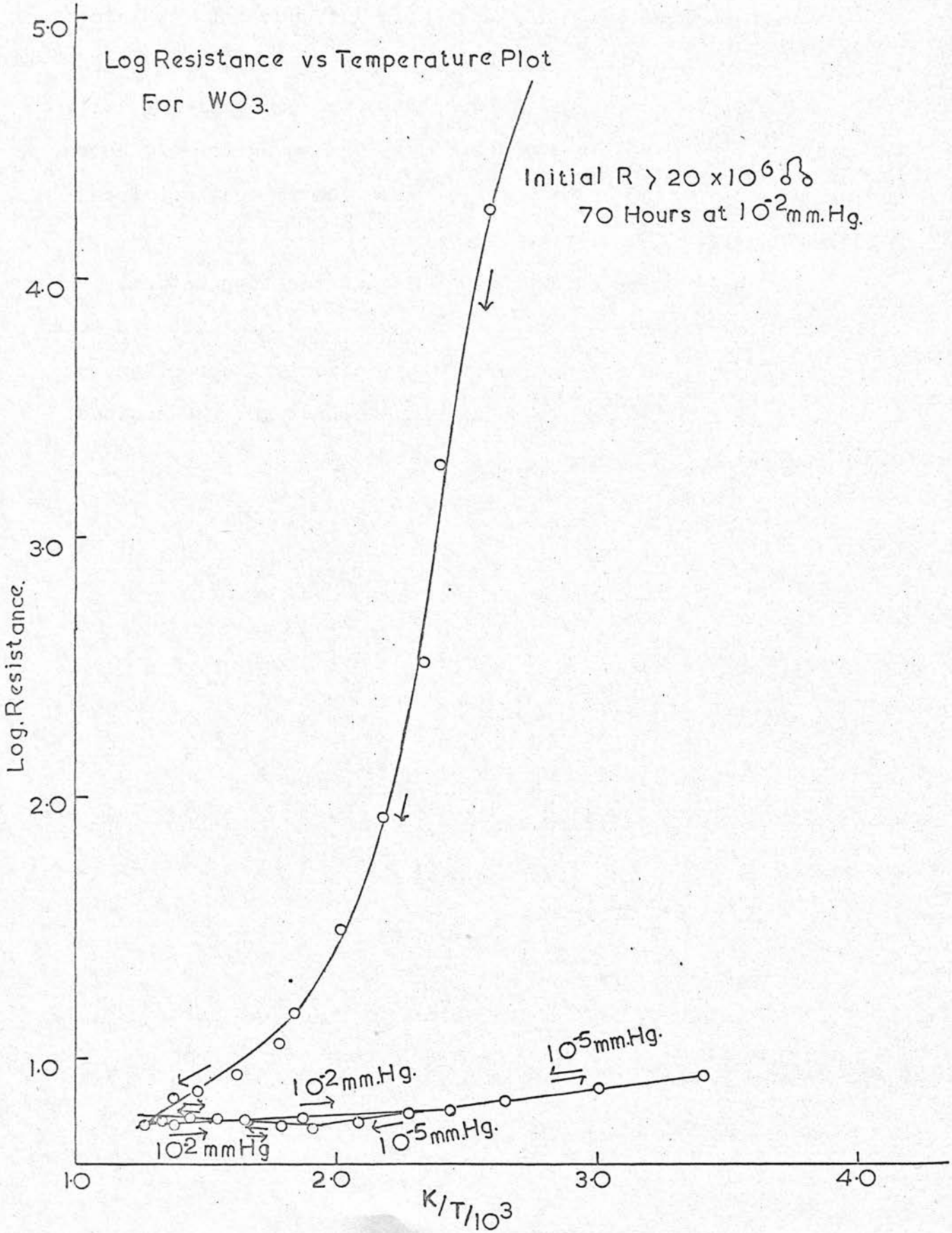
Log Resistance vs Temperature Plot
For WO3.
Initial R > 20 x 10^6 Ω
70 Hours at 10^-2 mm.Hg.
5·0
4·0
3·0
2·0
1·0
Log. Resistance.
10^-5 mm.Hg.
10^-2 mm.Hg.
10^-5 mm.Hg.
10^-2 mm Hg
1·0
2·0
3·0
4·0
K/T/10^3

Letters A-E on graph 15, have been introduced to explain the function of graphs 15-18.

After introduction of the sample to the conductivity cell, the cell was outgassed at a pressure of 10^{-5} mm Hg for ~20 hours, during which time the resistance was observed to decrease from ~1300 ohms to ~90 ohms (point A).

On subsequently raising and lowering the temperature, whilst maintaining the pressure constant, the resistance was then found to decrease to points B and C respectively. Thereafter, an alternatively raising and lowering the temperature, the sequence D-E-B and B-E-D was followed.

Graph 19.

Resistance/ Time Curve For WO_3.

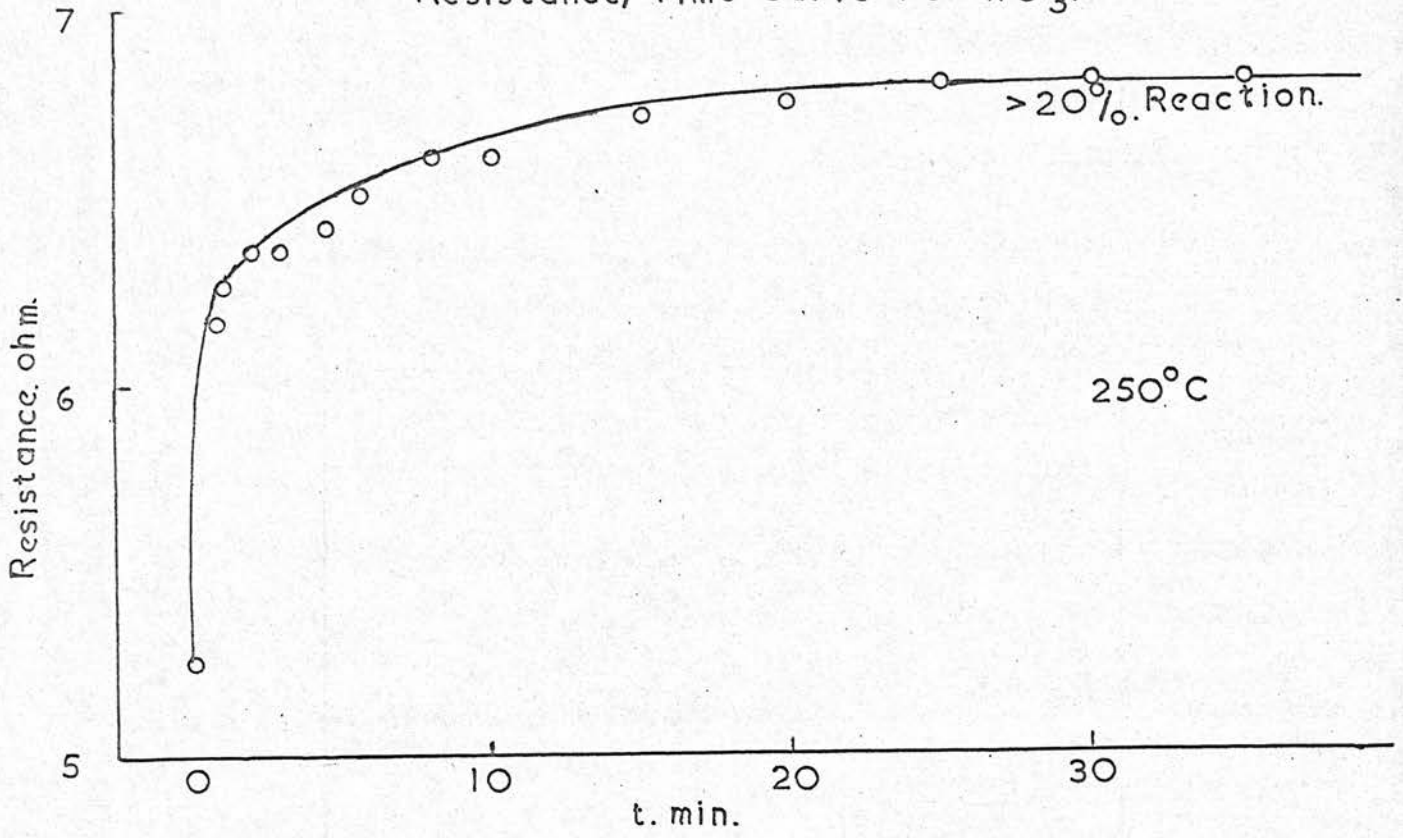

Graph 20

Resistance/ Time Curve For $Na_{0.11}WO_3$

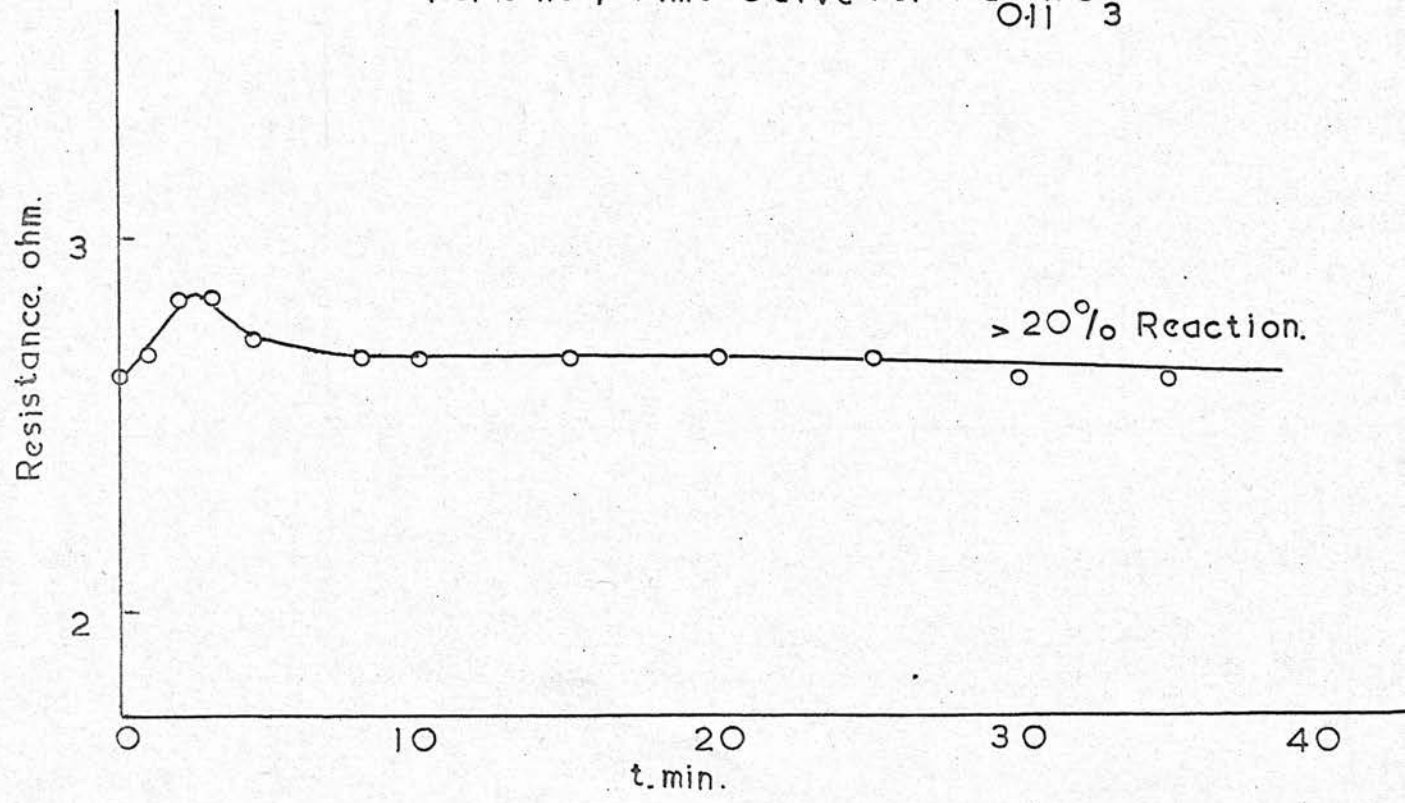

Table 17

Example of Resistance/Time Plot for Formic Acid Decomposition on WO_3 at 250°C

Time (mins)	Resistance (ohms)
0	5.25
$^1/_2$	6.15
1	6.25
2	6.35
3	6.35
4	6.40
6	6.50
8	6.60
10	6.60
15	6.70
20	6.75
25	6.80
30	6.80
35	6.80

Table 18

Example of Resistance/Time Plot for Formic Acid Decomposition on $Na_{0.11}WO_3$ at 200°C

Time (mins)	Resistance (ohms)
0	2.70
$^1/_2$	2.75
1	2.70
2	2.90
3	2.90
4	2.80
6	2.75
8	2.75
10	2.75
15	2.75
20	2.75
25	2.75
30	2.70

Graph 21.

Resistance/Time Plot For Oxygen Adsorption On $Na_{0.11}WO_3$.

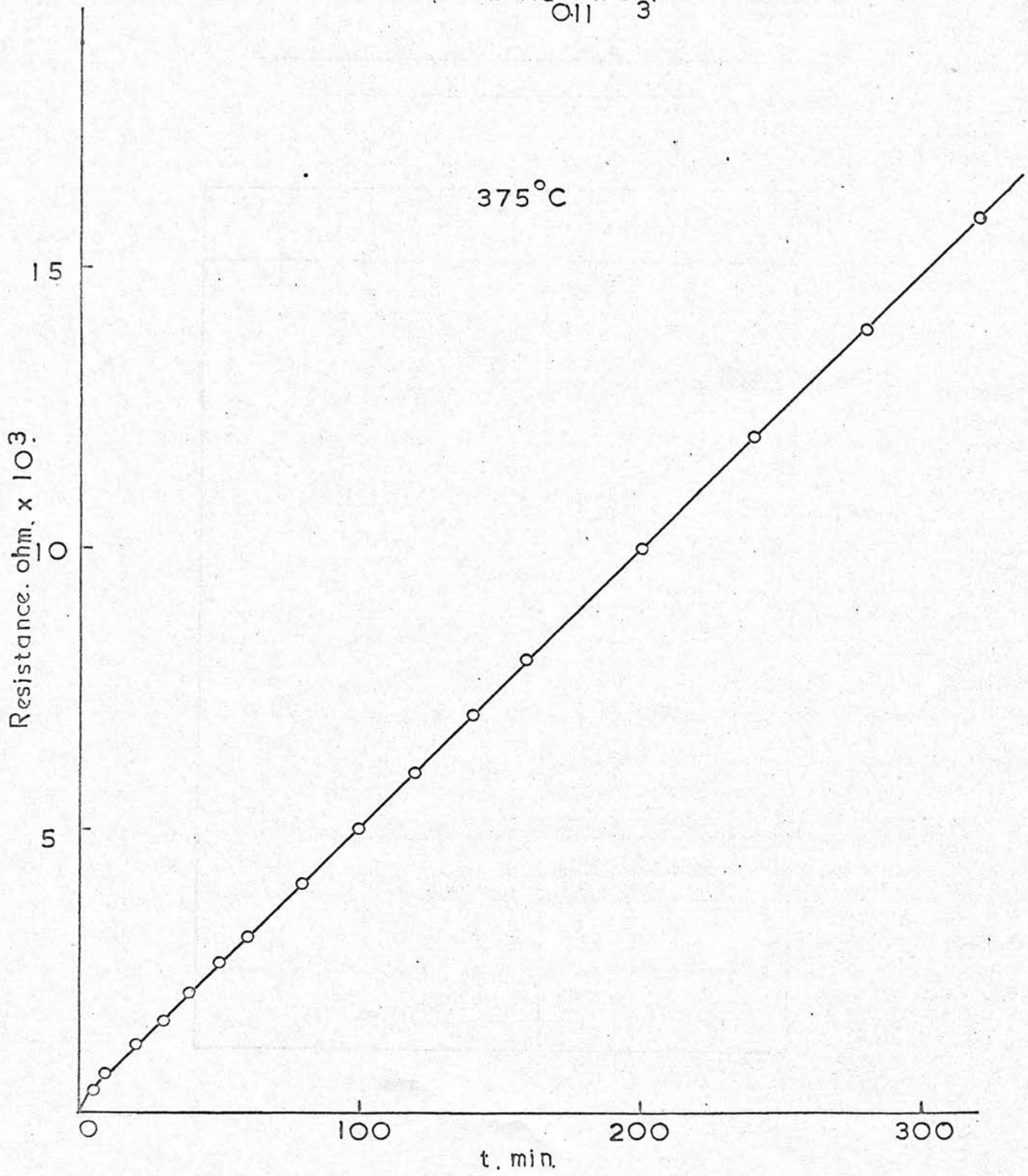

Table 19

Example of Resistance/Time Plot for Oxygen Adsorption on $Na_{0.11}WO_3$ at 375°C

Time (mins)	Resistance (ohms)
0	70
10	720
20	1,220
30	1,650
40	2,150
50	2,630
60	3,120
80	4,100
100	5,080
120	6,060
140	7,040
160	8,020
200	10,000
240	12,000
280	13,950
320	15,900

Graph 22a

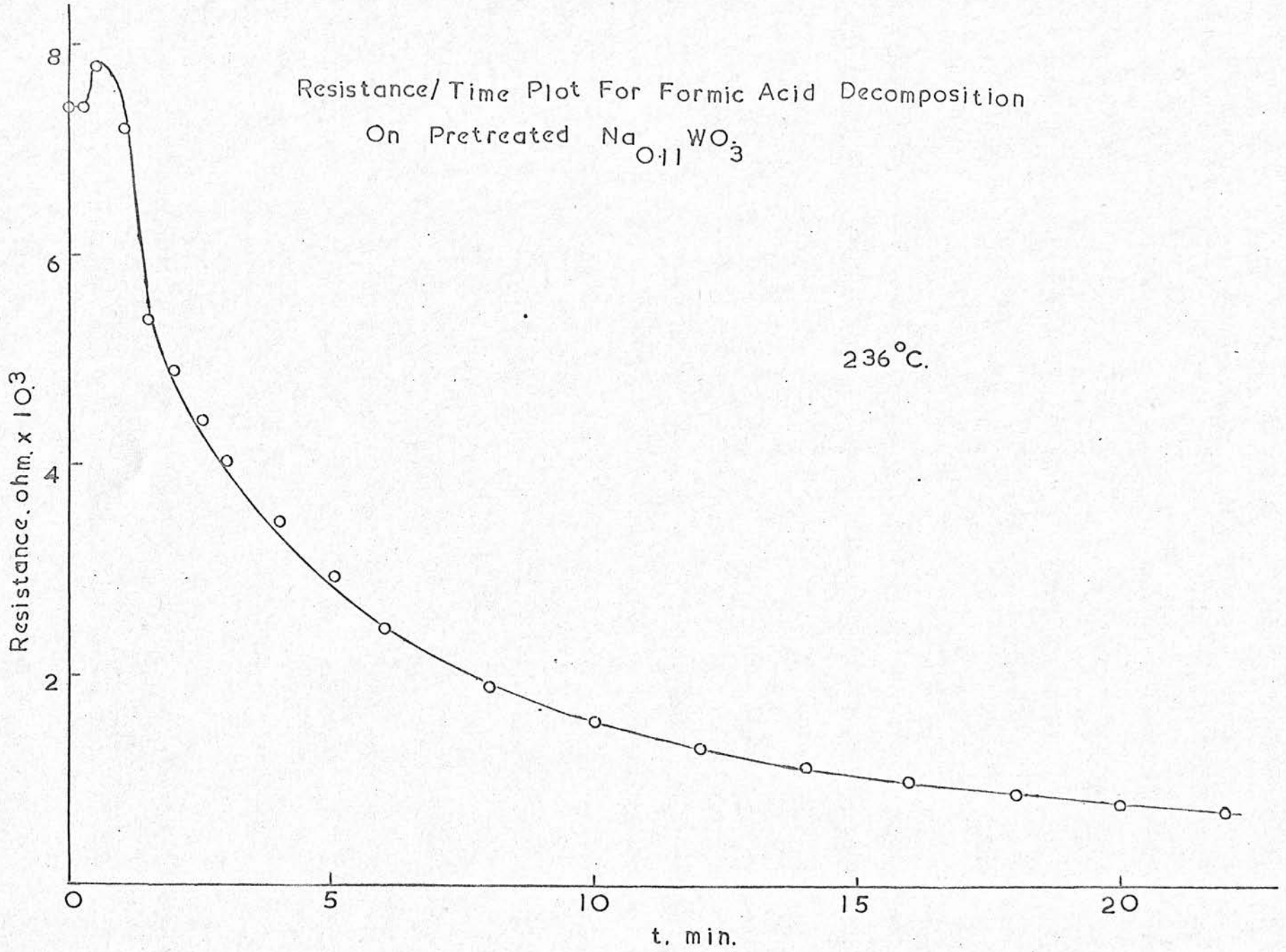
Resistance/ Time Plot For Formic Acid Decomposition
On Pretreated $Na_{0.11}WO_3$
236 °C.
Resistance. ohm. x 10^3
8
6
4
2
0
5
10
15
20
t. min.

Graph 22 b

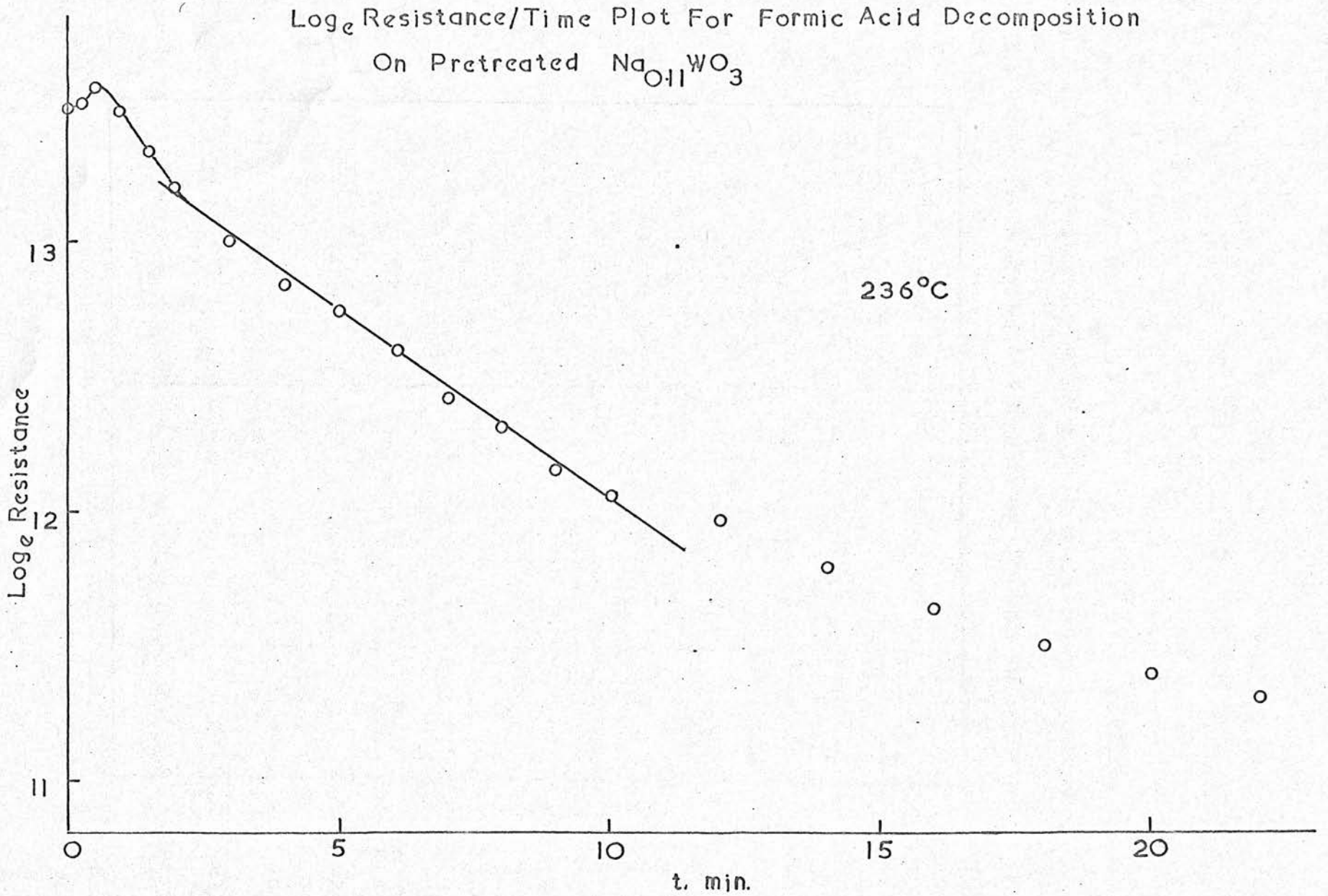
Log$_e$ Resistance/Time Plot For Formic Acid Decomposition
On Pretreated $Na_{0.11}WO_3$
236°C
Log$_e$ Resistance
13
12
11
0
5
10
15
20
t. min.

Table 20

Examples of Resistance and $\log_e$ Resistance/Time Plots for Formic Acid Decomposition on Oxygen Pretreated $NaO._{11}WO_3$

Time	Resistance x 10^3	$\log_e$ Resistance
0	740	13.51
$^1/_4$	740	13.51
$^1/_2$	780	13.57
1	720	13.49
$1^1/_2$	540	13.34
2	490	13.20
3	405	13.01
4	345	12.85
5	295	12.75
6	247	12.60
7	222	12.42
8	191	12.31
9	172	12.16
10	157	12.06
12	132	11.96
14	114	11.79
16	99	11.64
18	88	11.50
20	81	11.39
22	74	11.30
24	67	11.21

DISCUSSION.

The sodium tungsten bronzes, Na_xWO_3, where as x varies there are pronounced changes in electrical properties with only minor changes in crystal structure, would appear to constitute a favourable subject of study in relation to the electronic theory of catalysis (107).

With this in mind, it was decided to carry out a thorough investigation of the formic acid decomposition reaction on these compounds. This reaction is especially suited to a study of the electronic factor in that it involves only one molecular species, the rate of decomposition being followed easily by pressure measurements, and since it is catalysed by a wide range of oxides and metals (93).

In order to examine the value of using these compounds for a study of this nature, an attempt will be made to explain the observed results in terms of a model (as far as electronic properties are concerned) constructed from an appraisal of researches by Sienko and Crowder (12,61), Mackintosh (62), and particularly by Fuchs (63). Owing to the large degree of uncertainty, necessarily incurred when working with catalytic reactors, the proposed model will, in general, be less sophisticated than any one of these approaches.

The earlier view (43), that non stoichiometric oxides contained mixtures of several oxidation states has now been

Fig 11

(a) $x = 0.2$.

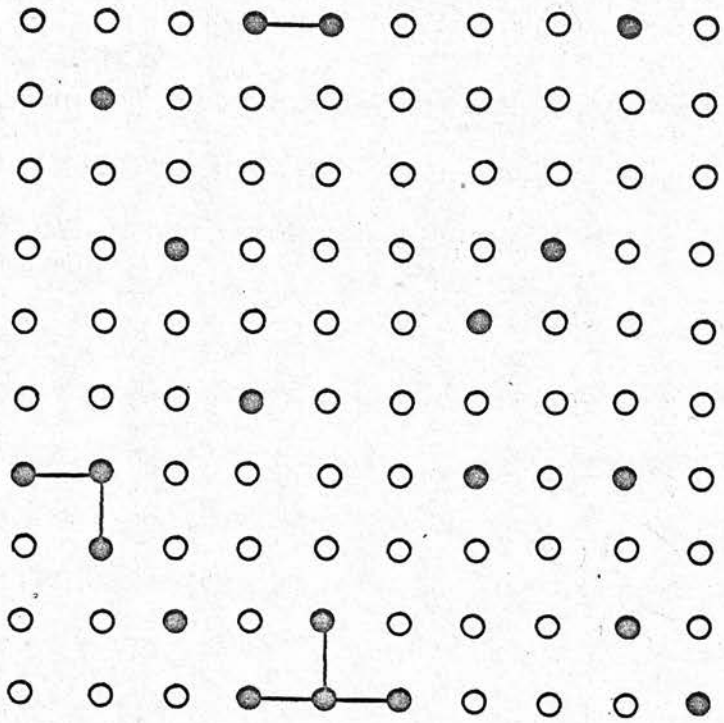

(b) $x = 0.45$.

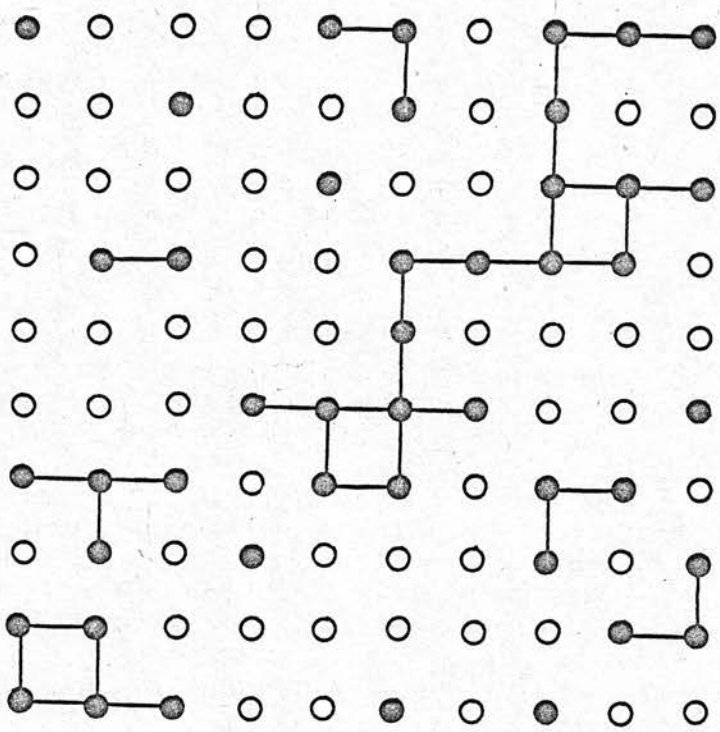

Na_xWO_3

○ Empty Sodium Sites.

● Filled " "

superceded in the alkali tungsten bronzes by replacing the hypothetical pentavalent tungsten in $xMW^{V}O_3(1-x)\ W^{VI}O_3$ by a degenerate 'electron gas' formed from the valence electrons of ionised M atoms in $M_xW^{VI}O_3$.

To explain the formation of this degenerate 'electron gas', Sienko and Crowder (12, 61), Mackintosh (62) and Fuchs (63) have each in turn, adopted essentially covalent models based on the Molecular Orbital theory, in which the common feature is that each sodium atom contributes one electron to a conduction band. Sienko (12, 61) and Mackintosh (62) adopted models in which the conduction band was derived by overlap of tungsten $5d_{\epsilon}$ (t_{2g}) and sodium p atomic orbitals respectively, whereas Fuchs postulated that clusters of sodium atoms may occur in the bronzes.

Fuchs's model may be explained with the aid of figure 11 (a and b), which shows a model of Na_xWO_3 at two values of x. Here electrons would be localised more diffusely so that they would extend over the tungsten and oxygen ions next to the sodium ions. It is perhaps, important to note in this model that the conduction electrons avoid the sodium vacancies, being concentrated in regions of occupied sodium sites. It should be observed that the clusters erroneously appear finite in figure 11 (a and b) only because a single atomic plane is shown in each case. On the basis of this approach, he was able to explain the changeover from a metallic to semiconducting state at $x \simeq 0.25$ (figure 5) (78), and not at $x \simeq 0.31$ as predicted by Sykes and Essam (108). In so doing,

he was able to invalidate the earlier suggestion by Sienko and Mackintosh of an explanation based on Mott's theory for the disappearance of metallic conductivity at $x \simeq 0.25$. Mott's theory (81) requires that there be a uniform electron density within the system, a condition most unlikely for the sodium bronzes in which the electron gas is highly non uniform.

From their measurements of the spin-lattice relaxation times for the ^{23}Na resonance, Fromhold and Narath (76) were able to deduce that there was a serious deviation from randomness in samples with x between 0.56 and 0.89, providing further support for the presence of clusters of sodium atoms. With the aid of this information, Fuchs was able to explain the earlier support, both for (24-5, 82) and against (60) the presence of an ordered structure at $x \simeq 0.75$, whilst at the same time providing an explanation for the observation by Juretschke (82) that the minimum in resistivity was much less than is customarily associated with such ordered structures. The serious deviation from randomness, leading to a system neither wholly ordered nor random in nature would result in a partially ordered structure, with a broader minimum in resistivity, extending from $x \sim 0.6$ to 0.9.

Finally, this picture is able to explain the observations (83-4) that the density of states, and hence the number of conduction electrons, is proportional to the sodium concentration x over the range $0.5 < x < 0.9$. This can be explained using figure 11 (a and b) and taking into account the various possible arrangements

of filled sodium sites in this figure. It can be seen, at some critical value of x, that a continuous conduction process will come into operation, with each filled sodium site having at least one other as nearest neighbour, a result leading to an unlimited sphere of movement, excluding of course, sodium vacancies, for any one arbitrarily chosen conduction electron.

In order to be of use in the present study, the picture outlined above has to be modified to take account of the oxygen deficiencies, introduced by vacuum heat treatment. This effect, referred to by Crowder and Sienko (37, 61), Derén and Polaczkowa (90) and others (45, 49, 91) as a result of studies on the electronic properties of tungsten trioxide, leads to a rapid increase in conductivity, with the final attainment of a 'Quasi metallic' state. It would now appear that, under vacuum conditions, a changeover from metallic-semiconductor properties, earlier thought to take place at $x \simeq 0.25$, may occur at much lower values of x, or indeed may never occur at all. However, this in itself does not necessarily invalidate the postulates of Fuchs (63) and others (12, 61-3), formulated with the aid of Mott's theory (81) for metal-semiconductor transitions. That the electrical properties of samples of WO_3 in vacuo are qualitatively different to the corresponding properties before such treatment, has been demonstrated by Sienko and Crowder (37,61).

These workers, observing that the effects were reversible, pointed out that the impurities responsible for the electrical

conductivity of WO_3 in air, were not due to oxygen deficiencies. A quantitative measure of this effect has been made by Kudrak and Sienko (91), who were able to show that each missing oxygen atom was equivalent to the presence of two alkali atoms. This equivalence of oxygen defect and alkali metal in the WO_3 system has been further demonstrated by Sienko and Banerjee (45), by the fact that the magnetic behaviour as a function of x is the same in WO_{3-x} as in $Mx\ WO_3$.

It is thus imperative to appreiciate, that without exception, measurements of the electrical properties of tungsten trioxide and the sodium bronzes have provided, unavoidably, measures of the total conductivity, it being virtually impossible, practically, to gain a better understanding of the actual component conduction processes within these compounds. Hence, whereas the available data, both past (37, 45,49,61, 90-1) and present, point to the attainment of a 'Quasi metallic' state under vacuo, this may in fact only refer to structurally defined boundaries within the crystal lattice, the overall effect misleadingly giving an oversimplified view of the conduction processes actually involved.

The results obtained in the present study from measurements of the change in resistance with temperature (and time) under vacuo (graphs 15-8, inclusive) are in agreement with those of Derén and Polaczkowa (90). All samples studied, rapidly became

highly conducting and without exception, exhibited positive thermal coefficients of resistivity, consistent with metallic behaviour. WO_3 and to a lesser extent $Na_{0.11}WO_3$, were also seen to exhibit semiconducting behaviour, the transition from a semiconducting to a metallic state occurring at ~250 °C and 110 °C respectively.

The marked increase in the resistance of WO_3 in the presence of formic acid (graph 19) would appear to provide support for those workers (93, 95) favouring the presence of a negatively charged formate ion as surface intermediate, especially since no appreciable change in resistance was observed in the presence of the individual product gases. Whether this is a complete or partial transfer of an electron leading either to the presence of an ionic (109) or covalent $(110)_A^{\text{SPECIES}}$ on the surface is of course very much open to speculation, more especially because of the absence of suitable comparisons with analogous bulk formates, used so effectively by other workers (100, 111). If instead of alternatively heating and cooling under vacuo, samples were exposed to formic acid, the trend towards a highly conducting state was facilitated, in accord with the observations by Rabes and Schenk (92), that formic acid, a strong reducing agent quickly reduces the parent oxide WO_3. The strong reducing nature of formic acid may also be the cause of the immediate rapid fall in resistance observed when samples, having undergone pretreatment in oxygen, are exposed to this acid.

A further interesting feature in this section was provided by the increasing resistance to oxidation through the series, temperatures of 360°C, 400°C and 450°C being required by $Na_{0.11}WO_3$, $Na_{0.38}WO_3$ and $Na_{0.77}WO_3$ to initiate reaction with oxygen. These temperatures are the minimum ones at which any appreciable change in resistance was observed, and compare favourably with the results of Balandin and Sokolova (13), using sodium bronzes prepared by reduction of the paratungstate.

In addition to conductivity measurements, x-ray diffraction, magnetic susceptibility and electron spin resonance measurements were carried out on samples prepared for this work. It was established that the sodium bronzes used in this investigation, were analogous to those prepared by earlier workers (14-37) (Tables 1 and 2), following the same linear relationship (Vegard's law) as that outlined by Straumanis (39). Diffraction traces carried out on bronzes with x values between 0.3 and 0.4, indicated that either a cubic phase or both cubic and tetragonal phases could exist in this region, depending upon the rate of annealing during preparation. This is in agreement with the observations by Magnéli (20) and Ribnick, Post and Banks (32) that quenched samples around $Na_{0.35}WO_3$ may be cubic, while slowly annealed samples would consist of both tetragonal and cubic phases together.

Results from magnetic susceptibility work (Table 4) are in close agreement with those of earlier workers (43,45,50,58,76,83)

and strongly suggest that a model based on delocalised electrons is more appropriate for describing the tungsten oxides than is the more traditional mixed oxidation state model. The results for pretreated samples, with the exception of tungsten trioxide, exhibited little difference to those carried out under normal conditions. The observed slight decrease in the specific susceptibilities may be attributed to some reorganisation of the surface, contributing to a slightly increased diamagnetism. The increase observed for tungsten trioxide may be interpreted in terms of a reduction in surface oxygen leading to small centres of pentavalent tungsten (43).

Finally electron spin resonance studies are consistent with those of Sienko and Osterreicher (112), who supplemented an infra red study with e.s.r. measurements of the hydrogen tungsten bronzes, H_xWO_3 ($0.5 > x > 0.03$), prepared in the absence of air and maintained under vacuum. That these were analogs of the more commonly known sodium bronzes was shown by the presence of a band in the region usually associated with the metal-H deformation motions (690 cm^{-1}) and the absence of any hydroxyl frequencies in the I.R. spectrum. With one notable exception, $H_{0.10}WO_3$, which gave a broad asymmetric absorption of g value $\sim$ 1.97, they failed to obtain any detectable signal for those samples studied. This they attributed to the high values of x, which would preclude penetration of the microwave power to a finite portion of the sample, or to a too low concentration of spins with less

concentrated specimens. The absence of any signal in the range g = 1.4-1.7, characteristic of W(V) provides additional support for the presence of a delocalised electron gas in these compounds. The presence of a signal at g$\sim$1.6 for pretreated WO_3, provides further support for the conductivity and magnetic susceptibility data which was consistent with the presence of pentavalent tungsten on the surface.

When attempting to assess the catalytic activities of substances using a test reaction, it is desirable that either the mechanism of the reaction is already understood or that during investigation an effort is made to elucidate the mechanism. It is with this in mind that an attempt will be made to outline certain relevant features of the formic acid decomposition reaction with regard to the present study, whilst referring one to other, more comprehensive texts (93), for a more detailed study of this reaction. Of greater importance, will be the use of this 'test' reaction to gain an understanding of the observed catalytic properties of the sodium bronzes, whilst at the same time attempting to explain these observations in terms of the proposed model.

As has already been referred to, formic acid may decompose either by dehydration to yield carbon monoxide and water, or by dehydrogenation to yield carbon dioxide and hydrogen. On some catalysts both reactions occur. In the absence of surfaces exhibiting acidic properties, the formic acid decomposition

Fig 12.

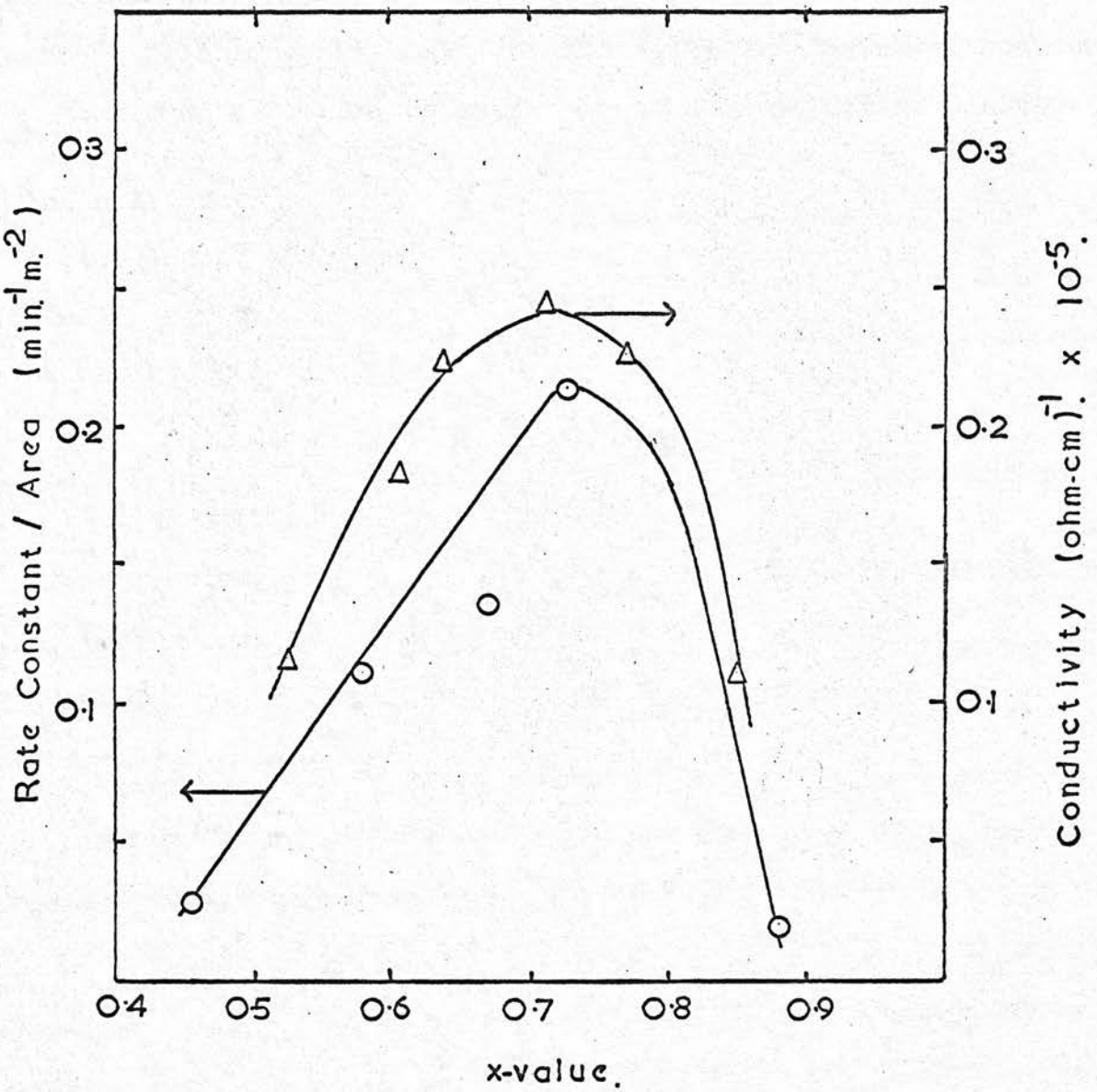

Dependence of Catalytic Activity for Conversion (O)

and Electrical Conductivity (Δ) on Bronze Composition

reaction has been shown (93-5) to proceed via a formate ion as surface intermediate. For a more detailed account of the mechanism, reference should be made to the first chapter of this text.

In their study of the ortho-para hydrogen conversion and hydrogen-deuterium exchange reactions, Jones and Loebh (85), using bronzes with $0.30 < x < 0.98$, were able to show that their results could be correlated with the electronic properties of the bronzes.

They observed that the marked dependence of the rate constant and the pre-exponential factor on composition, passing through a maximum at $x \triangleq 0.70$, closely paralleled the maximum in electrical conductivity reported for these samples (24-5, 82). This relationship is shown in figure 12, where both rate constant per. unit. area. and conductivity are plotted as a function of bronze composition. Conductivities were calculated from the data of Brown and Banks (25).

Of additional interest was the observed independence of the activation energy for the para hydrogen conversion on composition, being close to the gas phase value of 6 K cals/ mol.

Closer inspection of these results revealed that the desorption:adsorption rate constant ratio was largely responsible for the maximum in activity at $x \triangleq 0.7$. They propounded that if hydrogen is present on the surface as adsorbed ions and

. . .

neutralisation is necessary before desorption can occur, then the enhanced desorption rate can be interpreted as an enhanced accessibility of conduction electrons from the solid. Alternatively, if the diffusion of hydrogen atoms along the surface prior to desorption is rate determining, enhanced electrical conductivity should lead to greater mobility of adsorbed atoms and an increased rate of desorption.

The observations that the bronzes underwent an 'Activation process' in hydrogen, they attributed to the known fact that oxide catalysts require an adaptation period in the presence of reactant gas before obtaining reproducible results. Stone (113) has explained this activation process as a gradual enrichment of the surface layers with interstitial metal cations. Such a process would appear to be too permanent to explain the rapid reversible deactivation which occurs when hydrogen is removed from the sodium bronzes, or the irreversible poisoning when oxygen is admitted to the activated surface. They proposed that a more acceptable explanation would be that the activation process consists of diffusion of hydrogen into the lattice to alter the electronic properties of the surface and several adjacent layers. Accepting this, they recognised that the conversion necessarily still had to occur predominantly on the surface owing to the slow diffusion of hydrogen out of the lattice. Irreversible oxygen poisoning could then result if oxygen atoms were allowed to diffuse into the hydrogenated

lattice to form H_2O or OH trapped in interstitial positions.

These findings provide a more than useful basis from which some of the observed features of the present study may be explained. Consideration of Stone's (113) explanation of the activation process in terms of a gradual enrichment of the surface layers, leads to the query as to why the samples used in this study, underwent much more rapid adaptation prior to obtaining reproducible results; for example, whereas the samples used by Jones and Loebh (85) underwent slow activation, the process lasting approximately 5 days, those used in this work attained this very same condition after only 1-2 days. This question may be suitably answered by inspection of the various adsorption processes involved. It has already been established that formic acid is adsorbed as a formate ion species, whether or not this is in fact completely ionic or just dipolar in nature is immaterial, the important feature being that this intermediate will at some stage decompose, yielding among other things, hydrogen, initially in the form of atoms but later desorbed as the molecular species. As is well known, hydrogen atoms have much greater reducing powers than molecular hydrogen and hence must be a major contributor to the known strong reducing action of formic acid. This is further borne out by the conductivity data for pretreated samples, for which it was observed that only carbon monoxide and hydrogen, of the product gases, were able to lower the resistance to any appreciable

extent, with the overall rate of change of resistance being a thousandfold slower than that observed for formic acid. It would thus be expected that the adsorption of molecular hydrogen, in the form used by Jones and Loebh (85), would lack the necessary reducing power to effect as rapid an activation as that outlined above.

This factor could also explain the irreversible loss of activity, experienced by Jones and Loebh (85), on exposure to air (22×10^{-3} mm. Hg.) at temperatures as low as 175°C. Since in the present study, activities could easily be recovered after exposure to oxygen at similar low pressures and temperatures, (the 'irreversible deactivation' only recurred, for values of $x > 0.11$, at temperatures in excess of 350°C, depending upon the sodium content), further support is provided for the opinion that molecular hydrogen lacks the necessary reducing action to rejuvenate the surface of the bronzes used by Jones and Loebh. Whether or not this activity (85) could have been recovered with the aid of formic acid, will, it would seem, remain a matter for speculation.

If one is able to accept the view of the majority of workers (93) that the dehydrogenation reaction is a measure of metallic character, then it can be seen that there is a striking resemblance between graph 13, representing the individual contribution of the dehydrogenation reaction to the overall activity, and figure 12, representing the electrical conductivity.

The maximum occurring at $x \simeq 0.73$, whilst consistent with the maximum in conductivity, postulated by various workers (24-5, 82), does not necessarily conflict with the evidence by Juretschke (82), in support of Fuchs's picture (63) of a broad maximum in conductivity, extending from $x \sim 0.6$ to 0.9. This may be compared with the sudden changeover in selectivity, with a preference for the dehydrogenation reaction, occurring at $x \simeq 0.66$, and continuing for the remaining, higher members of the series.

Conversely, accepting that the dehydration reaction is inversely proportional to metallic character, it can be seen that there is also a close analogy between the results obtained for the dehydration component of the total activity in the present study, shown in graph 14, and those of Balandin and Sokolova (13) on the decomposition of isopropyl alcohol and ethanol, using bronzes prepared by reduction of sodium paratungstate. These workers observed that the dehydrating power of the bronzes was less than that of WO_3 or the unreduced paratungstate, and also that it decreased with increased degree of reduction, becoming almost zero in the case of the most completely reduced orange-yellow bronze ($x = 0.91$). In addition, an apprieciable increase in activity, to a value of the order of that observed for the original paratungstate, was observed for all bronzes studied, after pretreatment in oxygen in an analogous manner to that adopted in this work. These results, comparing favourably with the trend observed in the present study, they

attributed to oxidation of the bronzes.

Preliminary investigation, by these workers, of the formic acid decomposition reaction in a flow system on the orange-yellow bronze (x = 0,91) and the unreduced paratungstate, resulted in both dehydrogenation and dehydration, with a greater percentage of the latter reaction. Both catalysts promoted the decomposition in the same manner, yielding almost identical CO_2/CO ratios, with the paratungstate being more active than the bronze. Of significance is the absence of any reference to any washing procedure, or surface area data for the samples used in their study. An explanation of their results may be understood by consideration of certain important features of the present study. For instance, the low CO_2/CO ratios obtained prior to washing for the higher bronzes, may be accounted for by the presence of apprieciable quantities of unreacted WO_3, Na_2WO_4 and W on the surface of the unwashed bronzes. Further, the apparent lower, overall activity observed for the higher unwashed bronzes, was compensated for by the much lower specific surface areas of these samples.

In the comparision above of the present results with those of Balandin and Sokolova, no regard has been taken of the fact that all the bronzes used to establish graphs 13 and 14, representing dehydrogenation and dehydration respectively, were in a highly conducting state. It may therefore be profitless to attempt to correlate the observed dehydrogenation and dehydration

activity of the bronzes with conductivities (figure 12), determined under atmospheric conditions.

Henceforth, an attempt will be made to demonstrate how the results may also be interpreted using a mechanism based on the Multiplet theory (86) and analogous to that used by Balandin and Sokolova (13). In so doing, it will necessarily illustrate how well the conductivity data are able to provide conclusive evidence for this latter mechanism, whilst at the same time illustrating the suitability of both approaches.

The extent of zero order reaction, which was found to increase from 7 % (graph 4) for the lowest members of the series, to 30 % (graph 1) of total reaction for the highest members, may largely be accounted for by inspection of the CO_2/CO product distribution ratios. For example, the sudden changeover from largely dehydrating to dehydrogenating activity, occuring at $x \simeq 0.6$, closely parallels the marked increase in the extent of this linear relationship, the point of departure from zero order kinetics increasing from 12 % (graph 3) to 25 % of total reaction, as x increases from 0.6 to ~0.66. This also corresponds to the broad minimum in resistivity, postulated by Fuchs to occur between $x = 0.6$ and 0.9. This increased conductivity may in some way facilitate the formation of a formate intermediate whose configuration may favour the dehydrogenation reaction. Earlier it was observed that only

water of the product gases, caused any appreciable retardation of the decomposition rate, whilst at the same time, adsorption experiments failed to detect any significanct adsorption with any of these species. However, it should be pointed out that this retardation in the presence of water, only occurred to any large extent when appreciable quantities of water were present (pressure of HCOOH / pressure of $H_2O \simeq 1$ in the reaction system), so that it would appear that inhibition by H_2O is not related to the sudden increase in the extent of zero order reaction.

A more likely explanation may involve the formate intermediate or intermediates present on the surface. Should only one species be present, then this may undergo a change in configuration, tending to favour the dehydrogenation reaction at the expense of the dehydration reaction at some critical value of x. However, in the event of there being two opposing species, residing on the surface, then an exactly analogous situation may arise, except that in this case, the two species would still retain their individual character. An insight into this changeover, may, moreover, be gained from a scrutiny of the work by Jones and Loebl (85), who explained the enhanced activity at $x \simeq 0.7$, in terms of an activation process consisting of diffusion of hydrogen into the bronze lattice, resulting in an alteration in the electronic properties of the surface and several adjacent layers.

Before any attempt is made to specify any one mechanism, consistent with the observed results, mention will be made of the other anomalies of the present study. These have included the dependence of the CO_2/CO ratio on percentage reaction; the CO_2/H_2 ratios which are substantially greater than unity and the absence of any water-gas shift reaction.

The increase in CO_2/CO ratio (graphs 5b-8b) with percentage reaction, observed for the majority of catalysts used in the present study, has also been referred to by Mars, Scholten and Zwietering (93) for oxide catalysts. These workers, carrying out an infra red study of the decomposition on MgO, an essentially dehydrogenating oxide, were able to show that the intensity of the -OH bands decreased more rapidly than the other bands, in agreement with their observations of an initial rapid formation of water.

The CO_2/H_2 ratios, being substantially greater than unity are consistent with the view that apprieciable quantities of hydrogen are retained by the surface. This affinity for hydrogen, already referred to by Jones and Loebl (85), may be understood from the fact that hydrogen analogs of the sodium tungsten bronzes occur with almost identical lattice parameters (13,112). Sienko and Osterreicher (112) have succeeded in preparing hydrogen tungsten bronzes, H_xWO_3 with $0.5 > x > 0.03$. Owing to the ready oxidation by air under normal conditions, these were necessarily retained under vacuum.

Finally, the absence of any water-gas shift reaction is in keeping with the view of Mars (114) that zero order reactions, involving formic acid, result when species are quite strongly adsorbed onto the surface, so that no favourable sites, with respect to this secondary process, are left exposed on the surface.

Consideration now of the mechanism postulated by Balandin and Sokolova (13), and discussed in detail in the first chapter of this text, would seem to indicate that an explanation of the present results in terms of this approach might be justified. The rapid trend towards the highly conducting state may serve to account for the similarity in activities, for the decomposition reaction (graph 12), through the series. Whereas, previously an explanation of the changing CO_2/CO ratio has been interpreted in terms of a purely electronic model, which has neglected the oxygen vacancies and hence the high conducting nature of the whole series, it now appears that a more acceptable picture of the mechanism would involve participation of the various surface defects, due to both oxygen and sodium vacancies which are present throughout the series. Studies of the change of resistance with temperature (and time), magnetic susceptibilities and e.s.r. spectra of samples, the latter two more especially for WO_3, have provided conclusive evidence for the presence of the oxygen vacancies so necessary for this approach. Further evidence for the use of these oxygen vacancies has come from adsorption experiments with formic acid (Table 5), from which it

may be observed that the degree of adsorption of HCOOH was less on pretreated samples of WO_3 and $Na_{0.11}WO_3$ than on the normal catalysts.

Inspection of the results shown in Table 5, for the normal catalysts, reveals that the degree of adsorption of HCOOH for those members with $x > 0.60$, is larger than that for the lower members in the series. This would seem to invalidate a mechanism based solely on one adsorbed formate species, as used by Balandin and Sokolova (13), because of the smaller number of the necessary adjacent sodium and oxygen vacancies, understandably present at higher sodium concentrations. Had only the one type of formate species been present, these adsorption experiments should have shown smaller degrees of adsorption of HCOOH on ascending the series. These results are, however, consistent with a mechanism involving the presence of two separate formate species on the surface.

The close parallel between the results obtained for the dehydration component of the decomposition reaction (graph 14) and those of Balandin and Sokolova (13) on the dehydration of isopropyl alcohol and ethanol, would seem to indicate that a mechanism involving the use of the adjacent sodium and oxygen vacancies would be justified.

One may, therefore, picture the formation of a reaction intermediate of the following type:-

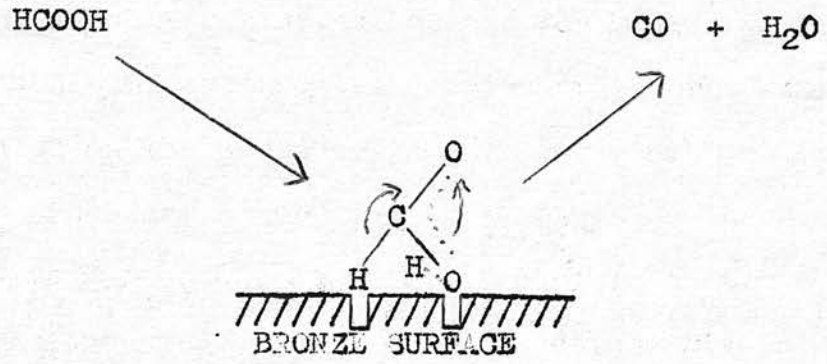

Whether this involves a partial or complete transfer of electrons is, however, still very much in doubt (109,110). Measurements of the change in resistance of the wholly dehydrating catalyst WO_3, in the presence of formic acid, have provided evidence for the transfer of electrons away from the catalyst. Similar measurements carried out on the bronzes have been less easily interpreted, little or no change in resistance being observed for all samples studied. The more easily distinguishable resistance change for WO_3, may, however, be a consequence of the greater density of adsorbed formic acid molecules on the surface, there being ~ 0.56 molecules of HCOOH/ cube face as opposed to ~ 0.23 molecules of HCOOH/ cube face with $Na_{0.11}WO_3$. It is also possible that the competing dehydration and dehydrogenation reactions give rise to oppositively charged formate ions on the surface. These would then cancel one another out, resulting in little or no observable change in the resistance of the bronzes. Another explanation for the possible absence of any distinct change in resistance, being observed for the mainly dehydrogenating

bronzes, may have been due to the fact that the bronzes were initially of very low resistance so that very little change would be expected.

From consideration of the various molecular parameters, it can be seen that the adsorbed formic acid complex may adopt a configuration similar to that of the alcohol in figure 6. Although the (H····O) distance in formic acid ($\sim$2.0 A), is less than the corresponding distance in alcohols ($\sim$2.35 A), it is to be expected that deformation will also play its part, with the (C····H) and (C····O) distances in the activated complex being larger than in the normal molecule. This will increase the (H····O) distance and thus make it closer to the bronze (Na····O) distance of 2.74 A. Furthmore, on increasing the number of sodium defects in going from the hypothetical $Na_{1.0}WO_3$ to those of lower x value, the WO_6 octahedra will be deformed, decreasing the lattice parameter from a = 3.86 in $Na_{1.0}WO_3$ to $\sim$3.75 in WO_3, so that the (Na····O) distance in the bronze will be closer to the (H····O) distance in formic acid. Thus it would be expected that the lower members would more easily facilitate the formation of the formate intermediate, since less strain will be involved in bringing the (H····O) distance closer to the (Na····O) distance in the bronze. This may also serve to explain the earlier departure from zero order kinetics observed for the lower members, since less deformation of the (C····O) and (H····O) bonds will result in a more strongly

bound formate species on the surface, so that there will be a greater possibility of poisoning the surface with respect to further reaction. It would appear, on the strength of the present results, that the breakdown of this intermediate is in fact the rate determining step in the decomposition. That any number of the available sodium vacancies may be used to form complexes of the above type has been demonstrated by the existence of hydrogen tungsten bronzes with x values as high as 0.5 (112).

Before forwarding arguements, both for and against the possible sites available for the dehydrogenation component of the decomposition, it is imperitive to note the apparent ease of reaction, with the departure from zero order kinetics occurring at a much later stage, when dehydrogenation is the major contributor to the overall decomposition, i.e. when $x > 0.60$. The indications are therefore, that the dehydrogenation mechanism involves a formate intermediate, less strongly bound to the surface of the bronze.

That this component is unlikely to proceed on filled sodium sites has been shown by Shabrowa (115), who demonstrated that sodium carbonate does not catalyse the decomposition of formic acid owing to the formation of a stable sodium formate.

The most probable sites would appear to involve either the adjacent tungsten and oxygen filled sites or isolated tungsten

atoms, using the mechanism presented by Eucken and Heuer (116), Eucken (117), and Wicke (118) or via the formation of a stable salt respectively. Adsorption between tungsten atoms has been ruled out owing to the great distance between adjacent tungsten atoms within the lattice (~ 3.86 Å).

Eucken and Heuer (116), Eucken (117) and Wicke (118), based their ideas on the mechanism of the analogous dehydrogenation of alcohols on their observation that dehydrogenation takes place in particular on oxides with a large cation radius and a smaller cation valency. As in such oxides the cation can only be incompletely surrounded, these authors supposed that the reaction proceeds via hydrogen addition to metal ions present on the surface; in analogy with this view, the dehydrogenation of formic acid could be visualised as follows:-

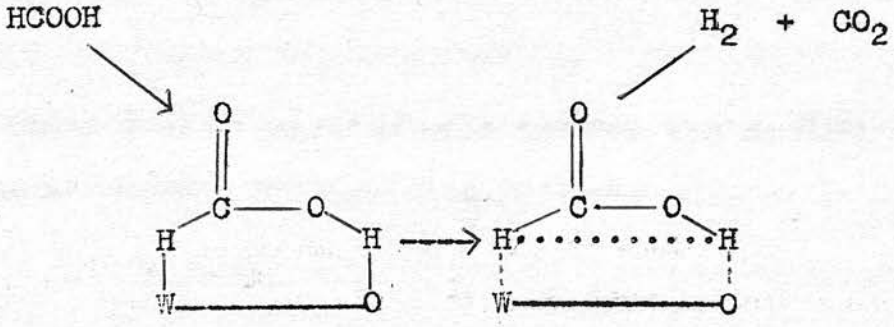

The high CO_2/H_2 ratios, however, would be inconsistent with this approach which was postulated before the importance of the formate and other ions as reaction intermediates was known.

Whether the mechanism will involve the formation of a salt, such as an oxalate or carbonate (93) will depend on, among other things, the stabilities of the oxalate and carbonate. The absence of any reliable data from the literature does in fact limit the use of this approach. In general, however, the stabilities of salts derived from dehydrogenating oxides appear to be of the same order as those of the corresponding formates.

The more recent evidence for the bimolecular type of mechanism, given by Hirota (95) and Lawson (97) and outlined in the first chapter of this text, would it seem to offer a realistic answer to this problem. In deriving the mechanism involving the formation of the intermediate complex shown earlier (page 15), they argued that strongly bound formate ions are sites for adsorption of weakly bound formic acid molecules in the presence of the gas phase. Decomposition of this intermediate species could then occur according to reaction paths (a) and (b), with (a) being favoured by Lawson and (b) by Hirota et. al.

$$HCOOH\ HCOO^- + Hads = 2CO_2 + 2H_2 \qquad (a)$$

$$HCOOH\ HCOO^- + Hads = CO_2 + H_2 + HCOO^- + Hads \qquad (b)$$

Even allowing for the fact that these researches were carried out on metal films, it may be that this approach is what is required to explain the results for the dehydrogenation component of the decomposition in the present study.

For instance, it would not seem unfavourable to consider the higher members of the series, i.e. where $x \geq 0.66$, as metals, a consequence which in itself would point to a bimolecular type mechanism, since recent studies (95,97) have indicated that a mechanism of this type is the one consistent with the results of the majority of workers (93). Although the larger degree of adsorption of HCOOH for those bronzes with $x \geq 0.66$ may also be consistent with this picture of a double layer of HCOOH molecules on the surface, it can also be seen to be in agreement with a monomolecular type mechanism.

Whether or not a bimolecular type mechanism is in fact in operation will, it would appear, remain a matter for speculation, as will any attempt, from the present study, to explain the similarly high degree of adsorption observed for WO_3.

Adoption of a bimolecular mechanism to explain the observed results would necessarily require that a slight modification be made to the picture outlined above in order to explain the high CO_2/H_2 ratios. It may be for example, that all hydrogen atoms are initially adsorbed prior to desorption as molecular hydrogen.

The correspondence between this higher degree of adsorption of HCOOH and the increased extent of zero order kinetics observed for those members with $x \geq 0.66$, may also be explained

from a consideration of simple Langmuir Adsorption.

An adequate explanation of the increased extent of zero order kinetics at $x \geqslant 0.66$, may be obtained from a consideration of the work by Jones and Loebl (85). On the basis of their results, the necessary prerequisite for a high percentage of dehydrogenation would apparently be attainment of a certain critical high conductivity, providing the necessary high quota of electrons to ensure a rapid adsorption together with desorption of hydrogen to and from the surface. An explanation along these lines may also account for the increasing CO_2/CO ratio with percentage decomposition for a given set of reaction conditions. If, as was thought possible by these workers, the diffusion of hydrogen atoms is a contributing factor to the behaviour of the surface to further reaction, then it would seem likely that some of the hydrogen atoms would occupy vacant sodium sites, with the result that these would remain essentially poisoned to further reaction. This type of process would explain the almost complete absence of hydrogen in the reaction system with the lower bronzes, there being a greater number of these sodium vacancies available for hydrogen occupation, and also apparently (112) no limit as to the amount taken up. Degassing procedure indicated that this hydrogen was easily removed, in accord with the ready reproducibility of rate measurements.

Finally, the presence of a compensation effect (93) has been shown in graph 11.

Summary

From a consideration of the various arguements, presented in this chapter, it would appear that the sodium bronzes conform with the electronic theory of catalysis with respect to the formic acid decomposition reaction. The CO_2/CO ratio would appear, however, to be governed by the number of occupied sodium sites present on the surface of the bronze, it being assumed, on the basis of conductivity, mass spectrometric and e.s.r. work, that the oxygen vacancies remain essentially constant for the bronzes, with the exception of WO_3. This necessarily invoked the use of an approach based on the Multiplet theory to present suitable mechanisms for the dehydrogenation and dehydration component reactions, consistent with the results. The close parallel between the decrease in the extent of dehydration and the decrease in adjacent sodium and oxygen vacancies in ascending the series has led to a mechanism in which use is made of these vacancies to explain the dehydration component of the decomposition . The insufficient number of such vacancies, together with the apparent higher degree of adsorption of HCOOH for those members with $x \geqslant 0.66$, has necessarily led to a different approach. Here, in formulating a mechanism for the dehydrogenation component, analogy has been drawn between these higher bronzes and the decomposition of formic acid on metals. In addition, arguements have been directed in support of a bimolecular and a monomolecular process for the dehydrogenation and dehydration

component reactions respectively.

It would appear that there is a critical value of x where the preference for dehydration is superceded by one for dehydrogenation. T he fine dividing line at which this occurs would, from the observed results, seem to be associated with that value of x at which each sodium has at least another sodium atom as nearest neighbour, leading to an unlimited sphere of movement for any one arbitrarily chosen conduction electron. At this point, for example, one may envisage a 'free run' for adsorbed hydrogen atoms in any direction, and so making it possible for favourable sites to undergo further reaction. This diffusion of hydrogen atoms has also been used to explain the shift towards higher CO_2/CO ratios during the reaction, these atoms occupying and essentially poisoning the sodium vacancies with respect to further reaction

REFERENCES.

1. Wöhler, F., Pogg. Ann., 2, 350 (1824).
2. Philipp, J., Schwebel, P., Ber., 12, 2234 (1879).
3. Scheibler, J., J. prakt. Chem., 83, 321 (1861).
4. Laurent, A., Ann. Chim. Physique (2), 67, 215 (1838).
5. Knorre, von. G., J. prakt. Chem., 27, 58 (1883).
6. Feit, W., Ber. Chem. Ges., 21, 134 (1888).
7. Brunner, "Beiträge zur Kennt nischer Wolfram bronzen", Dissert. Zurich, (1903).
8. Spitzen, V., Z. anorg. Allgem. Chem., 148, 69 (1925).
9. Spitzen, V., Kaschtanov, L., Z. anal. Chem., 75, 440 (1928).
10. Spitzen, V., Kaschtanov, L., Z. anorg. Allgem. Chem., 157, 141 (1926).
11. Straumanis, M.E., Z. Kristallogr., 102, 432 (1940).
12. Sienko, M.J., Adv. Chem. Ser. No. 39, 224 (1963).
13. Balandin, A. A., Sokolova, N.P., Izvest. Akad., Nauk. SSSR., Otdel, Khim. Nauk., 214-23 (1959).
14. Bracken, H., Z. Kristallogr., 78, 484 (1931).
15. Ueda, R., Ichinokawa, T., Phys. Rev., 80, 1106 (1950).
16. Wyart, J., Foex, M., Compt. rend., 232, 2459 (1951).
17. De Jong, von. W.F., Z. Kristallogr., 81, 314 (1932).
18. De Jong, von. W.F., Z. Kristallogr., 83, 496 (1932).
19. Hägg, G., Z. Physik. Chem., B29, 192 (1935). Nature, 135, 874 (1935).
20. Magnéli, A., Ark. Kemi. Mineral Geol., 1, 269 (1949).
21. Magnéli, A., Acta. Chem. Scand., 3, 88 (1949).
22. Brimm, E.O., Bentley, J.C., Lorenz, J.A., Jellineck, M.H., J. Amer. Chem. Soc., 73, 5427 (1951).

23. Andersson, G., Acta. Chem. Scand., 7, 154 (1953).

24. Gardner, W.R., Danielson, G.C., Phys. Rev., 93, 46 (1953).

25. Brown, B.W., Banks, E.J., J. Amer. Chem. Soc., 76, 963-6 (1954).

26. Westman, S., Magnéli, A., Acta. Chem. Scand., 12, 303 (1958).

27. Klug, H.P., Brasted, R.C., Comprehensive Inorg. Chem., 7, 289 (1959).

28. Dickens, P.G., Whittingham, M.S., Trans. Farad. Soc., 61, 1226 (1965). Quart. Rev., 22, 30 (1968).

29. Hägg, G., Magnéli, A., Arkiv. Mineral Geol., 19A, 2 (1944).

30. Magneli, A., Nova. Acta. Regiae. Soc. Sci. Upsaliensis, 14, 3 (1950).

31. Ward, R., Prog. Inorg. Chem., 1, 517-8 (1959).

32. Ribnick, A.S., Post, B., Banks, E., Adv. Chem. Ser. No. 39, 246 (1963).

33. Matthias, B.T., Wood, E.A., Phys. Rev., 84, 1255 (1951).

34. Rosen, C., Banks, E., Post, B., Acta. Cryst., 9, 475 (1956).

35. Peri, J.A., Banks, E., Post, B., J. Appl. Phys., 28, 1272 (1957).

36. Kepert, D.L., Prog. Inorg. Chem., 4, 232 (1962).

37. Crowder, B.L., Sienko, M.J., J. Inorg. Chem., 4, 73 (1965).

38. Bond, G.C., Catalysis by Metals (Academic Press, London and New York, 1962).

39. Straumanis, M.E., J. Amer. Chem. Soc., 71, 679 (1949).

40. Hägg, G., Magnéli, A., Rev. Pure and Appl. Chem. (Aust) 4, 235 (1954).

41. Magneli, A., J. Inorg. and Nucl. Chem., 2, 350 (1956).

42. Danitz, J.D., Orgel, L.E., Inorg. and Radio Chem., 2, 49 (1960).

43. Sienko, M.J., Kupka, F., J. Chem. Phys., 18, 1296 (1950).

44. Glemser, O., Sauer, H., Z. anorg. Chem.,252, 144 (1944).

45. Sienko, M.J., Banerjee, B., J. Amer. Chem. Soc., 83, 4149 (1961).

46. Gadó, P., Acta. Cryst., 16, A182 (1963).

47. Ackermann, R.J., Rauk, E.G., J. Phys. Chem., 67, 2596 (1963).

48. Magnéli, A., Gadó, P., Acta. Chem. Scand., 19, 1514 (1965).

49. Gebert, E., Ackermann, R.J., Inorg. Chem., 5, 36 (1966).

50. Selwood, P.W., Magneto Chemistry, Interscience (New York), p. 151 (1943).

51. Straumanis, M.E., Brimm, E.O., J. Amer. Chem. Soc., 73, 5427 (1951).

52. Straumanis, M.E., Hsu, S.S., ibid, 72, 4027 (1950).

53. Magnéli, A., Blomberg, B., Acta. Chem. Scand., 5, 372 (1951).

54. Huibregste, E.J., Barker, D.B., Danielson, G.C., Phys. Rev., 84, 142 (1951).

55. Huibregste, E.J., Iowa State Coll. J. Sci., 26, 222 (1952).

56. Straumanis, M.E., Irani, K.K., J. Amer. Chem. Soc., 74, 2114 (1952).

57. Ozerov, R.P., Dokalady Akad., Nauk, SSSR, 99, 93-5 (1954).

58. Stubbin, P.M., Mellor, D.P., Proc., N.S.Wales, 82, 225 (1948).

59. Sienko, M.J., Conroy, L.E., J. Amer. Chem. Soc., 79, 4048 (1957).

60. Ellerbeck, L.D., Shanks, H.R., Sidles, P.H., Danielson, G.C., J. Chem. Phys., 35, 298-302 (1961).

61. Crowder, B.L., Sienko, M.J., ibid, 38, 1576 (1963).

62. Mackintosh, A.R., ibid, 38, 1991 (1963).

63. Fuchs, R., ibid, 42, 3781 (1965).

64. Frohlich, H., Mott, N.F., Proc. Roy. Soc., (London), A171, 496 (1939).

65. Howarth, D., Sonheimer, E., Proc. Roy. Soc., (London), A219, 53 (1953).

66. Lee, T.D., Low, F.E., Pines, D., Phys. Rev., 90, 297 (1953).

67. Low, F.E., Pines, D., ibid, 91, 193 (1953).

68. Low, F.E., Pines, D., ibid, 98, 414 (1955).

69. Mellor, J.W., A Treatise on Inorg. and Theoretical Chemistry, Vol XI, p.753.

70. Sawada, S., Danielson, G.C., Phys. Rev., 113, 1005 (1959).

71. Dorothy, R.G., Lynch, D.W., Bull. Am. Phys. Soc., 7, 221 (1962).

72. Sienko, M.J., J. Amer. Chem. Soc., 81, 5556 (1959).

73. Barnes, R.G., Hultsch, R.A., Jones, W.H., Jnr., Bull. Am. Phys. Soc. Sec. II, 4, 166 (1959).

74. Jones, W.H., Jnr., Garbaty, E.A., Barnes, R.G., J. Chem. Phys., 36, 494 (1962).

75. Narath, A., Wallace, D.C., Phys. Rev., 127, 724 (1962).

76. Fromhold, A.T., Jnr., Narath, A., ibid, 152(2), 585-91 (1966).

77. McNiell, W., Dissert. Abstr., 22, 60-1 (1961).

78. Shanks, H.R., Sidles, P.H., Danielson, G.C., Adv. Chem. Ser. 39, 237 (1963).

79. Mahlestein, C.D., Danielson, G.C., Phys. Rev., 158(3), 825-32 (1967).

80. Sienko, M.J., Truong, T.B.N., J. Amer. Chem. Soc., 83, 3131 (1961).

81. Mott, N.F., Nuovo. Cimento., 7, 312 (1958), Phil. Mag., 6, 287 (1961).

82. Juretschke, L., Phys. Rev., 86, 124 (1952).

83. Greiner, J.D., Shanks, H.R., Wallace, D.C., J. Chem. Phys., 34, 772 (1962).

84. Vest, R.W., Griffel, M., Smith, J.F., ibid, 28, 293 (1958).

85. Jones, F.T., Loebl, E.M., J. Phys Chem., 73, 894 (1969).

86. Trapnell, B.M.W., Adv. Cat., 3, 1 (1951).

87. Mills, G.A., Weller, S., Hindin, S.O., Milliken, T.H., Z. Elektrochem, 60, 823 (1956).

88. Ormont, B.F., Structure of Inorganic Compounds, Moscow-Leningrad, Gostekhterizdat, 1945.

89. Ozerov, R.P., Proc. Acad. Sci., USSR., 99, 93 (1954) Progr. Chem., 24, 951 (1955).

90. Derén, J., Polaczkowa, E., Bull. Akad., Polon., 5, 313 (1959).

91. Sienko, M.J., Kudrak, D.R., Inorg. Chem. 6, 880 (1967).

92. Rabes, von I., Schenck, R., Z. anorg. Chem., 259, 201 (1949).

93. Mars, P., Scholten, J.J.F., Zwietering, P., Adv. Cat., 14, 35 (1963).

94. Yagodovskii, V.D., Poso, P., Kinet. Katal., 9(1), 110-16 (1968)(Russ).

95. Kishi, K., Ogawa, T., Hirota, K., J. Cat., 5, 464 (1966).

96. Suzuki, C., Matuura, I., Nippon Kagaka Zasshi, 89, 35-7, (1968).

97. Lawson, A., J. Cat., 11, 295 (1968).

98. Ewing, A.J., J. Chem. Soc., 105, 354 (1914). Coolidge, A.S., J. Amer. Chem. Soc., 52, 1874 (1930).

99. Brunnauer, S., Emmett, P.H., Teller, E., J. Amer. Chem. Soc., 60, 309 (1938).

100. Inglis, H.S., Studies on the Decomposition of Formic Acid on Transition metals. Ph. D. Thesis Edinburgh.

101. Figgis, B., Nyholm, R., J. Chem. Soc., 4190 (1958).

102. Lewis and Wilkins, 'Modern Co-ordination Chemistry', Interscience Publishers, New York, 1960.

103. Ingram, D.J.E., Free Radicals as studied by Electron Spin Resonance, (Butterworths, 1958), p16-8.

104. Jackman, L.M., Wiley, R.H., J. Chem. Soc., 2881 (1960).

105. Blake, P.G., Hinshelwood, C., Proc. Roy. Soc., A255, 444 (1960).

106. Fahrenfort, J., Van Reijen, L.L., Sachtler, W.M.H., 'The Mechanism of Heterogeneous Catalysis', Elesevier Monograph, p.23, (1960).

107. Baker, M., Jenkins, G.I., Adv. Cat., 8, 1 (1955).

108. Sykes, M.F., Essam, J.W., Phys. Rev., A310, 133 (1964).

109. Dowden, D.A., Reynolds, P.W., Disc. Farad. Soc., 8, 184 (1950).

110. Eley, D.D., Luetic, P., Trans. Farad. Soc., 53, 1483 (1957).

111. Quinn, D.F., Studies on the Electronic Factor in Catalysis, Ph. D. Thesis, Edinburgh.

112. Sienko, M.J., Osterreicher, H., J. Amer. Chem. Soc., 90, 6568 (1968).

113. Stone, F.S., 'Chemistry of the Solid State', W.E. Garner, Ed., Butterworth and Co. Ltd., London, 1955, p.400.

114. Mars, P., Z. physik. Chem., 22, 309 (1959).

115. Shabrowa, G.M., Doklady Akad. Nauk SSSR., 133, 1375 (1960).

116. Eucken, A., Heuer, K., Z. physik. Chem., 196, 40 (1950).

117. Eucken, A., Naturwissenschaften, 36, 48 (1959).

118. Wicke, E., Z. Elektrochem. 53, 279 (1949).